82 Semiclassical and Continuum Limits of Four-Dimensional CDT

四维 CDT 的半经典极限与连续统极限

Jakub Gizbert-Studnicki

雅各布·吉斯贝特-施图德尼茨基

Contents

目录

Abstract

摘要

This chapter discusses the infrared and the (perspective) ultraviolet limits of four-dimensional Causal Dynamical Triangulations (CDT). CDT is a non-perturabtive and background-independent approach to quantization of Einstein's gravity, based on a lattice regularization of the quantum-gravitational path integral. It is shown that inside the, so-called, de Sitter phase, one recovers a four-dimensional semiclassical universe, where behavior of the scale factor is consistent with classical solutions of Einstein's field equations and fluctuations of the scale factor are very accurately described by a simple minisuperspace effective action. It is argued that some of the phase transitions surrounding the semiclassical phase are higher-order transitions, which opens a possibility of defining a continuum limit of CDT. Finally, it is discussed how to define the renormalization group flow in CDT and then how to search for a UV fixed point in which, in the spirit of asymptotic safety, quantum theory of gravity could become non-perturbatively renormalizable and thus valid up to arbitrarily short distance scales.

本章讨论四维因果动态三角剖分 (CDT) 的红外与 (预期) 紫外极限。CDT 是爱因斯坦引力量子化的非微扰、不依赖背景的方法，以量子引力路径积分的格点正则化为基础。研究表明，在所谓德西特相内可以重新得到四维半经典宇宙，其中标度因子的行为与爱因斯坦场方程的经典解一致，且标度因子的涨落可被简单的超空间最小化有效作用量非常精确地描述。本文论证包围半经典相的部分相变是高阶相变，这为定义 CDT 的连续极限提供了可能。最后，本文讨论如何在 CDT 中定义重整化群流，以及如何寻找紫外不动点——在渐近安全的理念下，引力量子理论可在该不动点处实现非微扰可重整，从而在任意短距离尺度下都成立。

J. Gizbert-Studnicki (☑)

J. Gizbert-Studnicki (☑)

Institute of Theoretical Physics, Jagiellonian University, Kraków, Poland

波兰克拉科夫雅盖隆大学理论物理研究所

Mark Kac Center for Complex Systems Research, Jagiellonian University, Kraków, Poland e-mail: jakub.gizbert-studnicki@uj.edu.pl

波兰克拉科夫雅盖隆大学马克·卡克复杂系统研究中心电子邮箱:jakub.gizbert-studnicki@uj.edu.pl

---

Keywords

关键词

Lattice quantum gravity - Causal Dynamical Triangulations (CDT) - Quantum geometry - Semiclassical limit - Phase transitions - Renormalization group (RG) - Continuum limit - Asymptotic safety

格点量子引力——因果动态三角剖分 (CDT)——量子几何——半经典极限——相变——重整化群 (RG)——连续极限——渐近安全

Introduction

引言

Three out of four fundamental interactions are very accurately described by a quantum field theory (QFT), the infamous exception being the gravitational interaction. Therefore, a quantum description of gravity remains an important goal of theoretical physics. Despite many different approaches described in this Handbook, yet to date there is still no fully consistent theory of quantum gravity. One of the problems one encounters when trying to apply QFT framework to quantization of General Relativity, which is currently our best description of the classical gravitational interaction, is that such an approach is perturbatively non-renormalizable. It means that the naïve application of the perturbation theory would result in infinitely many counterterms and related coupling constants appearing in the theory in the ultraviolet (UV) limit, which cannot be eliminated via renormalization, thus yielding the theory to be unpredictive. However, as suggested in Weinberg's seminal work [1], the definition of renormalizability might be generalized to the non-perturbative regime as described by the asymptotic safety conjecture. Asymptotic safety (for more details check the part of the Handbook dedicated to the asymptotically safe quantum gravity and for the links of asymptotic safety with CDT refer to > Chap. 76, "The Causality Road from Dynamical Triangulations to Quantum Gravity That Describes Our Universe") predicts that the renormalization group (RG) flow of the bare gravitational couplings leads to the non-Gaussian UV fixed point(s), in which the quantum theory of gravity becomes scale-invariant (which by construction guarantees a finite limit, making the theory predictive), but also in the UV limit, the dimensionless gravitational couplings do not need to be small (thus invalidating the naïve use of perturbation theory). The actual calculations using the functional renormalization group make approximations which can be difficult to control, and it is therefore important to verify the results by independent methods. This motivates a complementary lattice QFT approach which can potentially be used for testing the asymptotic safety scenario. In the lattice formulation, the UV fixed point should appear as a higher-order critical point. The

reason is the following: the divergent correlation length, characteristic for a higher-order phase transition, should allow taking the lattice spacing to zero while simultaneously keeping physical observables fixed; as the lattice spacing a plays a role of a UV regulator (providing the UV cutoff of the QFT of order $1/a$), the cutoff will be removed in the continuum limit, which hopefully should correspond to the UV fixed point of quantum gravity. At the same time, the lattice QFT in question should be able to correctly reconstruct the infrared (IR) limit of gravity, hopefully consistent with classical Einstein's field equations. In principle one should also be able to define how to renormalize the dimensionless bare lattice coupling constants when taking the lattice spacing to zero (or alternatively the UV cutoff to infinity). The RG flow of the couplings with decreasing lattice spacing should define some path(s) in the lattice coupling constant space leading from the IR semiclassical limit to the UV continuum limit.

四种基本相互作用中已有三种可以被量子场论 (QFT) 非常精准地描述，广为人知的例外便是引力相互作用。因此，给出引力的量子描述仍是理论物理学的重要目标。尽管本手册阐述了诸多不同研究方案，迄今为止仍不存在一个完全自洽的量子引力理论。目前广义相对论是经典引力相互作用的最佳描述，当人们尝试用量子场论框架对其量子化时，遇到的一个问题是该方法在微扰下不可重整。这意味着，微扰论的朴素应用会在理论的紫外 (UV) 极限产生无穷多个抵消项和相关耦合常数，这些无法通过重整化消除，导致理论失去预言能力。但正如温伯格开创性工作 [1] 所提出的，可重整性的定义可以推广到非微扰区域，即渐近安全猜想所描述的内容。渐近安全 (更多细节参见本手册中关于渐近安全量子引力的部分，渐近安全与 CDT 的关联可参考 > 第 76 章，“从动力学三角剖分到描述我们宇宙的量子引力的因果性路径”) 预言，裸引力耦合的重整化群 (RG) 流会流向非高斯紫外不动点，量子引力理论在此处变为标度不变 (由构造保证存在有限极限，使理论具备预言能力)，但同时在紫外极限下，无量纲引力耦合不必很小 (因此朴素微扰论不再成立)。使用泛函重整化群的实际计算包含难以控制的近似，因此需要用独立方法验证结果，这催生了互补的格点量子场论方法，它有可能用来检验渐近安全方案。在格点表述中，紫外不动点应当表现为高阶临界点，原因如下: 高阶相变的特征是关联长度发散，这允许我们在格点间距趋于零的同时保持物理可观测量不变；由于格点间距 a 是紫外调节器 (为量子场论提供量级为 $1/a$ 的紫外截断)，截断会在连续极限中被移除，而这个连续极限有希望对应量子引力的紫外不动点。同时，我们讨论的这个格点量子场论应当能够正确重构引力的红外 (IR) 极限，且有希望与经典爱因斯坦场方程自洽。原则上，我们还应当能够定义，当格点间距趋于零 (或等价地说紫外截断趋于无穷) 时，如何对无量纲裸格点耦合常数进行重整化。耦合随格点间距减小的重整化群流，会在格点耦合常数空间中定义出若干路径，从红外半经典极限通向紫外连续极限。

As will be argued below, one of the most successful lattice formulations of quantum gravity is that of Causal Dynamical Triangulations (CDT) (for more details about the CDT formulation see Chap. 76, "The Causality Road from Dynamical Triangulations to Quantum Gravity That Describes Our Universe" and review articles [2-4]), at least in the sense that it seems to admit a well-defined semiclassical description, and, at the same time, it has a rich phase structure, where some of the phase transitions might be higher-order transitions, and one can also define how to renormalize the bare couplings of CDT when the lattice spacing is changed; an open question remains if the flow of couplings really leads from the IR to the UV fixed point of quantum gravity. The approach is based on the lattice regularization of the quantum-gravitational path integral over metric degrees of freedom (with Lorentzian signature):

下文将说明，因果动力学三角剖分 (CDT) 是最成功的量子引力格点表述之一 (关于 CDT 表述的更多细节参见第 76 章“从动力学三角剖分到描述我们宇宙的量子引力的因果性路径”以及综述文献 [2-4])，它至少满足: 能给出良定义的半经典描述，同时拥有丰富的相结构，其中部分相变可能是高阶相变，还能够定义改变格点间距时如何重整化 CDT 的裸耦合；耦合流是否真的能从量子引力的红外区流向紫外不动点仍是一个开放问题。该方法建立在对度量自由度 (洛伦兹号差) 的量子引力路径积分做格点正则化的基础上:

$$Z_{QG}(G,\Lambda) = \int \mathcal{D}\left[g_{\mu v}\right] e^{iS_{EH}[G,\Lambda;g_{\mu v}]}, \tag{1}$$

where $\mathcal{D}\left[g_{\mu v}\right]$ is a measure term, which enables one to integrate over geometries, i.e., diffeomorphism-invariant equivalence classes of metrics $g_{\mu v}$, and S_{EH} is the Einstein-Hilbert action, dependent on Newton' s constant G and the cosmological constant Λ . In the four-dimensional CDT, the continuous geometries are approximated by lattices (called triangulations) constructed from four-dimensional simplicial building blocks with fixed edge lengths (called four-simplices), fulfilling some additional topological constraints. The interior of each four-simplex is isomorphic to a (part of) flat Minkowski spacetime, and the geometry is encoded in the way the building blocks are ”glued” together. This idea originates from earlier methods of Euclidean Dynamical Triangulations (EDT), see Chap. 73, ”Lattice Quantum Gravity: EDT and CDT”, which assumed Euclidean (local SO(4) symmetry) instead of Lorentzian (local SO(3;1) symmetry) spacetime geometry. In EDT all simplices were equilateral and identical and the time direction was not distinguished. In contrast to that, in CDT one assumes that the (Lorentzian) spacetimes are globally hyperbolic, and thus they admit a time foliation into spatial hypersurfaces, called slices, of constant cosmological time. It is also required that the spatial topology $\sum$ of each slice is fixed and preserved in the time evolution. As a result the spacetime topology is that of $[0,1]\times\sum$. The (three-dimensional) geometry of a spatial slice at time t_k (k denotes the lattice time coordinate, $k\in\mathbb{Z}$) is represented by a triangulation $\mathcal{T}_k^{(3)}$ (with the fixed topology $\sum$) constructed from identical equilateral three-simplices (tetrahedra). Any two such triangulations $\mathcal{T}_k^{(3)}$ at time t_k and $\mathcal{T}_{k+1}^{(3)}$ at time t_{k+1} constitute boundaries of a (four-dimensional) triangulation $\mathcal{T}_{k:k+1}^{(4)}$ of a slab between t_k and t_{k+1} , which can be constructed from four types of four-simplices, denoted $T^{(4,1)}, T^{(1,4)}, T^{(3,2)}$, and $T^{(2,3)}$, where the numbers in parentheses represent the numbers of vertices that each simplex has in time t_k and t_{k+1} , respectively; see Fig. 1. The four-simplices are ”glued” together in such a way that there are no topological defects in the slab and thus any spatial hypersurface in time $t\in(t_k,t_{k+1})$ will also have the requested fixed topology $\sum$. The construction is repeated for $k=1,2,\ldots k_{\max}$ to obtain a full four-dimensional triangulation $\mathcal{T}$ with spatial boundaries $\mathcal{T}_1^{(3)}$ and $\mathcal{T}_{k_{\max}}^{(3)}$. In practice, in order to avoid the necessity of defining spatial boundary conditions, one usually identifies $\mathcal{T}_1^{(3)}$ and $\mathcal{T}_{k_{\max}+1}^{(3)}$, i.e., one fixes the spacetime topology to be $S^1\times\sum$ instead of $[0,1]\times\sum$. The distinction between space and time introduced by the foliation is also present in the (fixed) edge lengths of the four-simplices. This is quantified by the parameter α , defined by

其中 $\mathcal{D}\left[g_{\mu v}\right]$ 是测度项，它允许我们对几何 (即微分同胚不变的度量等价类 $g_{\mu v}$) 进行积分，S_{EH} 是依赖于牛顿常数 G 和宇宙学常数 Λ 的爱因斯坦-希尔伯特作用量。在四维因果动态三角剖分 (CDT) 中，连续几何由格点 (称为三角剖分) 近似，这类格点由固定边长的四维单形构造块 (称为四维单形) 构成，并满足一些额外拓扑约束。每个四维单形的内部同构于 (一部分) 平坦闵可夫斯基时空，几何信息编码在构造块的“粘合”方式中。这一思想源自欧几里得动态三角剖分 (EDT) 的早期方法，参见第 73 章“格点量子引力:EDT 与 CDT”，EDT 假设时空是欧几里得 (局部 SO(4) 对称) 而非洛伦兹 (局部 SO(3;1) 对称) 几何。EDT 中所有单形都是等边且全等的，不区分时间方向。与之相对，CDT 假设 (洛伦兹) 时空是整体双曲的，因此可以将时空按照宇宙学时间切片叶理化为空间超曲面 (称为切片)。它还要求每个切片的空间拓扑 $\sum$ 固定，并在时间演化中保持不变，因此时空拓扑为 $[0,1] \times \sum$ 。时间 t_k 处空间切片的 (三维) 几何 (k 表示格点时间坐标，$k \in \mathbb{Z}$) 由三角剖分 $\mathcal{T}_k^{(3)}$ 表示 (具有固定拓扑 $\sum$)，该三角剖分由全等的等边三维单形 (四面体) 构造而成。时间 t_k 的三角剖分 $\mathcal{T}_k^{(3)}$ 和时间 t_{k+1} 的三角剖分 $\mathcal{T}_{k+1}^{(3)}$ ，共同构成了 t_k 与 t_{k+1} 之间 slab 区域的 (四维) 三角剖分 $\mathcal{T}_{k:k+1}^{(4)}$ 的边界，该四维三角剖分可由四类四维单形构造，分别记为 $T^{(4,1)}, T^{(1,4)}, T^{(3,2)}$ 和 $T^{(2,3)}$ ，括号中的数字分别代表每个单形在时间 t_k 和时间 t_{k+1} 的顶点数；参见图 1。四维单形按如下方式粘合:slab 区域内不存在拓扑缺陷，因此任意时刻 $t \in (t_k, t_{k+1})$ 的空间超曲面也具有要求的固定拓扑 $\sum$。对 $k = 1, 2, \ldots k_{\max}$ 重复该构造，即可得到带有空间边界 $\mathcal{T}_1^{(3)}$ 和 $\mathcal{T}_{k_{\max}}^{(3)}$ 的完整四维三角剖分 $\mathcal{T}$ 。实际操作中，为了避免定义空间边界条件，通常将 $\mathcal{T}_1^{(3)}$ 与 $\mathcal{T}_{k_{\max}+1}^{(3)}$ 等同，也就是将时空拓扑固定为 $S^1 \times \sum$ 而非 $[0,1] \times \sum$。叶理化引入的时空区分也体现在四维单形固定的边长中，这由参数 α 量化，其定义为

$$a_t^2 = -\alpha a_s^2, \tag{2}$$

where a_t and a_s are the lattice spacing in the time and the spatial direction, respectively. According to Regge calculus [5], the curvature of a piecewise flat simplicial manifold constructed from four-simplices is defined through a deficit angle located at two-dimensional subsimplices (triangles) and depends on the number of four-simplices sharing a given triangle. Using Regge's prescription one can compute the Einstein-Hilbert action for a CDT triangulation $\mathcal{T}$, the so-called Regge action, see Chap. 76, "The Causality Road from Dynamical Triangulations to Quantum Gravity That Describes Our Universe" [6]:

其中 a_t 和 a_s 分别是时间方向与空间方向的晶格间距。根据里奇微积分 [5]，由四单形构造的分段平坦单纯流形的曲率通过位于二维子单形 (三角形) 处的亏缺角定义，且依赖于共享给定三角形的四单形数量。利用里奇公式可以计算 CDT 三角剖分 $\mathcal{T}$ 的爱因斯坦-希尔伯特作用量，即所谓的里奇作用量，参见第 76 章“从动力三角剖分到描述我们宇宙的量子引力的因果性道路”[6]:

$$S_R\left[k_0, k_4, \Delta; \mathcal{T}\right] = -\left(k_0 + 6\Delta\right) N_0 + k_4\left(N_4^{(4,1)} + N_4^{(3,2)}\right) + \Delta N_4^{(4,1)}. \tag{3}$$

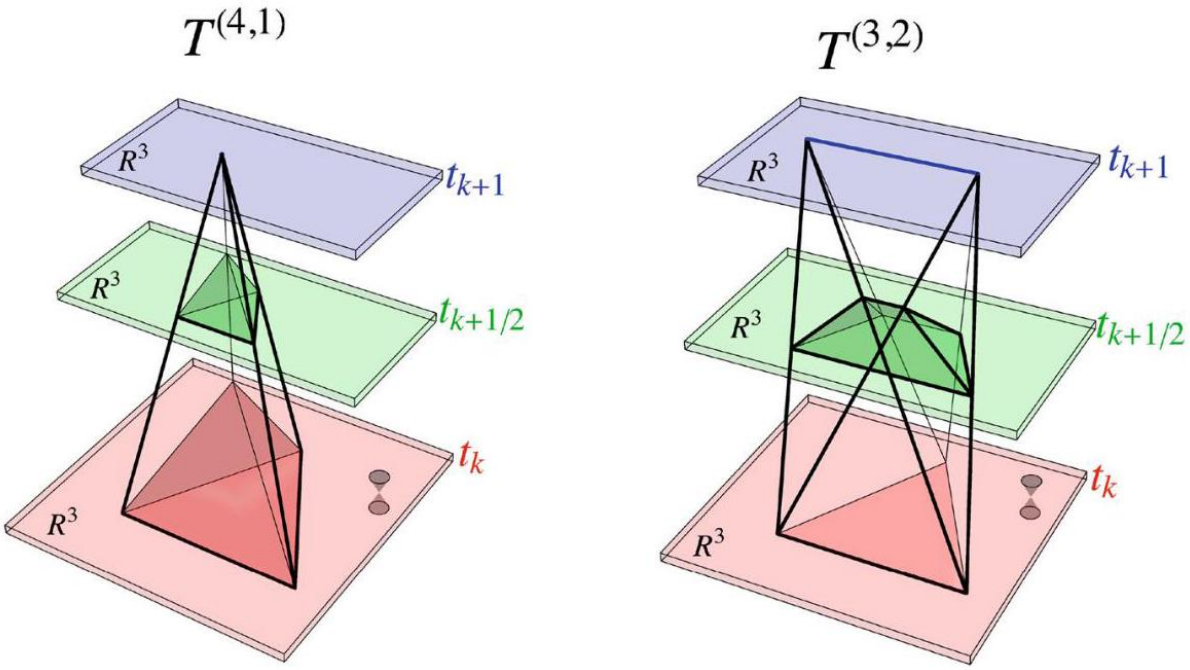

Fig. 1 The building blocks of the four-dimensional CDT triangulation: the $T^{(4,1)}$ simplex (left panel) and the $T^{(3,2)}$ simplex (right panel). The other two types, $T^{(1,4)}$ and $T^{(2,3)}$, are time-mirrored versions of them

Fig. 1 四维 CDT 三角剖分的构造块: $T^{(4,1)}$ 单形 (左图) 和 $T^{(3,2)}$ 单形 (右图)。另外两种类型 $T^{(1,4)}$ 和 $T^{(2,3)}$ 是二者的时间镜像版本

The action is a linear combination of N_0, denoting the total number of vertices, $N_4^{(4,1)}$, the total number of $T^{(4,1)}$ and $T^{(1,4)}$ four-simplices, and $N_4^{(3,2)}$, the total number of $T^{(3,2)}$ and $T^{(2,3)}$ four-simplices, in the triangulation $\mathcal{T}$. The three dimensionless bare coupling constants are k_0, related to the inverse Newton's constant; k_4, related to the cosmological constant; and Δ, related to the parameter α defined in Equation (2).

该作用量是以下项的线性组合: 表示三角剖分 $\mathcal{T}$ 中顶点总数的 N_0、表示 $T^{(4,1)}$ 型和 $T^{(1,4)}$ 型四单形总数的 $N_4^{(4,1)}$，以及表示 $T^{(3,2)}$ 型和 $T^{(2,3)}$ 型四单形总数的 $N_4^{(3,2)}$。三个无量纲裸耦合常数分别为: 与逆牛顿常数相关的 k_0、与宇宙学常数相关的 k_4，以及与式 (2) 定义的参数 α 相关的 Δ。

Using the CDT discretization, the (formal) quantum-gravitational path integral (1) can be defined by

利用 CDT 离散化，可将 (形式化的) 量子引力路径积分 (1) 定义为

$$Z_{CDT}^{(L)}\left(k_0, k_4, \Delta, \sum\right) = \sum_{\mathcal{T}\in\mathcal{T}^{(L)}} \frac{1}{\mathcal{C}_{\mathcal{T}}} e^{iS_R^{(L)}[k_0,k_4,\Delta;\mathcal{T}]}, \tag{4}$$

where the sum is over all possible CDT triangulations $\mathcal{T}$ described above, the measure term $1/\mathcal{C}_{\mathcal{T}}$ is the size of the automorphism group of $\mathcal{T}$ and S_R is the Regge action (3), and we have used the index (L) to emphasize the Lorentzian setting. It is important to stress that despite the fact that in CDT one discretizes quantum geometries using triangulated manifolds with some finite lattice spacing a, it is not assumed that the physical spacetime is discrete in any sense, and the UV cutoff $\sim 1/a$ (which regularizes the theory) is aimed to be removed in the continuum limit, if it exists. The four-dimensional CDT, defined by the lattice regularized

path integral (4), cannot be solved analytically, and in order to investigate its properties one is forced to use numerical methods, which require a change from the Lorentzian to the Euclidean signature. Due to the introduced time foliation, the metric signature change is well defined. Wick rotation can be achieved by an analytic continuation $\alpha \to -\alpha\,(\alpha > 7/12)$ in the lower half of the complex α -plane. As a result the interior of each four-simplex becomes isomorphic to a (part of) flat Euclidean space, and the Regge action is changed accordingly such that $iS_R^{(L)} = -S_R^{(E)}$ (both the Lorentzian $S_R^{(L)}$ and the Euclidean $S_R^{(E)}$ Regge actions have the same form as that of Equation (3), just the functional dependence of the CDT bare coupling constants k_0, k_4, Δ on G, Λ, α must be appropriately adjusted). The Euclidean Regge action $S_R^{(E)}$ is purely real and thus the CDT path integral (4) becomes a partition function:

其中求和遍历上述所有可能的 CDT 三角剖分 $\mathcal{T}$，测度项 $1/\mathcal{C}_{\mathcal{T}}$ 是 $\mathcal{T}$ 的自同构群大小，S_R 为里奇作用量 (3)，我们使用指标 (L) 强调这是洛伦兹框架。需要重点强调: 尽管 CDT 用带有有限格点间距 a 的三角剖分流形对量子几何做了离散化，但这并不意味着物理时空在任何意义上是离散的；用来正规化理论的紫外截断 $\sim 1/a$，若存在连续极限，则会在连续极限中被移除。由格点正规化路径积分 (4) 定义的四维 CDT 无法解析求解，要研究其性质必须使用数值方法，这要求我们将洛伦兹号差改为欧几里得号差。得益于预先引入的时间叶状结构，度规的号差变换是良定义的。我们可以通过在复 α 平面下半部分做解析延拓 $\alpha \to -\alpha\,(\alpha > 7/12)$ 完成维克转动。最终每个四单纯形的内部同构于平坦欧几里得空间 (的一部分)，里奇作用量也相应发生改变，得到 $iS_R^{(L)} = -S_R^{(E)}$ (洛伦兹 $S_R^{(L)}$ 和欧几里得 $S_R^{(E)}$ 里奇作用量都具有与方程 (3) 相同的形式，仅需对 CDT 裸耦合常数 k_0, k_4, Δ 关于 G, Λ, α 的函数依赖做适当调整)。欧几里得里奇作用量 $S_R^{(E)}$ 是纯实的，因此 CDT 路径积分 (4) 变成配分函数:

$$Z_{CDT}^{(E)}\left(k_0, k_4, \Delta, \sum\right) = \sum_{\mathcal{T}\in\mathcal{T}^{(E)}} \frac{1}{\mathcal{C}_{\mathcal{T}}} e^{-S_R^{(E)}[k_0,k_4,\Delta;\mathcal{T}]}. \tag{5}$$

Note that the (Euclidean) triangulations $\mathcal{T}$ appearing in the above sum must respect the imposed time foliation and the fixed spatial topology $\sum$ of the original (Lorentzian) triangulations; thus, a memory of the Lorentzian setting is still kept.

注意，上述求和中出现的 (欧几里得) 三角剖分 $\mathcal{T}$ 必须满足原始 (洛伦兹) 三角剖分的强制时间叶状结构和固定空间拓扑 $\sum$；因此，洛伦兹框架的特征仍被保留了下来。

The partition function (5) can be investigated using Monte Carlo (MC) methods. One performs MC simulations for a fixed topology $\sum$ and a choice of points in the CDT bare coupling constants space (k_0, k_4, Δ) . The results of such simulations show that for fixed values of k_0 and Δ , the partition function behaves in the leading order as

我们可以使用蒙特卡洛 (MC) 方法研究配分函数 (5)。我们针对固定拓扑 $\sum$，并在 CDT 裸耦合常数空间 (k_0, k_4, Δ) 中选取一组点进行 MC 模拟。模拟结果表明，对于固定的 k_0 和 Δ，配分函数的领头阶行为为

$$Z_{CDT}^{(E)}\left(k_0, k_4, \Delta, \sum\right) \propto e^{(k_4^c - k_4)N_4}, \tag{6}$$

where $N_4 = N_4^{(4,1)} + N_4^{(3,2)}$. The factor $e^{-k_4 N_4}$ comes directly from the bare cosmological constant k_4 appearing in the Regge action (3). The factor $e^{k_4^c N_4}$ comes from the number of states (triangulations with N_4

four-simplices) with the same value of the action, as the number of possible configurations grows (approximately) exponentially with N_4 , and the exponent k_4^c depends on k_0 and Δ . If $k_4 < k_4^c$, the partition function is divergent and the CDT theory becomes ill-defined. For $k_4 > k_4^c$ the size of the system remains finite. Therefore, taking the infinite volume limit ($N_4 \to \infty$) requires at the same time fine-tuning $k_4 \to k_4^c$. In the MC simulations, it is convenient to let the total lattice volume N_4 fluctuate around a fixed value $\bar{N}_4$ and perform a series of measurements for various target volumes $\bar{N}_4$ (in practice one usually fixes the $N_4^{(4,1)}$ volume). For each $\bar{N}_4$ the k_4 coupling constant is fine-tuned to the pseudo-critical value $k_4 \to k_4^c\left(\bar{N}_4\right)$. In the limit $\bar{N}_4 \to \infty$ the finite-size effects vanish and one effectively obtains $k_4 \to k_4^c \equiv k_4^c(\infty)$. By fixing $\bar{N}_4$ one in fact studies the properties of $Z_{CDT}^{(E)}\left(k_0, \Delta, \bar{N}_4, \sum\right)$, which is linked with $Z_{CDT}^{(E)}\left(k_0, k_4, \Delta, \sum\right)$ by the Laplace transform:

其中 $N_4 = N_4^{(4,1)} + N_4^{(3,2)}$ 。因子 $e^{-k_4 N_4}$ 直接来源于里奇作用量 (3) 中的裸宇宙学常数 k_4 。因子 $e^{k_4^c N_4}$ 来自于作用量取值相同的态的数量 (即含 N_4 个四单纯形的三角剖分), 因为可能构型的数量随 N_4 近似指数增长，且指数 k_4^c 依赖于 k_0 和 Δ 。若 $k_4 < k_4^c$ ，配分函数发散，CDT 理论不再良定义。对于 $k_4 > k_4^c$ ，系统尺寸保持有限。因此，取无限体积极限 ($N_4 \to \infty$) 需要同时对 $k_4 \to k_4^c$ 做精细调节。在蒙特卡洛模拟中，方便的做法是让总格点体积 N_4 在固定值 $\bar{N}_4$ 附近涨落，对不同的目标体积 $\bar{N}_4$ 进行一系列测量 (实际操作中通常固定 $N_4^{(4,1)}$ 体积)。对每个 $\bar{N}_4$ ，都将耦合常数 k_4 精细调节到伪临界值 $k_4 \to k_4^c\left(\bar{N}_4\right)$ 。在极限 $\bar{N}_4 \to \infty$ 下，有限尺寸效应消失，可有效得到 $k_4 \to k_4^c \equiv k_4^c(\infty)$ 。固定 $\bar{N}_4$ 实际上是研究 $Z_{CDT}^{(E)}\left(k_0, \Delta, \bar{N}_4, \sum\right)$ 的性质，它与 $Z_{CDT}^{(E)}\left(k_0, k_4, \Delta, \sum\right)$ 通过拉普拉斯变换关联:

$$Z_{CDT}^{(E)}\left(k_0, k_4, \Delta, \sum\right) = \int_0^\infty d\bar{N}_4 e^{-k_4 \bar{N}_4} Z_{CDT}^{(E)}\left(k_0, \Delta, \bar{N}_4, \sum\right). \tag{7}$$

As a result, for the fixed topology $\sum$ and the target lattice volume $\bar{N}_4$, the partition function effectively depends only on two bare coupling constants k_0 and Δ . As will be shown below, at least in some region of the CDT parameter space, the dependence on $\bar{N}_4$ turns out to be universal, and the $\bar{N}_4$ scaling analysis is a useful tool in discussing the semiclassical and the (perspective) continuum limits of CDT.

因此，对于固定拓扑 $\sum$ 和目标格点体积 $\bar{N}_4$ ，配分函数实际上仅依赖于两个裸耦合常数 k_0 和 Δ 。如下文所示，至少在 CDT 参数空间的某些区域，对 $\bar{N}_4$ 的依赖是普适的，$\bar{N}_4$ 标度分析是讨论 CDT 半经典极限和 (候选) 连续极限的有用工具。

The parameter space of the four-dimensional CDT spanned by k_0 and Δ has been largely investigated for the cases where the spatial topology $\sum$ was chosen to be either S^3 (the, so-called, spherical CDT) or T^3 (the toroidal CDT). Four phases with distinct geometric properties have been found [7-9]; see Fig. 2. Phase A is observed for sufficiently large values of the bare (inverse) cosmological constant k_0 . A typical configuration consists of many disjoint "baby universes" with a short time extension; see Fig. 3. In phase A the three-dimensional spatial volumes, quantified by the number of tetrahedra $N_3(k)$ forming a spatial slice with the lattice time coordinate $k \in \mathbb{Z}$, are uncorrelated. Phase B is realized for small values of the bare coupling Δ . In contrast to phase A , inside phase B the whole geometry "collapses" into a single spatial slice containing almost all spatial volume. The slice ends in the "past" and the "future" in a vertex of very high coordination number (belonging to almost all four-simplices). The spatial volume outside the collapsed slice is close to the cutoff size; see Fig. 3. It is believed that these two phases can be understood essentially from the dynamics of the three-dimensional EDT geometries of the slices of constant (lattice) time. The spatial slices in phase A are presumably realizations of branched polymers which dominate the path integral of three-dimensional Euclidean quantum gravity for large k_0 , whereas the extended part of the geometry in phase B corresponds to the Euclidean geometry in the, so-called, crumpled phase, which is characterized by the presence of very

few vertices with extremely high coordination number. The important feature of CDT, earlier unobserved in EDT, is the existence of two new phases of quantum geometry. For sufficiently small values of κ_0 and positive, but not too-large Δ , one can observe phase C_b . It shares some features with phase B , namely, it contains vertices of very large coordination number, but, at the same time, it has a time-extended geometry; see Fig. 3. The presence of high-order vertices surrounded by volume clusters means that the geometry is quite inhomogeneous. Finally, for even higher values of the bare coupling Δ , one reaches phase C_{dS} , whose generic geometry depends on the spatial topology choice; see Fig. 3. In the spherical CDT, the geometry consists of the time-extended blob, where most three-volume is placed, and the spatial volume changes quite smoothly with the time coordinate, whereas in the toroidal CDT, one observes a constant volume profile. The observed shape of the quantum universe closely resembles classical cosmological solutions of General Relativity. Therefore, the phase C_{dS} can be considered to be related to the semiclassical limit of CDT.

由 k_0 和 Δ 张成的四维 CDT 参数空间，已针对空间拓扑 $\sum$ 取 S^3 (即所谓球面 CDT) 或 T^3 (环面 CDT) 的情况开展了大量研究。研究已发现四种具有不同几何性质的相 [7-9]，参见图 2。当裸 (逆) 宇宙学常数 k_0 足够大时，会观测到 A 相。典型构型由许多时间延拓很短的不相交“婴儿宇宙”组成，参见图 3。在 A 相中，由构成格点时间坐标 $k \in \mathbb{Z}$ 空间切片的四面体数量 $N_3(k)$ 量化得到的三维空间体积是不相关的。当裸耦合常数 Δ 取值较小时，会形成 B 相。与 A 相相反，在 B 相内部，整个几何“坍缩”为单个空间切片，几乎包含了全部空间体积。该切片在“过去”和“未来”终止于一个配位数极高的顶点 (几乎属于所有四维单形)。坍缩切片外的空间体积接近截断尺寸，参见图 3。目前认为，这两个相本质上可以从恒定 (格点) 时间切片的三维 EDT 几何动力学得到解释。A 相中的空间切片大概率是分支聚合物的实现，在大 k_0 下主导三维欧几里得量子引力的路径积分；而 B 相几何的延展部分对应所谓皱缩相的欧几里得几何，该相的特征是存在极少配位数极高的顶点。CDT 一个重要的、此前在 EDT 中未被发现的特征是存在量子几何的两个新相。当 κ_0 足够小且 Δ 为正但不太大时，可以观测到 C_b 相。它与 B 相有一些共同特征，即都包含配位数极大的顶点，但同时它具有时间延展的几何，参见图 3。被体积团簇包围的高阶顶点说明几何是非均匀的。最后，当裸耦合常数 Δ 取值更大时，会进入 C_{dS} 相，该相的一般几何取决于空间拓扑的选择，参见图 3。在球面 CDT 中，几何由一个时间延展的团块构成，大部分三体积都位于该团块中，且空间体积随时间坐标变化相当平缓；而在环面 CDT 中，观测到的体积廓线是恒定的。观测得到的量子宇宙形状与广义相对论的经典宇宙学解高度相似。因此，C_{dS} 相可以认为与 CDT 的半经典极限相关。

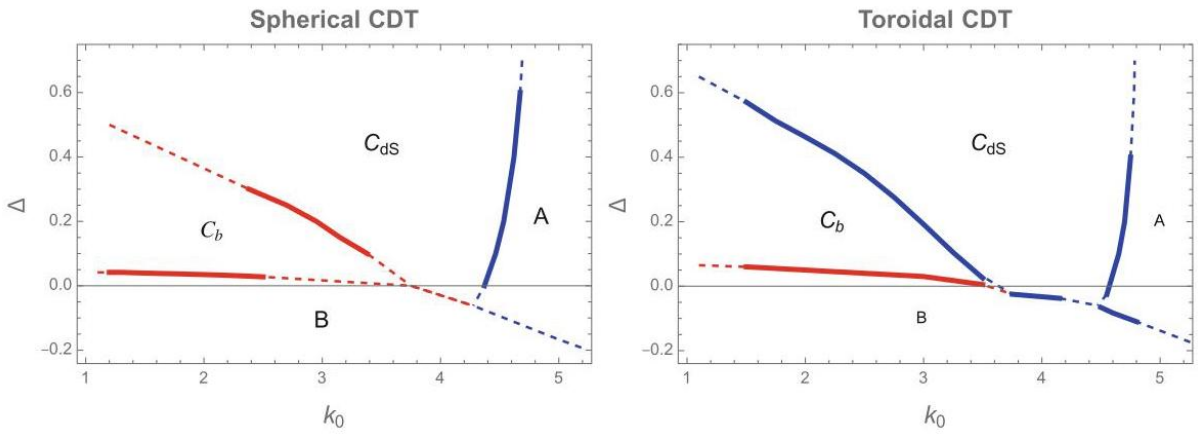

Fig. 2 The phase diagram(s) of the spherical (left panel) and the toroidal (right panel) CDT. Solid lines denote measured phase transition lines, where first-order transitions are shown in blue while higher-order

transitions in red. Dashed lines are extrapolations

图 2 球面 (左图) 与环面 (右图)CDT 的相图。实线为测得的相变线，一阶相变用蓝色表示，高阶相变用红色表示，虚线为外推结果

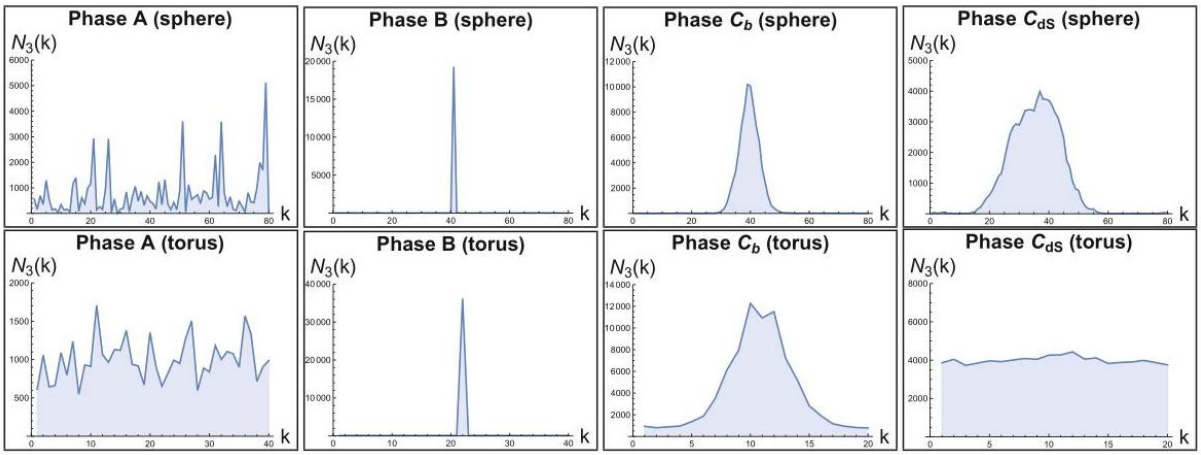

Fig. 3 Spatial volume profiles $N_3\,(k)$ of generic CDT configurations in different phases. Top, spherical CDT, A, B, C_b, C_{dS} ; bottom, toroidal CDT, A, B, C_b, C_{dS} , respectively

图 3 不同相中一般 CDT 构型的空间体积廓线 $N_3\,(k)$ 。上方分别为球面 CDT，A, B, C_b, C_{dS} ；下方分别为环面 CDT，A, B, C_b, C_{dS}

The Semiclassical Limit

半经典极限

As already mentioned in the introduction, in the four-dimensional CDT, one obtains new phases of quantum geometry, earlier unobserved in EDT. The especially interesting one is the phase C_{dS} , also called the de Sitter or the semiclassical phase. The hallmark of this phase is the presence of a stable extended four-dimensional geometry, where on large scales, compared to the triangulations size, a homogeneous and isotropic semiclassical spacetime with superimposed quantum fluctuations emerges dynamically. As will be discussed below, in phase C_{dS} not only does the effective macroscopic dimension of spacetime emerge with the correct classical value, but, equally remarkably, the global shape of the universe has been shown to be related to a simple minisuperspace description, similar to that used in standard quantum cosmology.

正如引言中已经提到的，在四维因果动态三角剖分 (CDT) 中，我们得到了量子几何的新相，这些相此前在欧几里得动态三角剖分 (EDT) 中从未被观测到。其中最值得关注的是相 C_{dS} ，它也被称为德西特相或半经典相。该相的标志性特征是存在稳定的延展四维几何，在远大于三角剖分基本单元尺寸的大尺度上，会动态演生出一个叠加了量子涨落的均匀各向同性半经典时空。如下文将讨论的，在相 C_{dS} 中，不仅时空的有效宏观维度演生出了正确的经典值，同样值得注意的是，宇宙的整体形状已被证明可以用简单的超空间 (minisuperspace) 模型描述，这与标准量子宇宙学中使用的描述方式类似。

Evidence for the Effective Spacetime Dimension Four

有效时空维度为四的证据

It is important to stress that, in the path-integral formulation, the notion of spacetime dimension is an emergent concept. This is related to the fact that geometries entering the gravitational path-integral are not that of smooth four-dimensional manifolds and therefore the effective dimension can, and in general does, differ from the topological dimension. In the lattice regularized models, such as CDT, it exemplified by the fact that even though the four-simplices forming triangulations are four-dimensional objects, due to the nontrivial connectivity structure, the triangulations cannot be embedded in the four-dimensional space. One should therefore define some notion of an effective dimension, which can be different (both larger or smaller) from the topological dimension.

需要重点强调的是，在路径积分表述中，时空维度的概念是演生出来的。这一点源于: 进入引力路径积分的几何并非光滑四维流形的几何，因此有效维度会 (且一般来说确实) 不同于拓扑维度。在因果动态三角剖分 (CDT) 这类格点正规化模型中，即便构成三角剖分的四单形是四维对象，但由于非平凡连通结构，三角剖分无法嵌入四维空间，这恰好体现了上述性质。因此我们需要定义某种有效维度的概念，其取值可以不同于拓扑维度，可大可小。

The Hausdorff Dimension

豪斯多夫维数

Due to the imposed time foliation, one of the simplest observables (here, by an observable we mean a quantity measured in the numerical simulations, not a diffeomorphism-invariant observable) measured in the Monte Carlo simulations of CDT is the so-called spatial volume profile $N_3(k)$. Each spatial slice with the lattice time coordinate $k \in \mathbb{Z}$ and the corresponding (continuous) time coordinate $t_k = ka$, where a is the lattice spacing (in the following we will assume for simplicity that the effective lattice spacing a is the same in time and spatial directions, but one can generalize to different lattice spacing a_t and a_s) is a three-dimensional triangulation constructed from identical equilateral tetrahedra. Accordingly, the continuum three-volume $V_3(t_k)$ is proportional to the number $N_3(k)$ of spatial tetrahedra in lattice time k:

由于预设了时间叶化，在 CDT 的蒙特卡洛模拟中，最简单的可测量观测量之一就是所谓的空间体积剖面 $N_3(k)$ (此处观测量指数值模拟中测量的量，而非微分同胚不变观测量)。每个带有格点时间坐标 $k \in \mathbb{Z}$ 的空间切片对应连续时间坐标 $t_k = ka$，其中 a 是格点间距 (下文为简化假设有效格点间距 a 在时间方向和空间方向相同，但也可以推广到时间和空间采用不同格点间距 a_t 和 a_s 的情况)，它是由全等等边四面体构造而成的三维三角剖分。因此，连续三维体积 $V_3(t_k)$ 正比于格点时间 k 下空间四面体的数量 $N_3(k)$:

$$V_3(t_k) \propto a^3 N_3(k). \tag{8}$$

In the spherical CDT, the generic spatial volume profile observed in phase C_{dS} consists of an extended part, the so-called blob, whose ends are connected by a thin stalk where the spatial volume is of the minimal allowed cutoff size; see Fig. 3. During a MC simulation, due to the CDT time-translation symmetry, the blob

performs a slow random walk around the (periodic) time-axis. Therefore, if one performed a long-enough MC simulation (in practice such a simulation would take several years of computer time), the spatial volume profile averaged over configurations would be a constant, in accordance with the time-translation symmetry. At the same time, it is obvious that the presence of the blob means that individual CDT configurations in phase C_{dS} break the time-translation symmetry. One can take this into account when computing the average over configurations by appropriately shifting the center of volume of each individual MC generated configuration to a common time coordinate, say $k = 0$. As a result one gets a nontrivial one-point correlator, i.e., the average volume profile $\langle N_3(k)\rangle_{\bar{N}_4}$; see Fig. 4, where the index $\bar{N}_4$ denotes the constant target lattice volume fixed in a MC simulation.

在球面 CDT 中，相 C_{dS} 观测到的一般空间体积剖面包含一个延展部分，即所谓的 blob，其两端由细柄连接，细柄处的空间体积为允许的最小截断尺寸；参见图 3。在 MC 模拟过程中，由于 CDT 的时间平移对称性，blob 会沿 (周期性) 时间轴做慢随机游走。因此，如果进行足够长的 MC 模拟 (实际上这类模拟需要耗费数年计算机时间)，根据时间平移对称性，对构型平均得到的空间体积剖面会是一个常数。同时很明显，blob 的存在说明相 C_{dS} 中的单个 CDT 构型破缺了时间平移对称性。在对构型求平均时，可以通过将每个 MC 生成构型的体积中心适当平移到公共时间坐标 (例如 $k = 0$) 来处理这个问题。最终我们会得到一个非平凡的一点关联函数，即平均体积剖面 $\langle N_3(k)\rangle_{\bar{N}_4}$；参见图 4，其中下标 $\bar{N}_4$ 表示 MC 模拟中固定的常数目标格点体积。

If the effective spacetime dimension is d_H, then, using textbook scaling arguments, one should expect that the spatially extended parts of the spacetimes measured for various effective four-volumes $\widetilde{N}_4 = \left\langle \sum_{k\in \text{blob}} N_3(k) \right\rangle_{\bar{N}_4}$, where the sum is over the extended part of the universe, can be mapped onto each other by rescaling the proper time and the spatial volumes according to

如果有效时空维数为 d_H，那么利用教科书标度论证，我们可以预期，对不同有效四维体积 $\widetilde{N}_4 = \left\langle \sum_{k\in \text{blob}} N_3(k) \right\rangle_{\bar{N}_4}$ (求和范围为宇宙的延展部分) 测量得到的时空延展部分，可以通过按如下方式重新标度固有时和空间体积实现相互映射:

$$k \to \tilde{k} = \frac{k}{\widetilde{N}_4^{1/d_H}}, \; N_3(k) \to \widetilde{N}_3(\tilde{k}) = \frac{N_3(k)}{\widetilde{N}_4^{1-1/d_H}}. \tag{9}$$

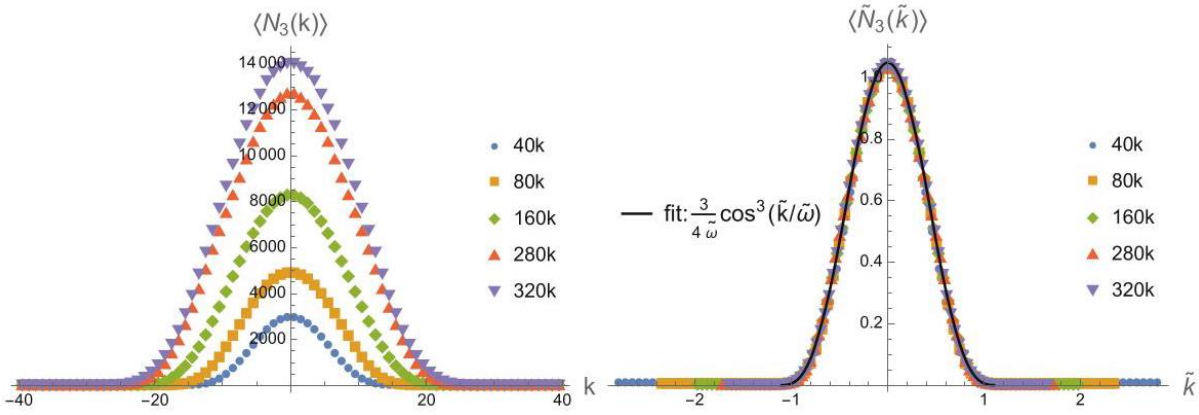

Fig. 4 Left panel: average volume profiles $\langle N_3(k)\rangle_{\tilde{N}_4}$ measured inside phase C_{dS} of the spherical CDT ($k_0 = 2.2, \Delta = 0.6$). Different colors denote different target lattice volumes $\tilde{N}_4^{(4,1)}$. Right panel: the volume profiles rescaled according to Equation (9) with Hausdorff dimension $d_H = 4$ and the fit of Equation (17)

图 4 左图: 球面 CDT ($k_0 = 2.2, \Delta = 0.6$) 相 C_{dS} 内部测量得到的平均体积剖面 $\langle N_3(k)\rangle_{\tilde{N}_4}$。不同颜色对应不同的目标格点体积 $\tilde{N}_4^{(4,1)}$。右图: 根据式 (9)，采用豪斯多夫维数 $d_H = 4$ 重标度后的体积剖面，以及式 (17) 的拟合

As a result

结果为

$$\langle N_3(k)\rangle_{\tilde{N}_4} = \widetilde{N}_4^{1-1/d_H} \left\langle \widetilde{N}_3\left(\tilde{k}\right)\right\rangle = \widetilde{N}_4^{1-1/d_H} H\left(\frac{k}{\widetilde{N}_4^{1/d_H}}\right) \tag{10}$$

can be expressed in terms of a universal function H. The Hausdorff dimension d_H can be then measured by performing a series of MC simulations for systems of various size $\widetilde{N}_4$ and fitting Equation (10) by applying the best overlap method. In Fig. 4 we show that indeed, to a good approximation, our MC generated data measured in phase C_{dS} of the spherical CDT fit the above scaling relation with a classical value of Hausdorff dimension $d_H = 4$.

可以用普适函数 H 表示。之后我们可以通过对不同尺寸 $\widetilde{N}_4$ 的系统进行一系列 MC 模拟，利用最佳重叠方法拟合式 (10)，测量得到豪斯多夫维数 d_H。图 4 向我们展示，在球面 CDT 的相 C_{dS} 中测得的 MC 生成数据，确实能在很好的近似下符合上述标度关系，得到的豪斯多夫维数为经典值 $d_H = 4$。

The Spectral Dimension

谱维数

Another way of obtaining an effective dimension of spacetime appearing in a non-perturbative quantum gravity is to study a diffusion process of a fictitious point particle, related to the, so-called, spectral dimension; for more details see also - Chap. 78, "Spectral Observables and Gauge Field Couplings in Causal Dynamical Triangulations". The diffusion process discussed here is related to the scalar spectral dimension; one can also consider a more general diffusion of k - forms; see [10]. Let us consider a smooth d -dimensional Riemannian manifold $\mathcal{M}$ equipped with a metric g_{ij}. The diffusion process is governed by the equation:

在非微扰量子引力中，获取时空有效维度的另一种方法是研究虚拟点粒子的扩散过程，这和所谓的谱维数相关；更多细节参见第 78 章“因果动态三角剖分中的谱可观测量与规范场耦合”。此处讨论的扩散过程对应标量谱维数，也可以考虑更一般的 k -形式扩散；参见文献 [10]。考虑一个配备了度量 g_{ij} 的光滑 d 维黎曼流形 $\mathcal{M}$，扩散过程由以下方程控制:

$$\frac{\partial}{\partial\sigma} K(x, x_0; \sigma) = \Delta_g K(x, x_0; \sigma), \tag{11}$$

where σ is the fictitious diffusion time and Δ_g is the Laplace-Beltrami operator of the metric g_{ij} , with the initial condition peaked at $x_0 \in \mathcal{M}$, i.e., given by a delta function $K(x, x_0; \sigma = 0) = \delta^d(x - x_0)$. The heat kernel $K(x, x_0; \sigma)$ represents the probability density of finding a particle at position $x \in \mathcal{M}$ after a diffusion time σ . The average return probability to the origin after time σ

其中 σ 是虚拟扩散时间，Δ_g 是度量 g_{ij} 的拉普拉斯-贝尔特拉米算子，初始条件集中在 $x_0 \in \mathcal{M}$ ，即由 δ 函数 $K(x, x_0; \sigma = 0) = \delta^d(x - x_0)$ 给出。热核 $K(x, x_0; \sigma)$ 代表扩散时间 σ 后，粒子出现在位置 $x \in \mathcal{M}$ 的概率密度。时间 σ 后粒子回到原点的平均返回概率

$$P_r(\sigma) = \frac{1}{V} \int dx \sqrt{g} K(x, x; \sigma), \tag{12}$$

where $V = \int dx \sqrt{g}$ is the volume of $\mathcal{M}$, has the following asymptotic expansion for small σ [11]

其中 $V = \int dx \sqrt{g}$ 是 $\mathcal{M}$ 的体积，对于小 σ 有如下渐近展开 [11]

$$P_r(\tau) \sim \sigma^{-\frac{d}{2}} \sum_{i=0}^{\infty} A_i \sigma^i \tag{13}$$

where A_i are in general complicated integrated functions of the metric g_{ij} . Note that the return probability (13) depends on the dimension d of the manifold. One can therefore compute the dimension from the return probability:

其中 A_i 一般是度量 g_{ij} 的复杂积分函数。注意到返回概率 (13) 依赖于流形的维度 d ，因此我们可以通过返回概率计算维度:

$$d = -2 \lim_{\sigma \to 0} \frac{d \log P_r(\sigma)}{d \log \sigma}. \tag{14}$$

The expression (14) can be generalized by dropping the limit $\sigma \to 0$ which defines the (running) spectral dimension

表达式 (14) 可以推广，去掉定义 (跑动) 谱维数的极限 $\sigma \to 0$ 后得到

$$d_s(\sigma) = -2 \frac{d \log P_r(\sigma)}{d \log \sigma}. \tag{15}$$

In CDT one deals with discretized geometries, and therefore one also has to discretize the diffusion Equation (11). One typically considers the discrete diffusion on the dual lattice, i.e., the graph whose nodes are four-simplices and whose links encode neighborhood relations between the four-simplices. The diffusion process is originated at a randomly chosen four-simplex of a given triangulation $\mathcal{T}$, and the return probability is computed for a range of discrete diffusion steps $\sigma = 0, \ldots, \sigma_{\max}$. Then, the (manifold) average return probability $P_r(\sigma)$ is estimated over a number of starting points $x_0 \in \mathcal{T}$. As we are interested in the expectation value of the above observable, the average $\langle P_r(\sigma) \rangle_{\bar{N}_4}$ over the ensemble of triangulations is subsequently computed. Finally, the (expectation value of) spectral dimensions is calculated using Equation (15). The results obtained in phase C_{dS} of the spherical CDT are presented in Fig. 5, where we also included a phenomenological fit:

在因果动态三角剖分 (CDT) 中我们处理离散化几何，因此也需要对扩散方程 (11) 进行离散化。通常我们考虑对偶格点上的离散扩散，即该图的节点为四单纯形，连线编码四单纯形之间的邻接关系。扩散过程起始于给定三角剖分 $\mathcal{T}$ 中随机选取的一个四单纯形，我们对一系列离散扩散步长 $\sigma = 0, \ldots, \sigma_{\max}$ 计算返回概率。随后，对多个起始点 $x_0 \in \mathcal{T}$ 估计 (流形的) 平均返回概率 $P_r(\sigma)$。由于我们关心上述可观测量的期望值，接下来会对三角剖分整体系综计算平均 $\langle P_r(\sigma) \rangle_{\tilde{N}_4}$。最后利用 (15) 式计算谱维数的期望值。球形 CDT 相 C_{dS} 中得到的结果如图 5 所示，我们还加入了唯象拟合:

$$d_s(\sigma) = d + \frac{c}{\sigma + b}, \tag{16}$$

where the constants $d = 4.17 \pm 0.07, c = 146 \pm 28, b = 66 \pm 17$ were established from data in range $\sigma \in [30, 450]$. As can be seen the spectral dimension changes with the diffusion time σ , or otherwise with the geodesic distance, as the diffusion process probes larger and larger scales of the quantum geometry. One should note that for very large diffusion times σ , due to finite size effects, i.e., when the diffusion process probes the whole simplicial manifold (which is by construction closed in the chosen spacetime topology $S^1 \times S^3$), the zero modes of the Laplace-Beltrami operator dominate and the spectral dimension $d_s(\sigma)$ goes to zero. This part of the evolution is not shown on the plot and was not taken into account when fitting Equation (16). The remarkable feature of the curve $d_s(\sigma)$ is its slow approach to the asymptotic value of $d_s(\sigma = \infty) = 4.17 \pm 0.07$ consistent with the four-dimensional universe. This type of behavior is nontrivial and is not the case in other CDT phases. The other nontrivial phenomenon that has emerged dynamically is a scale dependence of the spectral dimension which goes to $d_s(\sigma = 0) \approx 2$ for short distances. It is related to nonclassical features of generic geometries appearing in the CDT path integral. This nontrivial "dimensional reduction" has been first found in [12] and confirmed in many other approaches to quantum gravity [13-16].

其中常数 $d = 4.17 \pm 0.07, c = 146 \pm 28, b = 66 \pm 17$ 由范围 $\sigma \in [30, 450]$ 内的数据确定。可见谱维数随扩散时间 σ 变化，或者说随测地线距离变化，因为扩散过程会探测量子几何越来越大的尺度。需要注意的是，当扩散时间 σ 极大时，由于有限尺寸效应，即当扩散过程探测整个单纯形流形 (所选时空拓扑 $S^1 \times S^3$ 中它本就是闭合的) 时，拉普拉斯-贝尔特拉米算子的零模占主导，谱维数 $d_s(\sigma)$ 会趋近于零。演化的这一部分未在图中展示，拟合方程 (16) 时也未纳入考量。曲线 $d_s(\sigma)$ 的显著特点是缓慢趋近与四维宇宙相符的渐近值 $d_s(\sigma = \infty) = 4.17 \pm 0.07$。这种行为是非平凡的，在 CDT 的其他相中并不存在。另一个动态涌现的非平凡现象是谱维数依赖于尺度，在短距离处谱维数趋近于 $d_s(\sigma = 0) \approx 2$。这与 CDT 路径积分中普遍几何的非经典性质相关。这种非平凡的“维度降低”最早在文献 [12] 中被发现，之后在量子引力的许多其他研究方法中得到了证实 [13-16]。

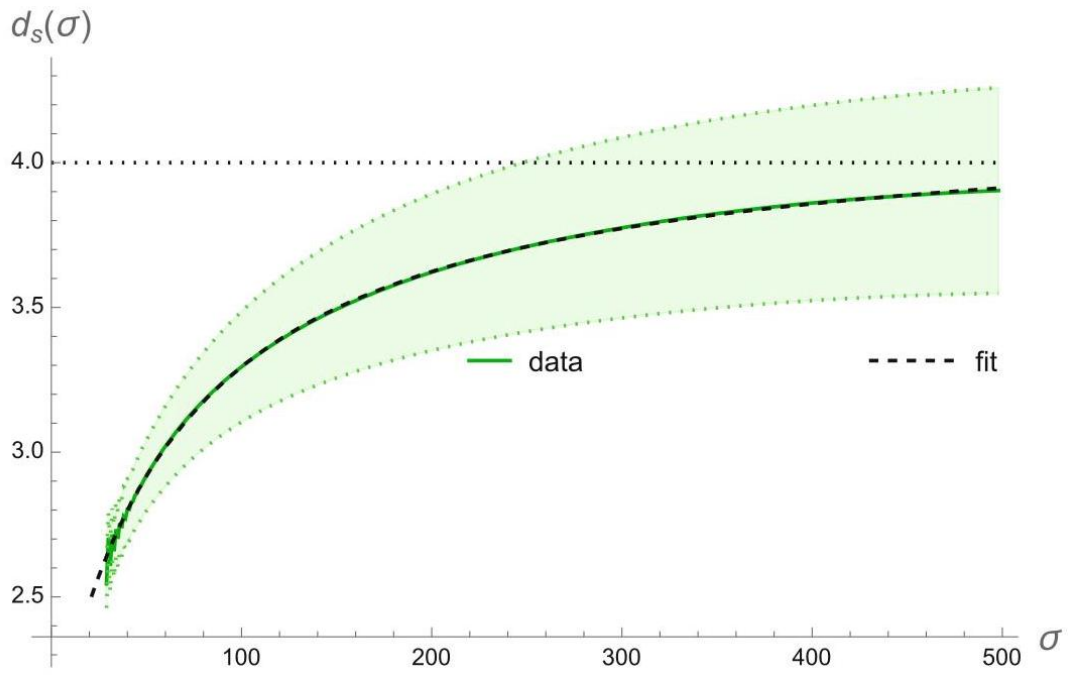

Fig. 5 The spectral dimension $d_s(\sigma)$ measured inside phase C_{dS} of the spherical CDT ($k_0 = 2.2, \Delta = 0.6$) and the fit of a phenomenological function (16). Shaded region indicates measurement errors

图 5 在球形 CDT ($k_0 = 2.2, \Delta = 0.6$) 的 C_{dS} 相内部测量得到的谱维数 $d_s(\sigma)$，以及唯象函数 (16) 的拟合结果。阴影区域表示测量误差

Summarizing this part, both the Hausdorff and the spectral dimensions measured in the C_{dS} phase point to the dynamically emerging macroscopic four-dimensional "average geometry". In the following we will provide evidence that indeed the geometry is consistent with a semiclassical four-dimensional universe.

综上，在 C_{dS} 相中测量得到的豪斯多夫维数与谱维数都表明，宏观四维“平均几何”是动态涌现的。下文我们将给出证据，证明该几何确实与半经典四维宇宙一致。

Evidence for an Effective Minisuperspace Action

有效超空间简化作用量的证据

The Semiclassical de Sitter Universe

半经典德西特宇宙

In the lattice formulation, one is interested in taking the thermodynamical (infinite volume) limit $\tilde{N}_4 \to \infty$, where one may hope to recover continuum physics. As already mentioned, inside phase C_{dS} of the spherical CDT, the one-point correlator, i.e., the average spatial volume, shows a nontrivial scaling behavior consistent with Hausdorff dimension four. One can therefore define a universal function $H(\tilde{k})$, describing the

(rescaled) volume profile; see Equation (10), which is independent of the lattice volume and thus it is also valid in the thermodynamical limit. A very nontrivial fact is that it is very well fitted by (cf. Fig. 4):

在格点 formulation 中，我们关注热力学 (无限体积) 极限 $\tilde{N}_4 \to \infty$，在此极限下我们有望得到连续统物理。如前所述，在球形 CDT 的 C_{dS} 相内部，单点关联函数 (即平均空间体积) 呈现出非平凡标度行为，与豪斯多夫维数为四的结论一致。因此我们可以定义一个描述 (重整化后) 体积分布的普适函数 $H\left(\tilde{k}\right)$，参见式 (10)，该函数与格点体积无关，因此在热力学极限下依然成立。一个非常不平凡的结论是，它可以被下式很好地拟合 (参见图 4):

$$H\left(\tilde{k}\right) = \frac{3}{4\widetilde{\omega}}\cos^3\left(\frac{\tilde{k}}{\widetilde{\omega}}\right), \tag{17}$$

resulting in the universal scaling

由此得到普适标度关系

$$\langle N_3\left(k\right)\rangle_{\tilde{N}_4} = \frac{3\widetilde{N}_4}{4}\frac{1}{\widetilde{\omega}\widetilde{N}_4^{1/4}}\cos^3\left(\frac{k}{\widetilde{\omega}\widetilde{N}_4^{1/4}}\right). \tag{18}$$

The above is of course valid only inside the extended part of the universe (the blob), i.e., for $-\frac{\pi}{2}\widetilde{\omega}\widetilde{N}_4^{1/4} \leq k \leq \frac{\pi}{2}\widetilde{\omega}\widetilde{N}_4^{1/4}$. The constant $\widetilde{\omega}$ appearing in Equation (18) is a function on the CDT bare couplings k_0 and Δ. Restoring continuum quantities one can write:

上述结论当然仅在宇宙的延伸部分 (团块区域) 成立，即对应 $-\frac{\pi}{2}\widetilde{\omega}\widetilde{N}_4^{1/4} \leq k \leq \frac{\pi}{2}\widetilde{\omega}\widetilde{N}_4^{1/4}$。式 (18) 中的常数 $\widetilde{\omega}$ 是 CDT 裸耦合 k_0 和 Δ 的函数。还原为连续统物理量后我们可以写出:

$$\langle V_3\left(t\right)\rangle = \frac{3V_4}{4}\frac{1}{\omega V_4^{1/4}}\cos^3\left(\frac{t}{\omega V_4^{1/4}}\right) =$$

$$= 2\pi^2\mathcal{R}^3\cos^3\left(\frac{t}{\mathcal{R}}\right), \tag{19}$$

which is the volume profile of a regular four-sphere with physical volume V_4 and radius $\mathcal{R} = \omega V_4^{1/4}$, and where t is the (Euclidean) proper-time. It corresponds to the Wick rotated (Euclidean) de Sitter universe, i.e., a vacuum solution of Einstein's field equations with positive cosmological constant $\Lambda = 3/\mathcal{R}^2$. Such a solution is obtained for a maximally symmetric (spatially homogeneous and isotropic) metric with the infinitesimal line element squared:

这是物理体积为 V_4、半径为 $\mathcal{R} = \omega V_4^{1/4}$ 的正则四维球面的体积分布，其中 t 是 (欧氏) 固有时间。它对应威克转动后的 (欧氏) 德西特宇宙，即正宇宙学常数 $\Lambda = 3/\mathcal{R}^2$ 下爱因斯坦场方程的真空解。该解对应最大对称 (空间均匀且各向同性) 度规，其无穷小线元平方为:

$$ds^2 = dt^2 + a^2\left(t\right)d\Omega_3^2, \tag{20}$$

where $a\left(t\right)$ is the scale factor and $d\Omega_3^2$ denotes the line element squared on the unit three-sphere, such that the spatial volume at proper-time t is $V_3\left(t\right) = 2\pi^2 a^3\left(t\right)$.

其中 $a(t)$ 是标度因子，$d\Omega_3^2$ 是单位三维球面上的线元平方，因此固有时间 t 处的空间体积为 $V_3(t) = 2\pi^2 a^3(t)$ 。

The Effective Action from Volume Fluctuations

源自体积涨落的有效作用量

So far we have looked only at the one-point function, i.e., the expected value of the spatial volume profile:

到目前为止，我们仅研究了单点函数，即空间体积轮廓的期望值:

$$\langle N_3(k)\rangle_{\tilde{N}_4} = \widetilde{N}_4^{3/4} H\left(\frac{k}{\widetilde{\omega}\widetilde{N}_4^{1/4}}\right). \tag{21}$$

One can as well measure the two-point (connected) correlator:

我们也可以测量两点 (连通) 关联函数:

$$\langle \delta N_3(k)\, \delta N_3(k')\rangle_{\tilde{N}_4}\,, \tag{22}$$

where

其中

$$\delta N_3(k) = N_3(k) - \langle N_3(k)\rangle_{\tilde{N}_4} \tag{23}$$

denote fluctuations around the dynamically emerging semiclassical average.

表示动力学产生的半经典平均值附近的涨落。

Let us first comment that the correlator (22) again shows the following universal scaling:

首先我们说明，关联函数 (22) 再次呈现出如下普适标度:

$$\langle \delta N_3(k)\, \delta N_3(k')\rangle_{\tilde{N}_4} = \widetilde{N}_4 F\left(\frac{k}{\widetilde{\omega}\widetilde{N}_4^{1/4}}, \frac{k'}{\widetilde{\omega}\widetilde{N}_4^{1/4}}\right) \tag{24}$$

with the same $\widetilde{\omega}$, as in Equation (21). The details of the function F are not important for the following discussion. Comparing Equations (21) and (24) implies that the (relative amplitudes of) quantum fluctuations scale as

其中的 $\widetilde{\omega}$ 与方程 (21) 中的相同。函数 F 的具体形式对下文讨论并不重要。对比方程 (21) 与 (24) 可知，量子涨落 (的相对振幅) 标度为

$$\frac{\sqrt{\langle \delta V_3^2(t_k)\rangle}}{\langle V_3(t_k)\rangle} = \frac{\sqrt{\langle \delta N_3^2(k)\rangle_{\bar{N}_4}}}{\langle N_3(k)\rangle_{\bar{N}_4}} \propto \frac{1}{\bar{N}_4^{1/4}}, \tag{25}$$

i.e., they vanish in the thermodynamical limit $\bar{N}_4 \to \infty$. As a result one obtains a fully classical spatial volume trajectory consistent with the de Sitter solution (19). Nevertheless, as will be shown below, analysis of quantum fluctuations described by the two-point correlator (24) is a useful tool to determine the effective action of CDT.

即它们在热力学极限 $\bar{N}_4 \to \infty$ 下消失。由此我们得到了完全经典的空间体积轨迹，与德西特解 (19) 一致。但下文将说明，分析由两点关联函数 (24) 描述的量子涨落是确定 CDT 有效作用量的有效工具。

Let us consider a continuous model of quantum fluctuations around a well-defined semiclassical trajectory $\bar{n}(t) \equiv \langle n(t)\rangle$. In a semiclassical approximation, the quantum fluctuations $\delta n(t)$ around this trajectory are described by a Hermitian operator $P(t,t')$ obtained by a quadratic expansion of the effective action:

我们考虑明确定义的半经典轨迹 $\bar{n}(t) \equiv \langle n(t)\rangle$ 附近量子涨落的连续模型。在半经典近似下，该轨迹附近的量子涨落 $\delta n(t)$ 由有效作用量二次展开得到的厄米算符 $P(t,t')$ 描述:

$$S_{\text{eff}}[\bar{n}(t) + \delta n(t)] = S_{\text{eff}}[\bar{n}(t)] + \frac{1}{2}\int dt dt' \delta n(t) P(t,t') \delta n(t'), \tag{26}$$

where we neglect all terms of order $O\left(\delta n^3\right)$ in fluctuations. In a discretized model

其中我们忽略了涨落中所有 $O\left(\delta n^3\right)$ 阶项。在离散模型中

$$S_{\text{ eff}}\left[\bar{n}(t_k) + \delta n(t_k)\right] = S_{\text{ eff}}\left[\bar{n}(t_k)\right] + \frac{1}{2}\sum_{kk'} \delta n(t_k) P_{kk'} \delta n(t_{k'}) \tag{27}$$

P becomes a matrix parametrized by a (discrete) time variable k :

P 成为由 (离散) 时间变量 k 参数化的矩阵:

$$P_{kk'} = \left.\frac{\partial^2 S_{\text{ eff}}}{\partial n(t_k)\,\partial n(t_{k'})}\right|_{n(t)=\bar{n}(t)}. \tag{28}$$

In such an expansion quantum fluctuations are Gaussian and the (discrete) two-point correlator, i.e., the covariance matrix, is given by the inverse of the propagator:

在该展开下量子涨落是高斯型的，(离散) 两点关联函数即协方差矩阵由传播子的逆给出:

$$C_{kk'} \equiv \langle \delta n(t_k)\, \delta n(t_{k'})\rangle = \left(P^{-1}\right)_{kk'}. \tag{29}$$

The problem can simply be inverted. In numerical simulations one can measure the covariance matrix C. The inverse of the C matrix defines the (propagator) P matrix and thus the effective action $S_{\text{ eff}}$, or at least its derivatives measured at the semiclassical solution (see Equation (28)).

该问题可以简单反推: 在数值模拟中我们可以测量协方差矩阵 C 。该 C 矩阵的逆定义了 (传播子) P 矩阵，进而得到有效作用量 S_{eff} ，或者至少得到半经典解处的导数 (见方程 (28))。

In order to apply the above method in the case of CDT, one should first check whether the quantum fluctuations are sufficiently well described by a quadratic effective action implying Gaussian fluctuations. This is indeed the case for the observed spatial volume fluctuations measured in the extended part of the CDT universe (the blob) in phase C_{dS} of the spherical CDT. Therefore, the method seems applicable in the physically interesting limit of large lattice volumes. The empirical matrix $\widehat{P}$, obtained by inverting the measured spatial volume-volume correlator $\widehat{C}$, has a simple tridiagonal structure, suggesting that there are only nearest neighbor interactions between adjacent spatial slices. Consequently, the effective action can be expressed in the following form:

为将上述方法应用于 CDT，我们首先需要验证量子涨落是否可以被蕴含高斯涨落的二次有效作用量良好描述。对于球对称 CDT C_{dS} 相，在 CDT 宇宙的延展区域 (团块) 中测量得到的空间体积涨落确实满足该条件。因此该方法适用于物理上有意义的大格点体积极限。对测量得到的空间体积-体积关联矩阵 $\widehat{C}$ 求逆得到经验矩阵 $\widehat{P}$ ，它具有简单的三对角结构，说明相邻空间切片之间仅存在最近邻相互作用。因此有效作用量可以写为如下形式:

$$S_{\text{eff}} = S_{\text{kin}} + S_{\text{pot}} = \sum_k K\left(N_3\left(k\right), N_3\left(k+1\right)\right) + \sum_k V\left(N_3\left(k\right)\right), \tag{30}$$

where the functions K and V , representing respectively the kinetic and the potential terms, have to be determined from empirical data. In order to do so, let us make an Ansatz about a possible form of the effective action. As already mentioned, the semiclassical spatial volume profile is consistent with the de Sitter spacetime with spherical spatial topology, obtained for the metric (20). Inserting the metric to the (Euclidean) Einstein-Hilbert action

其中分别代表动能项和势能项的函数 K 和 V 需要由经验数据确定。为此，我们先对有效作用量的可能形式做一个假设。如前所述，半经典空间体积轮廓与具有球形空间拓扑的德西特时空一致，该时空由度规 (20) 得到。将该度规代入 (欧几里得) 爱因斯坦-希尔伯特作用量

$$S_{HE}^{(E)} = -\frac{1}{16\pi G}\int dt \int d\Omega_3 \sqrt{g}\left(R - 2\Lambda\right) \tag{31}$$

one obtains the following minisuperspace action:

我们得到如下微型超空间作用量:

$$S_{MS}^{(S^3)} = -\frac{3\pi}{4G}\int dt \left(a\dot{a}^2 + a - \frac{\Lambda}{3}a^3\right). \tag{32}$$

The Euler-Lagrange equation of motion for the scale factor $a\left(t\right)$ derived from the action (32) is solved by

由作用量 (32) 导出的标度因子 $a\left(t\right)$ 的欧拉-拉格朗日运动方程的解为

$$\bar{a}\left(t\right) = \mathcal{R}\cos\left(\frac{t}{\mathcal{R}}\right), \tag{33}$$

where we have chosen the proper time to be in range $-\frac{\pi}{2}\mathcal{R} \leq t \leq \frac{\pi}{2}\mathcal{R}$, such that the maximum is located at $t = 0$. Reparametrizing $a(t)$ in terms of the spatial volume

其中我们已取固有时处于区间 $-\frac{\pi}{2}\mathcal{R} \leq t \leq \frac{\pi}{2}\mathcal{R}$ 内，使得最大值位于 $t = 0$。用空间体积重新参数化 $a(t)$

$$V_3(t) = \int d\Omega_3 \sqrt{g|_{S^3}} = 2\pi^2 a^3(t) \tag{34}$$

one indeed obtains a solution consistent with the average CDT solution (19):

确实可以得到与 CDT 平均解 (19) 自洽的解:

$$\bar{V}_3(t) = 2\pi^2 \mathcal{R}^3 \cos^3\left(\frac{t}{\mathcal{R}}\right) =$$

$$= \frac{3V_4}{4} \frac{1}{\omega V_4^{1/4}} \cos^3\left(\frac{t}{\omega V_4^{1/4}}\right), \; V_4 = \int_{-\frac{\pi}{2}\mathcal{R}}^{\frac{\pi}{2}\mathcal{R}} dt \bar{V}_3(t). \tag{35}$$

The constant $\omega = \left(\frac{3}{8\pi^2}\right)^{1/4}$ is set by a condition that the total four-volume of the sphere is equal V_4. The simplest discretization of the above continuum expression is given by

常数 $\omega = \left(\frac{3}{8\pi^2}\right)^{1/4}$ 由整个球体的四维体积等于 V_4 这一条件确定。上述连续统表达式的最简单离散化形式为

$$\bar{N}_3(k) = \frac{3\widetilde{N}_4}{4} \frac{1}{\widetilde{\omega}\widetilde{N}_4^{1/4}} \cos^3\left(\frac{k}{\widetilde{\omega}\widetilde{N}_4^{1/4}}\right), \; \widetilde{N}_4 = \sum_k \bar{N}_3(k). \tag{36}$$

Comparing Equations (35) and (36), one can identify:

对比方程 (35) 和 (36)，可以得到:

$$\frac{t_k}{\omega V_4^{1/4}} = \frac{k}{\widetilde{\omega}\widetilde{N}_4^{1/4}}, \; V_4 = C_4 \widetilde{N}_4 a^4, \tag{37}$$

where the (dimensionless) constant C_4 is the volume of a unit four-simplex, a is the lattice spacing, and the continuum proper-time $t_k = ka$, implying

其中无量纲常数 C_4 是单位四维单纯形的体积，a 是晶格间距，连续统固有时为 $t_k = ka$，由此可得

$$\widetilde{\omega} = \omega C_4^{1/4} \tag{38}$$

The minisuperspace action (32) can also be expressed in terms of the spatial volume (34):

微超空间作用量 (32) 也可以用空间体积 (34) 表示为:

$$S_{MS}^{(S^3)} = -\frac{1}{\Gamma}\int dt\left(\frac{\dot{V}_3^2}{V_3} + \mu V_3^{1/3} - \lambda V_3\right), \tag{39}$$

where $\Gamma = 24\pi G, \mu = 9\left(2\pi^2\right)^{2/3}$ and $\lambda = 3\Lambda$. The simplest discretization of the above action has the following form:

其中 $\Gamma = 24\pi G, \mu = 9\left(2\pi^2\right)^{2/3}$ 且 $\lambda = 3\Lambda$ 。上述作用量的最简单离散化形式如下:

$$S_{\text{eff}}^{(S^3)} = \frac{1}{\tilde{\Gamma}}\sum_k\left(2\frac{\left(N_3(k) - N_3(k+1)\right)^2}{N_3(k) + N_3(k+1)} + \tilde{\mu}N_3(k)^{1/3} - \tilde{\lambda}N_3(k)\right), \tag{40}$$

which is the Ansatz we were looking for. Note that the effective action of CDT agrees with the minisuperspace action up to an overall sign; see Conclusions for more discussion of this fact. The empirical propagator matrix $\widehat{P}$, measured inside phase C_{dS} of the spherical CDT, is indeed very well described by the proposed Ansatz [17,18]. The dimensionless coupling constants $\tilde{\Gamma}, \tilde{\mu}$, and $\tilde{\lambda}$ appearing in the discretized effective action (40) can be fitted from numerical data. Similarly to $\tilde{\omega}$ they all depend on the CDT bare couplings k_0 and Δ .

这正是我们寻找的拟设。注意 CDT 的有效作用量与微超空间作用量仅相差一个整体符号；关于这一点的更多讨论见结论部分。在球形 CDT 的 C_{dS} 相内测量得到的经验传播子矩阵 $\widehat{P}$ ，确实可以被该拟设很好地描述 [17,18]。离散化有效作用量 (40) 中出现的无量纲耦合常数 $\tilde{\Gamma}, \tilde{\mu}$ 和 $\tilde{\lambda}$ 可以通过数值数据拟合得到。与 $\tilde{\omega}$ 类似，它们都依赖于 CDT 裸耦合 k_0 和 Δ 。

By analyzing relations between dimensionful and dimensionless quantities appearing respectively in the continuum expression (39) and its discrete counterpart (40), one obtains:

通过分析连续统表达式 (39) 及其离散对应形式 (40) 中量纲量和无量纲量之间的关系，可得:

$$\sqrt{C_4}a^2\tilde{\Gamma}\tilde{\omega}^2 = \Gamma\omega^2, \tag{41}$$

$$\tilde{\mu}\tilde{\omega}^{8/3} = \mu\omega^{8/3}, \tag{42}$$

$$\tilde{\lambda}\tilde{\omega}^2 = \sqrt{C_4}a^2\lambda\omega^2. \tag{43}$$

Rewriting (41) in terms of Newton’ s constant $\left(\Gamma = 24\pi G; \omega = \left(\frac{3}{8\pi^2}\right)^{1/4}\right)$ leads to

将 (41) 用牛顿常数 $\left(\Gamma = 24\pi G; \omega = \left(\frac{3}{8\pi^2}\right)^{1/4}\right)$ 改写后得到

$$a^2 = \frac{6\sqrt{6}}{\sqrt{C_4}\tilde{\Gamma}\tilde{\omega}^2}G. \tag{44}$$

Assuming that (renormalized) Newton’ s constant G is fixed and, as suggested by the CDT results, the semiclassical description is still valid close to the Planck length $\ell_p = \sqrt{G}$ (in units where $c = \hbar = 1$), one can use Equation (44) to estimate the effective lattice spacing (in $\left[\ell_p\right]$). The lattice spacing depends on two scales:

the average size of the CDT universe expressed in lattice units (quantified by $\widetilde{\omega}$) and the amplitude of quantum fluctuations (quantified by $\sqrt{\tilde{\Gamma}}$). The lattice spacing at the "generic" point in phase C_{dS} $(k_0 = 2.2, \Delta = 0.6)$, where most of the CDT simulations were done, is estimated to be $a \approx 2\ell_p$ which translates into an average radius of the MC generated quantum geometries $\sim 10\ell_p$. It is remarkable that quantum universe at such short scales can be so well described by a semiclassical minisuperspace approximation.

假设 (重整化后的) 牛顿常数 G 固定，且如 CDT 结果所示，半经典描述在普朗克长度 $\ell_p = \sqrt{G}$ 附近仍然成立 (单位制取 $c = \hbar = 1$)，我们就可以用方程 (44) 估计有效晶格间距 (单位为 $[\ell_p]$)。晶格间距依赖两个标度: 以晶格单位表示的 CDT 宇宙平均大小 (由 $\widetilde{\omega}$ 量化) 和量子涨落的振幅 (由 $\sqrt{\tilde{\Gamma}}$ 量化)。在 C_{dS} $(k_0 = 2.2, \Delta = 0.6)$ 相内"一般"点 (大多数 CDT 模拟都在此处进行) 的晶格间距估计值为 $a \approx 2\ell_p$，对应的蒙特卡洛生成量子几何的平均半径为 $\sim 10\ell_p$。值得注意的是，如此短尺度下的量子宇宙仍能被半经典微超空间近似很好地描述。

The Effective Action from Transfer Matrix Method

利用转移矩阵法得到的有效作用量

As argued above, the spatial volume profile (or alternatively the scale factor) of the spherical CDT inside the S_{dS} phase is very well described by a simple discretization of the minisuperspace action (40). This result was obtained by analyzing a semiclassical approximation of volume fluctuations around the average (de Sitter) volume profile, where one could use the empirical covariance matrix to compute the propagator matrix. The problem with such an approach is that in a semiclassical approximation, the propagator matrix is defined by second derivatives of the effective action at the semiclassical solution. One should note that the form of the discretized effective action (40) suggests that, in the physically interesting blob region, the second derivatives, i.e., the elements of the propagator matrix, fall very fast with increasing volume (derivatives of the kinetic term behave as $N_3(k)^{-1}$ and of the potential term as $N_3(k)^{-5/3}$). As a result it is very difficult to observe any subleading corrections, especially in the effective potential. A natural question arises if one can measure the effective action without resorting to the semiclassical approximation, thus validating the above results.

如上所述，S_{dS} 相内球形 CDT 的空间体积分布 (或标度因子) 可以用微超空间作用量 (40) 的简单离散化很好地描述。该结果是通过分析平均 (德西特) 体积分布附近体积涨落的半经典近似得到的，在此方法中可以利用经验协方差矩阵计算传播子矩阵。这种方法的问题在于，在半经典近似下，传播子矩阵由有效作用量在半经典解处的二阶导数定义。需要注意的是，离散化有效作用量 (40) 的形式表明，在有物理意义的团块区域中，二阶导数即传播子矩阵的元会随着体积增大快速衰减: 动能项的导数行为符合 $N_3(k)^{-1}$，势能项的导数行为符合 $N_3(k)^{-5/3}$。因此，很难观测到任何次领头修正，尤其是有效势能中的次领头修正。一个自然的问题是，能否不借助半经典近似来测量有效作用量，从而验证上述结果。

The quasi-local form of the CDT discretized effective action (30) leads in a natural way to the path-integral representation of the spatial volume fluctuations:

CDT 离散化有效作用量的准定域形式自然导出了空间体积涨落的路径积分表示:

$$Z_{\text{eff}} = \sum_{\{N_3(k)\}} e^{-S_{\text{eff}}} \equiv \sum_{\{N_3(k)\}} \prod_{k=1,\ldots,k_{\max}} e^{-L_{\text{eff}}[N_3(k),N_3(k+1)]} = \operatorname{tr} M^{k_{\max}}, \tag{45}$$

where M is the effective transfer matrix defined by the effective Lagrangian

其中 M 是由有效拉格朗日量定义的有效转移矩阵

$$\langle N_3(k+1)|M|N_3(k)\rangle \propto \exp\left(-L_{\text{eff}}\left[N_3(k), N_3(k+1)\right]\right). \tag{46}$$

In the partition function (45), one assumes time-periodic boundary conditions, consistent with the CDT numerical setup. In such an approach one disregards all details of the geometric structure at a given spatial slice and looks only at the spatial volume $N_3(k)$.

配分函数 (45) 采用了时间周期边界条件，与 CDT 的数值设置一致。在该方法中，我们忽略给定空间切片上几何结构的所有细节，只关注空间体积 $N_3(k)$。

One should note that, by construction, CDT has a genuine transfer matrix $\mathcal{M}$ which relates a spatial geometry $\mathcal{T}_k^{(3)}$ at the lattice time k to a spatial geometry $\mathcal{T}_{k+1}^{(3)}$ at time $k+1$. The transfer matrix $\mathcal{M}$ is defined by a sum over all possible four-dimensional triangulations $\mathcal{T}_{k;k+1}^{(4)}$ of a slab between k and $k+1$ (with boundary three-dimensional triangulations $\mathcal{T}_k^{(3)}$ and $\mathcal{T}_{k+1}^{(3)}$):

需要注意，根据构造，CDT 存在一个真实转移矩阵 $\mathcal{M}$，它将格点时间 k 处的空间几何 $\mathcal{T}_k^{(3)}$ 与时间 $k+1$ 处的空间几何 $\mathcal{T}_{k+1}^{(3)}$ 关联起来。转移矩阵 $\mathcal{M}$ 由对 k 和 $k+1$ 之间 slab(边界三维三角剖分为 $\mathcal{T}_k^{(3)}$ 和 $\mathcal{T}_{k+1}^{(3)}$) 所有可能的四维三角剖分 $\mathcal{T}_{k;k+1}^{(4)}$ 求和定义:

$$\left\langle \mathcal{T}_{k+1}^{(3)}|\mathcal{M}|\mathcal{T}_k^{(3)}\right\rangle = \sum_{\mathcal{T}_{k;k+1}^{(4)}} e^{-S_R\left[\mathcal{T}_{k;k+1}^{(4)}\right]}, \tag{47}$$

where $S_R\left[\mathcal{T}_{k:k+1}^{(4)}\right]$ is the Regge action computed for the four-dimensional triangulation of the slab. Accordingly, the partition function of CDT (5) corresponding to $k_{\max}$ time steps (with time-periodic boundary conditions) can be expressed as

其中 $S_R\left[\mathcal{T}_{k:k+1}^{(4)}\right]$ 是 slab 的四维三角剖分对应的 Regge 作用量。相应地，对应 $k_{\max}$ 个时间步 (带时间周期边界条件) 的 CDT 配分函数 (5) 可以表示为

$$Z_{CDT} = \sum_{\left\{\mathcal{T}_k^{(3)}\right\}} \prod_{k=1,\ldots,k_{\max}} \left\langle \mathcal{T}_{k+1}^{(3)}|\mathcal{M}|\mathcal{T}_k^{(3)}\right\rangle = \operatorname{tr}\mathcal{M}^{k_{\max}}. \tag{48}$$

The effective transfer matrix elements can be formally computed as an average over the genuine transfer matrix elements:

有效转移矩阵元可以形式化为真实转移矩阵元的平均:

$$\langle N_3(k+1)\,|M|\,N_3(k)\rangle = \frac{1}{\mathcal{N}_{N_3(k+1)}\mathcal{N}_{N_3(k)}} \sum_{\substack{\mathcal{T}^{(3)}_{k+1}\in\mathcal{T}^{(3)}(N_3(k+1))\\ \mathcal{T}^{(3)}_{k}\in\mathcal{T}^{(3)}(N_3(k))}} \left\langle \mathcal{T}^{(3)}_{k+1}\,|\mathcal{M}|\,\mathcal{T}^{(3)}_{k}\right\rangle,$$

(49)

where $\mathcal{T}^{(3)}(N_3(k))$ denotes a subset of all three-dimensional triangulations with size $N_3(k)$ and the number of such triangulations equals $\mathcal{N}_{N_3(k)}$. The statement that one can use the matrix M defined above as an effective transfer matrix assumes that the standard deviation of the matrix elements $\left\langle \mathcal{T}^{(3)}_{k+1}\,|\mathcal{M}|\,\mathcal{T}^{(3)}_{k}\right\rangle$ in Equation (49) is sufficiently small and consequently

其中 $\mathcal{T}^{(3)}(N_3(k))$ 表示所有体积为 $N_3(k)$ 的三维三角剖分构成的子集，这类三角剖分的数量等于 $\mathcal{N}_{N_3(k)}$。认为可以使用上述定义的矩阵 M 作为有效转移矩阵的前提是，式 (49) 中矩阵元 $\left\langle \mathcal{T}^{(3)}_{k+1}\,|\mathcal{M}|\,\mathcal{T}^{(3)}_{k}\right\rangle$ 的标准差足够小，因此

$$\left\langle \mathcal{T}^{(3)}_{k+\Delta k}\left|\mathcal{M}^{\Delta k}\right|\mathcal{T}^{(3)}_{k}\right\rangle \sim \left\langle N_3(k+\Delta k)\left|M^{\Delta k}\right|N_3(k)\right\rangle, \tag{50}$$

for $\Delta k = 1, 2, \ldots k_{\max}$. In the following we will assume that the description of spatial volume fluctuations using the effective transfer matrix M is a sufficiently good approximation and use it to analyze the empirical (Monte Carlo generated) data. The consistency of such analysis will provide indirect evidence that the approach is correct.

对 $\Delta k = 1, 2, \ldots k_{\max}$ 成立。在下文中我们假设，利用有效转移矩阵 M 描述空间体积涨落是足够好的近似，并将其用于分析 (蒙特卡洛生成的) 经验数据。该分析的自洽性将为该方法的正确性提供间接证据。

Using the partition function (45) and the resulting effective transfer matrix M, one can compute the (two-point) probability distribution of measuring a combination of volumes $N_3(k) = n, N_3(k') = m\,(n, m \in \mathbb{N})$ in spatial slices separated by $\Delta k = k' - k$ time steps:

利用配分函数 (45) 及其得到的有效转移矩阵 M，可以计算被 $\Delta k = k' - k$ 个时间步分隔的空间切片中体积组合 $N_3(k) = n, N_3(k') = m\,(n, m \in \mathbb{N})$ 测量结果的 (两点) 概率分布:

$$P^{k_{\max}}_{\Delta k}\left(N_3(k) = n, N_3(k') = m\right) = \frac{1}{Z_{\text{eff}}}\left\langle n\left|M^{k_{\max}-\Delta k}\right|m\right\rangle\left\langle m\left|M^{\Delta k}\right|n\right\rangle, \tag{51}$$

where we again assumed time-periodic boundary conditions. Let us consider a CDT model with a very short time period $k_{\max} = 2$. It follows from Equation (51) that the two-point probability distribution of measuring $N_3(1) = n$ and $N_3(2) = m$ is given by

其中我们再次假设时间周期性边界条件。考虑一个时间周期极短为 $k_{\max} = 2$ 的 CDT 模型，由式 (51) 可得，测量得到 $N_3(1) = n$ 和 $N_3(2) = m$ 的两点概率分布为

$$P^{k_{\max}=2}_{\Delta k=1}\left(N_3(1) = n, N_3(2) = m\right) = \frac{\langle n\,|M|\,m\rangle\langle m\,|M|\,n\rangle}{\operatorname{tr} M^2}. \tag{52}$$

Due to time reflection symmetry, the transfer matrix M must be symmetric, leading to

由时间反射对称性，转移矩阵 M 必为对称矩阵，因此有

$$\langle n\,|M|\,m\rangle = \mathcal{N}_0\sqrt{P_{\Delta k=1}^{k_{\max}=2}\left(N_3\left(1\right)=n, N_3\left(2\right)=m\right)}. \tag{53}$$

The empirical two-point probability distribution $\widehat{P}_{\Delta k=1}^{k_{\max}=2}$ can be measured in the MC simulations of CDT and therefore used to estimate the transfer matrix elements (up to a normalization factor $\mathcal{N}_0$); see Fig. 6, where we show (the logarithm) of the transfer matrix elements measured in phase C_{dS} of the spherical CDT. The empirical transfer matrix can be then used to reconstruct the effective Lagrangian L_{eff} . According to Equation (46), one gets:

经验两点概率分布 $\widehat{P}_{\Delta k=1}^{k_{\max}=2}$ 可以在 CDT 的蒙特卡洛模拟中测得，因此可用于估计转移矩阵元 (相差归一化因子 $\mathcal{N}_0$)；参见图 6，我们在图中展示了球形 CDT C_{dS} 相中测得的转移矩阵元 (的对数)。得到的经验转移矩阵可进一步用于重构有效拉格朗日量 L_{eff} 。根据式 (46) 可得:

$$L_{\text{eff}}\left[n,m\right] = -\log\langle n\,|M|\,m\rangle + \log\mathcal{N}_0 \tag{54}$$

and the corresponding effective action is given by

对应的有效作用量为

$$S_{\text{eff}} = \sum_k L_{\text{eff}}\left[N_3\left(k\right), N_3\left(k+1\right)\right]. \tag{55}$$

For very small spatial volumes ($N_3 <\sim 300$) , the effective Lagrangian is dominated by lattice discretization artifacts (Fig. 6, left), but for larger volumes it is quite smooth (Fig. 6, right) and can be very well fitted by the following (discretized) Lagrangian [19]:

对于极小的空间体积 ($N_3 <\sim 300$) ，有效拉格朗日量由晶格离散化伪影主导 (图 6 左)，但体积较大时它相当光滑 (图 6 右)，可以用下述离散化拉格朗日量很好地拟合 [19]:

$$L_{\text{eff}}^{(S^3)}\left[n,m\right] = \frac{1}{\tilde{\Gamma}}\left[2\frac{\left(n-m\right)^2}{n+m-2n_0} + \tilde{\mu}\left(\frac{n+m}{2}\right)^{1/3} - \tilde{\lambda}\left(\frac{n+m}{2}\right)\right], \tag{56}$$

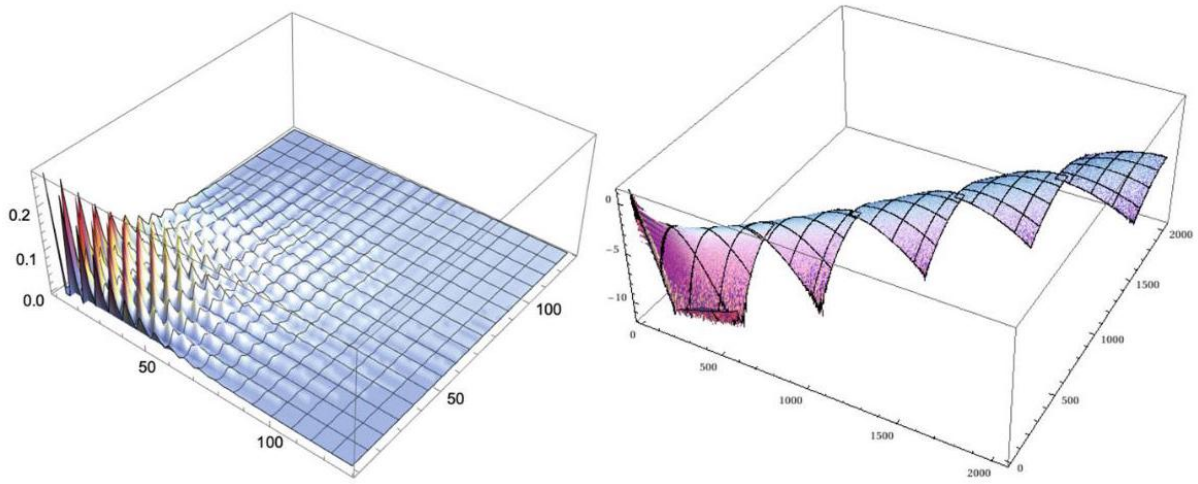

Fig. 6 Empirical transfer matrix measured for small (left panel) and large (right panel) spatial volumes in phase C_{dS} of the spherical CDT ($k_0 = 2.2, \Delta = 0.6$) . Right figure is in logarithmic scale

图 6 球形 CDT ($k_0 = 2.2, \Delta = 0.6$) C_{dS} 相中小空间体积 (左图) 与大空间体积 (右图) 测得的经验转移矩阵。右图为对数坐标

where we have omitted a constant term $\log \mathcal{N}_0$. Fitted values of the parameters $\tilde{\Gamma}, \tilde{\mu}$, and $\tilde{\lambda}$ agree within measurement errors with the parameters obtained using the covariance matrix method discussed before. In the above discretization, we have also included a finite-size correction n_0 . Fitted values of $|n_0| < 10$ are very small compared to macroscopic spatial volumes $N_3 > 300$, where discretization effects are negligible and the parametrization (56) holds. Note that in (56), we have also used a different discretization of the potential part of the effective Lagrangian than in Equation (40). Such a form better fits the transfer matrix data, but it gives exactly the same continuum effective action, consistent with the minisuperspace action (39).

其中我们省略了常数项 $\log \mathcal{N}_0$ 。参数 $\tilde{\Gamma}, \tilde{\mu}$ 和 $\tilde{\lambda}$ 的拟合值与之前协方差矩阵法得到的参数在测量误差范围内一致。在上述离散化中，我们还加入了有限尺寸修正 n_0 。与宏观空间体积 $N_3 > 300$ 相比，$|n_0| < 10$ 的拟合值非常小，此时离散化效应可以忽略，参数化形式 (56) 成立。注意 (56) 中有效拉格朗日量势项的离散化方式与式 (40) 不同。该形式能更好拟合转移矩阵数据，但得到的连续有效作用量完全一致，与微超空间作用量 (39) 相容。

In order to check the validity of the effective transfer matrix approach, one can compare the spatial volume fluctuations data measured in CDT and in a simplified effective model, defined by the partition function (45), where the spatial volume is the only degree of freedom. The transfer matrix M used in the effective model is obtained by smoothly joining the purely empirical transfer matrix $\widehat{M}$, measured for very small spatial volumes where dicretization artifacts prevail, with the theoretical transfer matrix $M_{th}^{(S^3)} \equiv \mathcal{N}_0 \exp\left(-L_{\text{eff}}^{(S^3)}\right)$ defined by the effective Lagrangian (56) (with fitted values of $\tilde{\Gamma}, \tilde{\mu}$ and $\tilde{\lambda}$), applicable to larger volumes, i.e.,

为了检验有效转移矩阵方法的有效性，可以对比 CDT 中测得的空间体积涨落数据，和由配分函数 (45) 定义的简化有效模型的结果，该有效模型仅以空间体积为自由度。有效模型中使用的转移矩阵 M 由两部分光滑连接得到: 一部分是离散化伪影占主导的极小空间体积区域测得的纯经验转移矩阵 $\widehat{M}$ ，另一部分是适用于较大体积的、由有效拉格朗日量 (56)(代入 $\tilde{\Gamma}, \tilde{\mu}$ 和 $\tilde{\lambda}$ 的拟合值) 定义的理论转移矩阵 $M_{th}^{(S^3)} \equiv \mathcal{N}_0 \exp\left(-L_{\text{eff}}^{(S^3)}\right)$ ，即:

$$\langle n \left| M \right| m \rangle = \begin{cases} \langle n \left| \widehat{M} \right| m \rangle \,, n < thr \text{ or } m < thr \\ \left\langle n \left| M_{th}^{(S^3)} \right| m \right\rangle, \text{ otherwise} \end{cases} , \tag{57}$$

where thr is a threshold (thr = 300). In Fig. 7 we compare the average spatial volume profile and the fluctuations profile measured in both the effective and the original CDT Monte Carlo simulations [20]. The agreement is indeed remarkable, thus validating the form of the effective action.

其中 thr 为阈值 (thr = 300)。在图 7 中，我们对比了在有效 CDT 蒙特卡洛模拟与原始 CDT 蒙特卡洛模拟 [20] 中测得的平均空间体积轮廓和涨落轮廓。二者的一致性确实十分出色，从而验证了有效作用量的形式。

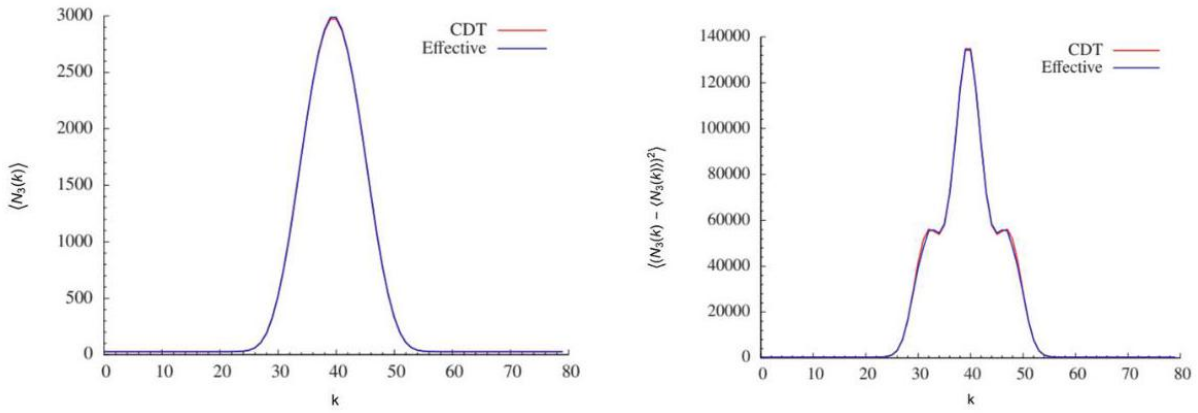

Fig. 7 Comparison of the full CDT results with the effective model of spatial volume fluctuations described in the text. Left panel shows the average volume profile $\langle N_3(k) \rangle$ and right panel the fluctuations profile $\left\langle (N_3(k) - \langle N_3(k) \rangle)^2 \right\rangle$. Data measured in phase C_{dS} of the spherical CDT ($k_0 = 2.2, \Delta = 0.6$)

图 7 完整 CDT 结果与本文描述的空间体积涨落有效模型的对比。左图为平均体积轮廓 $\langle N_3(k) \rangle$，右图为涨落轮廓 $\left\langle (N_3(k) - \langle N_3(k) \rangle)^2 \right\rangle$。数据取自球面 CDT ($k_0 = 2.2, \Delta = 0.6$) 的 C_{dS} 相

Impact of the Spatial Topology Choice

空间拓扑选择的影响

All the results discussed above were obtained in the CDT model with a (fixed) spherical spatial topology $\sum = S^3$. As discussed in the introduction, the spatial topology choice is an important ingredient of CDT; it is therefore important to check the impact of the topology choice on the results. So far, the only other spatial topology studied in the MC simulations was the toroidal topology $\sum = T^3 \equiv S^1 \times S^1 \times S^1$, and such a topology change (from spherical to toroidal) does not seem have impact on the CDT phase structure; see Fig. 2. All four phases (A, B, C_b, and C_{dS}) earlier observed in the spherical CDT are also present in the toroidal CDT. Also location of all phase transition lines is similar for both topologies; but, as will be discussed later, the order of the phase transitions can be different. Nevertheless, due to the different spatial topologies, the dynamically emerging background geometry observed in phase C_{dS} can be different. It is indeed the case as can be visualized by the spatial volume profiles measured in phase C_{dS}; see Fig. 3. In the spherical CDT the average volume profile was very well fitted by a $\cos^3$ function, cf. Equation (18), while in the toroidal CDT one rather observes a constant volume profile $\langle N_3(k) \rangle_{\tilde{N}_4} = \text{const}$.

上述所有结果均是在具有 (固定) 球形空间拓扑 $\sum = S^3$ 的 CDT 模型中得到的。正如引言中所述，空间拓扑选择是 CDT 的重要组成部分，因此检验拓扑选择对结果的影响十分重要。到目前为止，蒙特卡洛模拟中唯一研究过的其他空间拓扑是环面拓扑 $\sum = T^3 \equiv S^1 \times S^1 \times S^1$，这种 (从球形到环形的) 拓扑变化似乎并未对 CDT 的相结构产生影响，见图 2。此前在球形 CDT 中观测到的全部四个相 (A, B, C_b 和 C_{dS} 也同样存在于环面 CDT 中。两种拓扑下所有相变线的位置也相近；但正如后文将要讨论的，相变的阶数可能存在差异。尽管如此，由于空间拓扑不同，在相 C_{dS} 中观测到的动力学涌现背景几何也可能不同。实际情况确实如此，相 C_{dS} 中测得的空间体积分布可以直观体现这一点，见图 3。球形 CDT 中的平均体积分布可以用 $\cos^3$ 函数很好地拟合，参见式 (18)，而环面 CDT 中观测到的更接近恒定体积分布 $\langle N_3(k)\rangle_{\tilde{N}_4} = \text{const}$。

As discussed above, in the spherical CDT, the spatial volume fluctuations are very accurately explained by the minisuperspace effective action; see Equation (39), where the potential term $\propto V_3(t)^{1/3}$ comes from a (constant positive) curvature of the three-sphere and therefore is absent in the case of the (flat) topological torus. One can therefore expect that the toroidal version of phase C_{dS} should admit the following minisuperspace action:

如上所述，在球形 CDT 中，空间体积涨落可以被微超空间有效作用非常精确地解释，参见式 (39)，其中势能项 $\propto V_3(t)^{1/3}$ 来源于三维球面的 (恒定正) 曲率，因此在 (平直) 拓扑环面中不存在。因此我们可以预期，相 C_{dS} 的环面版本应当满足如下微超空间作用量:

$$S_{MS}^{(T^3)} = -\frac{1}{24\pi G}\int dt\left(\frac{\dot{V}_3^2}{V_3} - \lambda V_3\right), \tag{58}$$

where the above potential term is absent.

其中上述势能项不存在。

Using the covariance matrix of spatial volume fluctuations or the effective transfer matrix approach discussed above, one can again determine the form and parameters of the (discretized) effective action in the toroidal CDT, which is very well described by [21,22]

利用上文讨论的空间体积涨落协方差矩阵或有效转移矩阵方法，我们可以再次确定环面 CDT 中离散化有效作用量的形式与参数，该结果可以被 [21,22] 很好地描述

$$S_{\text{eff}}^{(T^3)} = \frac{1}{\tilde{\Gamma}}\sum_k\left(2\frac{\left(N_3(k) - N_3(k+1)\right)^2}{N_3(k) + N_3(k+1)} - \tilde{\lambda}N_3(k) + \tilde{\xi}N_3(k)^{\rho}\right), \tag{59}$$

where the best fit $\rho \approx -3/2$. Again, as in the spherical CDT, all dimensionless constants appearing in Equation (59), i.e., $\tilde{\Gamma}, \tilde{\lambda}$, and $\tilde{\xi}$ depend on the bare couplings of CDT (k_0 and Δ). The kinetic term and the cosmological part of the potential term in Equation (59) are consistent with the toroidal minisuperspace action (58) (as already noted, the CDT effective action and the minisuperspace action agree up to overall sign; see discussion in Conclusions). The additional potential term $\propto V_3^{-3/2}$, where we used the continuum physics notation, does not have a classical counterpart and therefore can be treated as a genuine quantum correction. At the moment it does not have a clear interpretation.

其中是最佳拟合 $\rho \approx -3/2$。与球形 CDT 的情况相同，式 (59) 中出现的所有无量纲常数，即 $\tilde{\Gamma}, \tilde{\lambda}$ 和 ξ 都依赖于 CDT 的裸耦合 (k_0 和 Δ)。式 (59) 中的动能项和势能项的宇宙学部分与环面微超空间作用量 (58) 一致 (如前所述，CDT 有效作用量与微超空间作用量仅整体符号不同，参见结论部分的讨论)。额外的势能项 $\propto V_3^{-3/2}$ (此处我们使用连续物理记号) 没有经典对应，因此可以被视为真正的量子修正。目前它尚无明确解释。

The Effective Action in Other Phases

其他相中的有效作用量

Using the transfer matrix method discussed before, one can as well determine the form of the effective action in other phases of CDT. In particular the effective transfer matrix data measured in phase A are well fitted by [20]

利用前文讨论过的转移矩阵法，我们同样可以确定因果动态三角剖分其他相中的有效作用量形式。具体来说，在 A 相测得的有效转移矩阵数据可以很好地通过文献 [20] 拟合

$$\left\langle n \left| M^{(A)} \right| m \right\rangle = \mathcal{N}_0 \exp\left(\tilde{\lambda}\,(n+m) - \tilde{\xi}\,(n^\rho + m^\rho)\right),\ \rho \approx 0.5, \tag{60}$$

yielding an effective action without a kinetic term. One can check that indeed when approaching the $A - C_{dS}$ transition from inside the semiclassical phase C_{dS} the measured value of $\tilde{\Gamma} \to \infty$, causing the kinetic term of the effective actions (40) and (59) disappear at the transition point. Lack of the kinetic term inside phase A can be therefore interpreted as the limit of the effective Newton’ s constant $G_{\text{eff}} \to \infty$, leading to a causal disconnection of different spatial slices.

由此得到了一个不含动能项的有效作用量。可以验证，当从半经典相 C_{dS} 内部趋近 $A - C_{dS}$ 相变时，测得的 $\tilde{\Gamma} \to \infty$ 值使得有效作用量 (40) 和 (59) 的动能项在相变点消失。因此，A 相内部缺少动能项可以解释为有效牛顿常数 $G_{\text{eff}} \to \infty$ 的极限，导致不同空间切片发生因果断开。

The situation is more complicated in phase C_b where the transfer matrix is well parametrized by [20]

在 C_b 相情况更为复杂，该相的转移矩阵可以通过文献 [20] 很好地参数化为

$$\begin{aligned}\left\langle n \left| M^{(C_b)} \right| m \right\rangle = \mathcal{N}_0 \Bigg[&\exp\left(-2\frac{\left((m-n) - \left[c_0\left(n+m-s^b\right)\right]_+\right)^2}{\tilde{\Gamma}\,(n+m-2n_0)}\right) + \\ &+ \exp\left(-2\frac{\left((m-n) + \left[c_0\left(n+m-s^b\right)\right]_+\right)^2}{\tilde{\Gamma}\,(n+m-2n_0)}\right)\Bigg] \exp\left(-V\left[n+m\right]\right),\end{aligned} \tag{61}$$

where $[\ldots]_+ \equiv \max(\ldots, 0)$, and the potential part $V[n+m]$ was not determined precisely. As can be seen from Equation (61), the kinetic term of the effective transfer matrix bifurcates for the spatial volume $n+m > s^b$ (the bifurcation point). Hence, the other name of the phase C_b , which is also called the bifurcation phase. When approaching the $C_b - C_{dS}$ phase transition from inside the bifurcation phase C_b , one observes $s_b \to \infty$ and $c_0 \to 0$, resulting in the effective action change at the transition point. Accordingly, in phase

C_{dS} one recovers the standard kinetic term of the minisuperspace action. It can be shown that the bifurcation of the kinetic term in phase C_b is related to the appearance of high-order vertices in generic triangulations observed in that phase. Such vertices are surrounded by large volume clusters, causing that the volume density is manifestly nonhomogeneous, and therefore the minisuperspace description ceases to be valid inside the bifurcation phase C_b .

其中 $[\ldots]_+ \equiv \max(\ldots, 0)$，而势能部分 $V[n+m]$ 尚未被精确确定。从式 (61) 可以看出，有效转移矩阵的动能项在空间体积 $n+m > s^b$ 处分叉 (该点为分叉点)。因此 C_b 相又有另一个名称: 分叉相。当从分叉相 C_b 内部趋近 $C_b - C_{dS}$ 相变时，可以观测到 $s_b \to \infty$ 和 $c_0 \to 0$，导致有效作用量在相变点发生改变。相应地，在 C_{dS} 相中我们可以重新得到极小超空间作用量的标准动能项。可以证明，C_b 相中动能项的分叉与该相观测到的一般三角剖分中高阶顶点的出现有关。这些顶点被大体积团簇包围，导致体积密度明显非均匀，因此极小超空间描述在分叉相 C_b 内部不再成立。

Summary of the Semiclassical Limit

半经典极限总结

We have shown that a quantum theory of gravity defined by the four-dimensional Causal Dynamical Triangulations correctly predicts a semiclassical universe with positive cosmological constant, which on large scales is extended and four-dimensional, and whose shape is compatible with a cosmological solution of classical General Relativity. Remarkably, these properties have been derived from first principles in the fully background independent and non-perturbative lattice QFT approach, in which the ground-state geometry emerges dynamically from quantum fluctuations. Inside phase C_{dS} the fluctuations of the scale factor are very well described by a simple minisuperspace action. In the thermodynamical limit (when the lattice size $N_4 \to \infty$) the (relative) amplitude of quantum fluctuations vanishes and one recovers a fully classical trajectory of the scale factor, matching our current understanding of the physics of the very early Universe, at least under the assumption of a spatially homogeneous and isotropic spacetime.

我们已经证明，由四维因果动态三角剖分定义的量子引力理论，正确预测了具有正宇宙学常数的半经典宇宙: 该宇宙在大尺度上是延展的四维宇宙，其形态与经典广义相对论的宇宙学解相容。值得注意的是，这些性质是通过完全背景独立的非微扰格点量子场论方法从第一性原理推导得出的，在该框架中基态几何从量子涨落中动态涌现。在 C_{dS} 相内，标度因子的涨落可以通过一个简单的超空间 (minisuperspace) 作用量很好地描述。在热力学极限下 (当格点大小 $N_4 \to \infty$ 时)，量子涨落的 (相对) 幅度消失，我们可以重新得到完全经典的标度因子演化轨迹，这与我们目前对极早期宇宙物理学的理解一致，至少在空间均匀各向同性时空的假设下是如此。

Search for a Continuum Limit

寻找连续极限

As already mentioned in the introduction, lattice field theories are well suited to study non-perturbative aspects of quantum field theories, such as a (potentially non-perturbatively renormalizable) QFT describing quantum gravity. In the lattice formulation, one regularizes a QFT in question by introducing a lattice of size

N , where the lattice spacing a plays a role of a UV cutoff $\sim 1/a$. Then, in order to define the continuum limit, one has to remove the cutoff by taking $a \to 0$ and $N \to \infty$ in a controlled way, such that the continuum physics quantities of a given

正如引言中已经提到的，格点场理论非常适合研究量子场论的非微扰方面，例如描述量子引力的 (潜在非微扰可重整化) 量子场论。在格点表述中，我们通过引入尺寸为 N 的格点对目标量子场论进行正则化，其中格点间距 a 充当紫外截断 $\sim 1/a$ 的角色。随后，为了定义连续极限，必须通过可控方式取 $a \to 0$ 和 $N \to \infty$ 来移除截断，使得给定

QFT remain unchanged. This is related to the renormalization group flow, which describes how the dimensionless bare lattice couplings should be adjusted when approaching the continuum limit. In particular, the QFT is usually characterized by some physical length scale which can be related to a correlation length ξ . While taking the continuum limit $a \to 0$, the correlation length ξ_a measured in terms of (decreasing) lattice units a must diverge, i.e., $\xi_a \to \infty$ when $a \to 0$, such that the physical correlation length $\xi = \xi_a a$ is kept fixed. The diverging correlation length is characteristic for a higher-order phase transition. Therefore, the presence of the higher-order transitions in a lattice theory is a sine qua non condition of the existence of the continuum limit and the related renormalization group fixed point(s). We thus have a space of (dimensionless) bare coupling constants associated with the lattice theory, and we want to locate regions in this parameter space where there are higher-order phase transitions. In this section we will discuss how the order of a phase transition can be measured using numerical MC methods, and we will provide evidence that (at least some of) the CDT phase transitions are indeed the higher-order transitions. Then, we will try to define the CDT renormalization group flow, following the paths of ”constant physics” in the direction of decreasing lattice spacing.

量子场论的连续物理量保持不变。这与重整化群流相关，重整化群流描述了在趋近连续极限时应当如何调整无量纲裸格点耦合。具体而言，量子场论通常由某个与关联长度 ξ 相关的物理长度尺度表征。在取连续极限 $a \to 0$ 时，以 (递减的) 格点单位 a 度量的关联长度 ξ_a 必须发散，即当 $a \to 0$ 时满足 $\xi_a \to \infty$ ，从而保持物理关联长度 $\xi = \xi_a a$ 固定。关联长度发散是高阶相变的特征。因此，格点理论中存在高阶相变是连续极限及相关重整化群不动点存在的必要条件。我们有一个与格点理论关联的 (无量纲) 裸耦合常数空间，我们想要定位该参数空间中存在高阶相变的区域。在本节中，我们将讨论如何使用数值蒙特卡洛方法测量相变的阶，并给出证据证明 (至少部分)CDT 相变确实是高阶相变。随后，我们将沿着“物理常数”路径向着格点间距减小的方向尝试定义 CDT 重整化群流。

Phase Transitions

相变

Phase transitions can typically be captured by analyzing some macroscopic properties of a given system and tracking their changes when varying coupling constants of a theory in question. The notion of an order of a phase transition was introduced by Ehrenfest, who proposed to characterize phase transitions using derivatives of thermodynamical potentials, such as free energy, measured at the transition point. According to the Ehrenfest classification, if all first $(n-1)$ derivatives of the free energy are continuous and the n -th order derivative diverges at the transition point, then one has the n -th order phase transition. This picture was refined by Landau and Ginzburg who introduced the notion of an order parameter (OP) . The order

parameter is related to the first-order derivative of the free energy, and it captures the symmetry difference between the two different phases. One should note that in some recent models of solid-state physics, the above characterization can fail, when a phase transition cannot be described by a local order parameter, but rather by long-range entanglement, called topological order. Nevertheless in the following we will stick to the Ehrenfest-Landau-Ginzburg classification of phase transitions. Since then the classification of phase transitions shifted toward distinguishing between two types of phase transitions: first-order, which has a divergent first-order derivative of the thermodynamic potential, and higher-order (also called continuous), where the first-order derivative is continuous but second-or higher-order derivatives diverge. Therefore, in the case of a first-order transition, an order parameter is discontinuous at the transition point, and one observes a δ -like singularity of susceptibility related to a second-order derivative of a thermodynamical potential. The behavior is different for a higher-order phase transition, where an order parameter is continuous, but it is nonanalytic at the transition point. As a consequence the second- or higher-order derivatives diverge in a specific way. Furthermore, in the above classification, there is a relation between the order of a transition and the correlation length. For a first-order transition, one typically has finite correlation length, while divergent correlation length signals a continuous phase transition. As will be discussed below, the distinction between orders of phase transitions using lattice methods is nontrivial. This is caused by the fact that in a lattice formulation, one deals with a large but finite number of degrees of freedom and thus both the thermodynamical potentials and all their derivatives are finite. Therefore, instead of observing true phase transitions, one in fact deals with pseudo-phase transitions (crossovers), causing much smoother transition signals. It is only in the thermodynamical limit, i.e., when the lattice size $N \to \infty$, that one recovers the true phase transitions. It is therefore necessary to analyze finite-size effects and discuss how the lattice results can be interpolated to the infinite volume (lattice size) limit.

相变通常可以通过分析给定系统的某些宏观性质，并追踪当改变所研究理论的耦合常数时这些性质的变化来得到。相变级数的概念由埃伦费斯特提出，他提出利用热力学势 (例如自由能) 在相变点测得的导数来表征相变。根据埃伦费斯特分类法，若自由能的所有一阶 $(n-1)$ 导数都连续，且 n 阶导数在相变点发散，则该相变就是 n 阶相变。朗道和金兹堡对这一理论进行了改进，引入了序参量 (OP) 的概念。序参量与自由能的一阶导数相关，它反映了两个不同相之间的对称性差异。需要注意的是，在近代一些凝聚态物理模型中，上述表征方法可能失效: 有些相变无法用局域序参量描述，而需要用长程纠缠 (即拓扑序) 来描述。但下文我们仍将采用埃伦费斯特-朗道-金兹堡的相变分类法。后来相变分类逐渐转向区分两种类型的相变: 一阶相变 (其热力学势的一阶导数发散) 和高阶相变 (也称为连续相变，其一阶导数连续，但二阶或更高阶导数发散)。因此，一阶相变的序参量在相变点不连续，并且可以观测到与热力学势二阶导数相关的磁化率呈现 δ 类奇点。高阶相变的行为则不同，它的序参量连续，但在相变点非解析，因此二阶或更高阶导数会以特定形式发散。此外，在上述分类中，相变的级数和关联长度之间存在关联。一阶相变的关联长度通常是有限的，而发散的关联长度是连续相变的标志。正如下文将要讨论的，用格点方法区分相变级数并非易事。这是因为在格点表述中，我们处理的自由度数量很大但仍是有限的，因此热力学势及其所有导数都是有限的。所以我们实际观测到的不是真正的相变，而是伪相变 (渡越)，其转变信号平缓得多。只有在热力学极限下，即当格点尺寸 $N \to \infty$ 趋于无穷时，我们才能得到真正的相变。因此有必要分析有限尺寸效应，讨论如何将格点结果插值到无限体积 (格点尺寸) 极限。

Ising Model Example

伊辛模型示例

As a toy model example, let us discuss the Ising model of a ferromagnet with the nearest neighbor interaction on a (d -dimensional) square lattice of size N (denoting the number of vertices where spins are placed), described by a partition function:

作为一个玩具模型示例，我们来讨论放置自旋的格点顶点数为 N 的 d 维正方形晶格上，具有最近邻相互作用的铁磁体伊辛模型，其配分函数表达式为:

$$Z(\beta, h) = \sum_{\{s_i\}} \exp\left(\beta \sum_{i \leftrightarrow j} s_i s_j + h \sum_i s_i\right), \; s_i = \pm 1, \tag{62}$$

where $\{s_i\}$ in the first sum denotes all possible spin configurations. In the model there are two (dimensionless) coupling constants β and h , related to the inverse temperature and the external magnetic field, respectively. Note that we used a (nonstandard) convention in which h is the inverse temperature $\times$ the external field. In the thermodynamical limit, for $d \geq 2$ dimensions and without external field ($h = 0$) , one has a second-order (continuous) phase transition between the ordered and the disordered phase occurring at the critical (inverse) temperature β_c (e.g., in $d = 2$ dimensions $\beta_c = \frac{1}{2}\ln\left(1+\sqrt{2}\right) \approx 0.44$) . The Ising model with external field can be also used to describe a first-order phase transition between positive and negative magnetization occurring for $\beta > \beta_c$ (low temperature) at $h_c = 0$.

其中第一个求和符号中的 $\{s_i\}$ 遍历所有可能的自旋构型。该模型包含两个无量纲耦合常数 β 和 h , 分别对应逆温度和外磁场。请注意我们采用了非标准约定: h 对应逆温度，$\times$ 对应外场。在热力学极限下，对于 $d \geq 2$ 维且无外场 ($h = 0$) 的情况，有序相和无序相之间会在临界逆温度 β_c 处发生二级连续相变 (例如在 $d = 2$ 维中结果为 $\beta_c = \frac{1}{2}\ln\left(1+\sqrt{2}\right) \approx 0.44$))。带外场的伊辛模型也可以描述一级相变: 在 $\beta > \beta_c$ (低温) 条件下，正负磁化之间会在 $h_c = 0$ 处发生一级相变。

Higher-Order Transition

高阶相变

Let us start with a second-order phase transition in the absence of the external field ($h = 0$) . The macroscopic properties of the system can be traced by magnetization (per spin):

我们从外场 ($h = 0$) 不存在情况下的二级相变开始讨论。系统的宏观性质可以通过 (单位自旋的) 磁化强度来描述:

$$m = \frac{1}{N}\sum_i s_i \tag{63}$$

It plays a role of an order parameter distinguishing between the low-temperature (high β) ordered phase, where the system is magnetized ($\langle m \rangle \neq 0$) , and the high-temperature (low β) disordered phase, where the magnetization vanishes ($\langle m \rangle \approx 0$). In the disordered phase, the spins are distributed randomly, and one

recovers a (spin inversion) Z_2 symmetry of the Hamiltonian (with $h = 0$), while in the ordered phase the spins prefer to align together and therefore spontaneously break the Z_2 symmetry. Accordingly, the order parameter captures the difference between symmetries of generic spin configurations observed in the two phases. Note that formally the Z_2 symmetry is present also in the ordered phase as in any positive temperature there is a nonzero probability of tunneling between the positive and the negative magnetizations, which are equally probable. This can be observed for small lattices. The tunneling probability decays exponentially with N ; thus, in practice for large lattices the tunneling never happens in the MC simulation time. The average magnetization

磁化强度作为序参数，区分低温 (高 β) 有序相和高温 (低 β) 无序相: 有序相中的系统拥有非零磁化强度 ($\langle m\rangle \neq 0$) ，而无序相中的磁化强度趋近于 ($\langle m\rangle \approx$ 零。在无序相中，自旋随机分布，保留了哈密顿量的 (自旋反转) Z_2 对称性 (当 $h = 0$ 时)；而在有序相中，自旋倾向于同向排列，因此自发破缺了 Z_2 对称性。相应地，序参数体现了两个相中典型自旋组态的对称性差异。需要注意，形式上 Z_2 对称性在有序相中依然存在: 因为在任意正温度下，磁化强度取正和取负之间存在非零隧穿概率，二者概率相等。这种现象在小晶格中可以观测到。隧穿概率随 N 指数衰减；因此在实际大晶格的蒙特卡洛模拟时间内，隧穿永远不会发生。平均磁化强度

$$\langle m\rangle = \frac{1}{N}\left\langle \sum_i s_i \right\rangle = \frac{1}{N}\frac{1}{Z}\sum_{\{s_i\}}\sum_i s_i \exp\left(\beta \sum_{i\leftrightarrow j} s_i s_j + h\sum_i s_i\right) = \frac{1}{N}\frac{\partial \ln Z}{\partial h},$$

(64)

is related to a first-order derivative of the free energy $F = -\frac{1}{\beta}\ln Z$.

和自由能 $F = -\frac{1}{\beta}\ln Z$ 的一阶导数相关。

One can as well compute the (magnetic) susceptibility χ which is the first-order derivative of the (average) magnetization and thus the second-order derivative of the free energy:

我们也可以计算 (磁) 磁化率 χ ，它是 (平均) 磁化强度的一阶导数，因此也就是自由能的二阶导数:

$$\chi = \frac{\partial\langle m\rangle}{\partial h} = \frac{1}{N}\frac{\partial^2 \ln Z}{\partial h^2}. \tag{65}$$

It follows that

由此可得

$$\frac{\chi}{N} = \langle m^2\rangle - \langle m\rangle^2 \tag{66}$$

so the susceptibility χ is proportional to the variance of magnetization. The susceptibility

因此磁化率 χ 正比于磁化强度的方差。磁化率

$$\chi = \frac{1}{N}\sum_{ij}\left(\langle s_i s_j\rangle - \langle s_i\rangle\langle s_j\rangle\right) = \frac{1}{N}\sum_{ij} G_c^{(2)}(i,j) = \sum_j G_c^{(2)}(0,j) \tag{67}$$

is also related to the (connected) two-point correlation function defined by

还和由下式定义的 (连通) 两点关联函数相关

$$G_c^{(2)}(i,j) = \frac{\partial^2 \ln Z}{\partial h_i \partial h_j}, \tag{68}$$

where we have introduced a space-dependent external field ($h \to h_i$) . Generically, away from the transition point the correlation function decays exponentially:

其中我们引入了依赖空间位置的外场 ($h \to h_i$) 。一般来说，远离相变点时关联函数指数衰减:

$$G_c^{(2)}(i,j) \sim e^{-|x_{ij}|/\xi}, \tag{69}$$

where $|x_{ij}|$ is the distance between two lattice points i and j and ξ is the correlation length, which depends on the parameters of the system, i.e., $\xi = \xi(N,\beta,h)$. Typically the correlation length is of order of a few lattice units a . Interesting physics arises when $\xi \to \infty$. This is achieved in the thermodynamical limit $N \to \infty$ by fine-tuning the coupling constant(s) to the critical value(s), i.e., for the Ising model $\beta \to \beta_c$. In the neighborhood of a continuous phase transition, the exponential falloff in Equation (69) vanishes, and the correlator starts to behave according to the power law:

其中 $|x_{ij}|$ 是两个格点 i 和 j 之间的距离，ξ 是关联长度，它依赖于系统的参数，即 $\xi = \xi(N,\beta,h)$ 。通常关联长度是几个晶格单位 a 的量级。当 $\xi \to \infty$ 时，有趣的物理就会出现。这可以通过将耦合常数精细调谐到临界值，在热力学极限 $N \to \infty$ 下实现，对伊辛模型来说就是 $\beta \to \beta_c$ 。在连续相变的邻域内，式 (69) 的指数衰减消失，关联函数开始按幂律行为变化:

$$G_c^{(2)}(i,j) \sim \frac{1}{|x_{ij}|^{d-2+\eta}} \tag{70}$$

where η is a critical exponent. As a result correlations extend to macroscopic distances $|x_{ij}| \gg a$, and the system starts to be insensitive to the short-distance details of the lattice. Therefore, in the vicinity of the higher-order critical point, one can possibly obtain a continuum limit of a theory microscopically defined on a lattice. As microscopic details of the lattice become unimportant, there will be many theories with a different microscopic formulation but the same properties in the continuum limit, such a phenomenon is called universality, and it is mostly governed by the same symmetries and dimensionality of different systems. The (universal) nonanalytic behavior near a continuous phase transition point is captured by scaling relations. In the thermodynamical limit $N \to \infty$, one has in the phase transition region

其中 η 是临界指数。因此关联延伸到宏观尺度 $|x_{ij}| \gg a$ ，系统开始对晶格的短程细节不敏感。因此，在高阶临界点附近，我们有可能得到原本微观定义在晶格上的理论的连续极限。由于晶格的微观细节不再重要，许多微观表述不同的理论可以拥有相同的连续极限性质，这种现象被称为普适性，它主要由不同系统共有的对称性和维度决定。连续相变点附近的 (普适) 非解析行为由标度关系描述。在热力学极限 $N \to \infty$ 下，相变区域满足

$$\xi \sim |\beta_c - \beta|^{-\upsilon}, \tag{71}$$

$$\langle m\rangle \sim |\beta_c - \beta|^{\alpha}, \tag{72}$$

$$\chi \sim |\beta_c - \beta|^{-\gamma}, \tag{73}$$

where υ, α , and γ are critical exponents (the critical exponent α is usually denoted β , but here we used a different notation to distinguish it from the (inverse) temperature). In the two-dimensional Ising model, one has $\upsilon = 1, \alpha = 1/8$, $\gamma = 7/4$. For a finite lattice of size N , the pseudo-critical point $\beta_c(N)$ is also shifted relative to the true critical point $\beta_c = \beta_c(\infty)$. This is caused by the fact that the largest length scale available on a finite lattice is of the order of the linear extension of the lattice $L = N^{1/d}$, and thus instead of the infinite correlation length at the phase transition point, one has $\xi(N) \sim N^{1/d}$. Using Equation (71) one obtains:

其中 υ, α 和 γ 是临界指数 (临界指数 α 通常记为 β ，但本文采用不同记号以将其与 (逆) 温度区分开)。二维伊辛模型中，可得 $\upsilon = 1, \alpha = 1/8$ 、$\gamma = 7/4$ 。对于尺寸为 N 的有限晶格，伪临界点 $\beta_c(N)$ 相对于真实临界点 $\beta_c = \beta_c(\infty)$ 也会发生偏移。这是因为有限晶格可达到的最大长度标度约等于晶格的线性延展长度 $L = N^{1/d}$ ，因此在相变点关联长度不会趋于无穷，而是为 $\xi(N) \sim N^{1/d}$ 。利用式 (71) 可得:

$$|\beta_c - \beta_c(N)|^{-\upsilon} \sim N^{1/d} \tag{74}$$

leading to the following finite-size scaling relation for the pseudo-critical point

由此推导出伪临界点的如下有限尺寸标度关系

$$\beta_c(N) = \beta_c - \text{ const } \times N^{-\tilde{\upsilon}},\ \tilde{\upsilon} = \frac{1}{\upsilon d}. \tag{75}$$

As suggested by Equation (73), for fixed lattice volume N , one can find a pseudocritical point $\beta_c(N)$ by observing a peak in susceptibility. The scaling exponent $\tilde{\upsilon}$ can be then computed numerically by performing a series of MC measurements for larger and larger lattices and fitting the scaling relation (75). For a higher-order (continuous) transition, one expects $\tilde{\upsilon} < 1$, e.g., for the two-dimensional Ising model, one has $\tilde{\upsilon} = 1/2$.

如式 (73) 所示，固定晶格体积 N 时，可通过观测磁化率的峰找到伪临界点 $\beta_c(N)$ 。随后对越来越大的晶格进行一系列蒙特卡洛测量，对标度关系 (75) 做拟合，即可通过数值计算得到标度指数 $\tilde{\upsilon}$ 。对于高阶 (连续) 相变，理论上满足 $\tilde{\upsilon} < 1$ ，例如二维伊辛模型中可得 $\tilde{\upsilon} = 1/2$ 。

Similarly, using Equation (74) one obtains the following finite size scaling relations:

类似地，利用式 (74) 可得如下有限尺寸标度关系:

$$\langle m\rangle \sim N^{-\tilde{\alpha}},\ \tilde{\alpha} = \alpha\tilde{\upsilon}, \tag{76}$$

$$\chi \sim N^{\tilde{\gamma}},\ \tilde{\gamma} = \gamma\tilde{\upsilon}. \tag{77}$$

The scaling exponents $\tilde{\alpha}$ and $\tilde{\gamma}$ can again be computed numerically by measuring the values of the (average) magnetization and susceptibility at the pseudo-critical points $\beta_c(N)$ and then fitting Equations (76) and (77), respectively. For higher-order transitions, one expects $\tilde{\alpha}, \tilde{\gamma} < 1$.

标度指数 $\tilde{\alpha}$ 和 $\tilde{\gamma}$ 同样可以通过数值方法计算: 分别测量伪临界点 $\beta_c(N)$ 处的 (平均) 磁化强度和磁化率，再分别对式 (76) 和式 (77) 做拟合即可。对于高阶相变，理论上满足 $\tilde{\alpha}, \tilde{\gamma} < 1$。

First-Order Transition

一级相变

The Ising model that we have been investigating also exhibits a phase transition between positive and negative magnetization which can be achieved for $\beta > \beta_c$ (low temperature) through the introduction of an external magnetic field h. By the symmetry it is expected that the transition occurs at $h_c = 0$, where the (average) magnetization $\langle m \rangle$ jumps from positive to negative values. The jump in magnetization means that there is a discontinuity of the first-order derivative of the free energy, and thus the transition is first-order. Consequently, one can also expect to observe a δ-like singularity in the magnetic susceptibility χ, which is a first-order derivative of the magnetization and the second-order derivative of the free energy.

我们一直在研究的伊辛模型在正磁化和负磁化之间也存在相变，该相变可在 $\beta > \beta_c$ (低温) 下通过引入外磁场 h 实现。根据对称性可知，相变发生在 $h_c = 0$ 处，此处 (平均) 磁化强度 $\langle m \rangle$ 从正值跳变为负值。磁化强度的跳跃意味着自由能的一阶导数存在不连续性，因此该相变是一级相变。由此，我们还可以预期磁化率 χ 会出现 δ 类奇点，磁化率是磁化强度的一阶导数，同时也是自由能的二阶导数。

Conversely to the higher-order transition case, the correlation length stays finite, and there are no long-range collective fluctuations in the system. As a result the rearrangement of spin configurations from positive to negative magnetization is difficult. In the thermodynamical limit $N \to \infty$, one observes a hysteresis which causes the phase change to occur at points slightly displaced from $h_c = 0$. The hysteresis occurs due to metastable states of positive and negative magnetization coexisting at the critical point. In numerical simulations, the hysteresis is visible only for large enough lattices, as for large N the MC simulation time is usually shorter than the MC autocorrelation time close to the transition point, which is large and grows exponentially with (some power of) N. For smaller lattices, where the autocorrelation time is much shorter than the MC simulation time, one can observe back and forth tunneling between the two metastable states in the transition region ($h \approx 0$). This smoothens the transition and causes thermodynamical quantities to become continuous and "rounded" for finite N, e.g., instead of the jump in magnetization, one observes a tanh-like behavior of $\langle m \rangle$, similarly instead of δ-like behavior of susceptibility, there is a smooth peak in χ. This shows that in practice the accurate estimation of jumps in the expectation value of an order parameter and singularities in its susceptibility at phase transitions which are only "weakly" first-order is particularly cumbersome and then even the distinction from second-order transitions may be a problem. Therefore, again one has to perform a careful finite-size scaling analysis in order to extrapolate from the smooth behavior of a finite system toward jumps and singularities of $N \to \infty$.

与高阶相变相反，一级相变的关联长度保持有限，系统中不存在长程集体涨落。因此自旋组态很难从正磁化重新排列为负磁化。在热力学极限 $N \to \infty$ 下，人们会观测到滞后现象，导致相变发生的位置相较于 $h_c = 0$ 发生小幅偏移。滞后现象的出现是因为正、负磁化的亚稳态在临界点共存。在数值模拟中，只有足够大的格点才能观测到滞后现象，因为对于大格点 N，蒙特卡洛模拟时间通常短于相变点附近的蒙特卡洛自关联时间，而相变点附近的自关联时间很大，且随 N 的 (某次幂) 指数增长。对于较小格点，自关联时间远短于蒙特卡洛模拟时间，人们可以在相变区域 ($h \approx 0$) 观测到两个亚稳态之间来回隧穿。这会平滑相变，使得有限 N 系统的热力学量变为连续并被“修圆”，例如，磁化强度不会发生跳跃，而是观测到 $\langle m \rangle$ 呈双曲正切类行为；类似地，磁化率不会呈现 δ 类行为，而是在 χ 处出现一个光滑峰。这表明，在实际中，对于仅为“弱”一级的相变，要准确估计序参量期望值的跳跃和磁化率的奇点格外困难，甚至可能无法区分一级相变和二级相变。因此，我们仍需要进行细致的有限尺寸标度分析，才能从有限系统的光滑行为外推得到 $N \to \infty$ 的跳跃和奇点。

Typically, in the case of a first-order transition, the probability distribution of an order parameter in the transition region can be described by a sum of two shifted Gaussians, centered at values characteristic for the two metastable states coexisting at the transition point. In particular, in the Ising model the behavior of magnetization m is well approximated by the following probability distribution [23]

通常，在一级相变的情况下，相变区域内序参量的概率分布可以描述为两个平移高斯分布的和，分布中心分别位于相变点共存的两个亚稳态各自的特征值处。具体而言，伊辛模型中磁化强度 m 的行为可以用以下概率分布很好地近似 [23]

$$p(m) = \mathcal{N} e^{hmN} \left[\exp\left(-\frac{(m-\bar{m})^2}{2\overline{\chi}/N} \right) + \exp\left(-\frac{(m+\bar{m})^2}{2\overline{\chi}/N} \right) \right] \tag{78}$$

$$= \widetilde{\mathcal{N}} \left[e^{h\bar{m}N} \exp\left(-\frac{\left(m-\bar{m}-h\overline{\chi}\right)^2}{2\overline{\chi}/N} \right) + e^{-h\bar{m}N} \exp\left(-\frac{\left(m+\bar{m}-h\overline{\chi}\right)^2}{2\overline{\chi}/N} \right) \right],$$

where $\mathcal{N}, \widetilde{\mathcal{N}}$ are normalization factors. For $h = 0$ one recovers two equally probable metastable states of magnetization centered at $\pm\bar{m}$, and the amplitude of fluctuations within each state is governed by $\overline{\chi}$ (note that $\overline{\chi}$ is not the total susceptibility but rather a susceptibility within each state). In other models the positions of states don't have to be symmetric w.r.t. zero and also the widths of the two Gaussians can differ. The width of the two Gaussians decreases with N, and in the limit $N \to \infty$, one obtains two shifted δ-functions. It is also visible that the nonzero external field h shifts the position of the two Gaussians in the direction of h, and the shift is proportional to h. At the same time, the relative probability of observing each state changes with h, such that for $h > 0$, the peak at positive m becomes exponentially larger than the peak at negative m, while for $h < 0$ the opposite happens and thus negative magnetization prevails, and the effect is stronger for larger N.

其中 $\mathcal{N}, \widetilde{\mathcal{N}}$ 是归一化因子。对于 $h = 0$，我们可以得到两个概率相等的磁化亚稳态，中心分别位于 $\pm\bar{m}$，每个状态内的涨落振幅由 $\overline{\chi}$ 决定 (注意 $\overline{\chi}$ 不是总磁化率，而是每个状态内部的磁化率)。在其他模型中，状态的位置不需要关于零对称，两个高斯分布的宽度也可以不同。两个高斯分布的宽度随 N 减小，在极限 $N \to \infty$ 下，我们得到两个平移的 $\delta\,\delta$ 函数。还可以看出，非零外场 h 会将两个高斯分布的位置向 h 的方向平移，平移幅度与 h 成正比。同时，观测到每个状态的相对概率随 h 变化: 对于 $h > 0$，正 m 处的峰比负 m 处的峰呈指数增长，而对于 $h < 0$ 则相反，负磁化占优，且 N 越大，该效应越明显。

It is a simple task to compute $\langle m \rangle$ and χ using probability distribution (78). One obtains:

利用概率分布 (78) 计算 $\langle m \rangle$ 和 χ 是一件简单的事，可得:

$$\langle m \rangle = \overline{\chi} h + \bar{m} \tanh\left(h \bar{m} N\right), \tag{79}$$

$$\chi = \frac{\partial \langle m \rangle}{\partial h} = \overline{\chi} + \bar{m}^2 N / \cosh\left(h \bar{m} N\right). \tag{80}$$

This explains the smoothed tanh-like behavior of magnetization (instead of a jump) as well as a smooth peak of height proportional to N in susceptibility (instead of a δ -like function) observed for finite N . Away from the critical point, i.e., for $|h| \gg |\bar{m} N|^{-1}$, one recovers the expected "bulk" behavior:

这就解释了在有限 N 下观测到的磁化强度呈现平滑双曲正切型行为 (而非跃变)，以及磁化率呈现高度正比于 N 的平滑峰 (而非 δ 型函数)。远离临界点时，即对于 $|h| \gg |\bar{m} N|^{-1}$ ，我们会重新得到预期的“体”行为:

$$\langle m \rangle \approx \overline{\chi} h \pm \bar{m}, \ \chi \approx \overline{\chi}, \tag{81}$$

whereas in the transition region, i.e., for $|h| \ll |\bar{m} N|^{-1}$, one has

而在相变区域，即对于 $|h| \ll |\bar{m} N|^{-1}$ ，我们有

$$\langle m \rangle \approx h \bar{m}^2 N, \ \chi \approx \bar{m}^2 N. \tag{82}$$

It follows that at the first-order critical point, one obtains the following universal finite-size scaling relations (for the Ising model, one formally has $\langle m \rangle = 0$ at $h_c = 0$) :

由此可得，在一阶临界点处满足如下普适有限尺寸标度关系 (对于伊辛模型，形式上有 $\langle m \rangle = 0$ 在 $h_c = 0$) :

$$\langle m \rangle \sim N, \ \chi \sim N. \tag{83}$$

Note that the only scaling which enters the above equations is related to the total volume of the system (lattice size N). This is different than the scaling observed for higher-order transitions; see Equations (76) and (77), where one has nontrivial scaling exponents. In the Ising model discussed here, due to the spin-inversion symmetry at $h = 0$, there will be no shift of the pseudo-critical point with N as always $h_c(N) = 0$. Nevertheless, in other models which exhibit first-order transitions, one can also expect a finite-size scaling of the pseudo-critical point, similar to Equation (75), where again the scaling will be related to the total volume N , i.e., one has a trivial scaling exponent $\tilde{\upsilon} = 1$, being the only power of N which comes into play for the first-order transition.

请注意，上述方程中仅有的标度与系统总容积 (晶格尺寸 N) 相关。这和高阶相变观测到的标度不同；参见方程 (76) 和 (77)，其中存在非平庸标度指数。在本文讨论的伊辛模型中，由于 $h = 0$ 处的自旋反转对称性，赝临界点不会随 N 移动，因为始终满足 $h_c(N) = 0$ 。尽管如此，在其他存在一阶相变的模型中，赝临界点也会出现有限尺寸标度，和方程 (75) 类似，标度同样和总容积 N 相关，即标度指数为平庸的 $\tilde{\upsilon} = 1$ ， N 的这一次幂是一阶相变中唯一发挥作用的。

CDT Phase Transitions

CDT 相变

As discussed above, phase transitions belonging to the same universality class will show the same type of finite-size scaling properties, which manifest by universal values of scaling exponents and in principle can be used to distinguish between first- and higher-order transitions. The Ising model example shows that a practical distinction between the two types of phase transitions using lattice methods is nontrivial and requires a careful analysis of finite-size effects. In both cases pseudocritical points can be found by tracking an order parameter $\mathcal{O}$, used to distinguish the two different phases, and observing a peak in its susceptibility:

如上所述，属于同一普适类的相变会展现出相同类型的有限尺寸标度性质，表现为标度指数的普适值，原则上可用于区分一级相变和高级相变。伊辛模型的例子表明，用格点方法对这两类相变进行实际区分并非易事，需要仔细分析有限尺寸效应。在两种情况下，都可以通过追踪用于区分两个不同相的序参量 $\mathcal{O}$ ，并观察其磁化率的峰来找到准临界点:

$$\chi_{\mathcal{O}} \equiv \bar{N}_4 \left(\langle \mathcal{O}^2 \rangle - \langle \mathcal{O} \rangle^2 \right), \tag{84}$$

where $\bar{N}_4$ denotes the lattice size, i.e., the (constant) target four-volume fixed in the MC simulations of CDT. In the MC simulations, for each lattice size $\bar{N}_4$, one typically changes values of one coupling constant (below denoted $\mathcal{C}$, in the case of CDT: $\mathcal{C} \equiv k_0$ or Δ , respectively) while keeping other coupling(s) fixed, and one can therefore measure the finite-size scaling of the pseudo-critical point $\mathcal{C}_c\left(\bar{N}_4\right)$:

其中 $\bar{N}_4$ 表示格点尺寸，即 CDT 的蒙特卡罗模拟中固定的 (常数) 目标四体积。在蒙特卡罗模拟中，对于每个格点尺寸 $\bar{N}_4$ ，通常固定其他耦合，改变一个耦合常数 (下文记为 $\mathcal{C}$ ，在 CDT 中分别为 $\mathcal{C} \equiv k_0$ 或 Δ)，因此可以测量准临界点 $\mathcal{C}_c\left(\bar{N}_4\right)$ 的有限尺寸标度:

$$\mathcal{C}_c\left(\bar{N}_4\right) = \mathcal{C}_c - \text{ const } \times \bar{N}_4^{-\tilde{\upsilon}}, \tag{85}$$

where the critical exponent $\tilde{\upsilon} = 1$ indicates a first-order transition while $\tilde{\upsilon} < 1$ a higher order transition. One could look as well at the average value of an order parameter $\langle \mathcal{O} \rangle$ or its susceptibility $\chi_{\mathcal{O}}$ measured at the pseudo-critical points $\mathcal{C}_c\left(\bar{N}_4\right)$ and use finite-size scaling relations:

其中临界指数 $\tilde{\upsilon} = 1$ 对应一级相变，$\tilde{\upsilon} < 1$ 对应高级相变。也可以考察准临界点 $\mathcal{C}_c\left(\bar{N}_4\right)$ 处测得的序参量 $\langle \mathcal{O} \rangle$ 平均值或其磁化率 $\chi_{\mathcal{O}}$ ，利用有限尺寸标度关系:

$$\langle \mathcal{O} \rangle \sim \bar{N}_4^{-\tilde{\alpha}}, \tag{86}$$

$$\chi_{\mathcal{O}} \sim \bar{N}_4^{\tilde{\gamma}} \tag{87}$$

where again $-\widetilde{\alpha} = 1$ and $\tilde{\gamma} = 1$ point to a first-order transition, while other values of the critical exponents indicate a higher-order transition. In practice the relations (86) and (87) are rarely used in CDT studies as the observed phase transitions are quite "narrow," and the resolution of the numerical data is insufficient to measure the average value of an order parameter at the transition point or the susceptibility peak value with good enough accuracy.

其中同样 $-\widetilde{\alpha} = 1$ 和 $\tilde{\gamma} = 1$ 对应一级相变，其他临界指数值对应高级相变。实际中 CDT 研究很少使用 (86) 和 (87) 式，因为观测到的相变相当“狭窄”，数值数据的分辨率不足以足够准确地测量相变点处序参量的平均值或磁化率峰值。

Another possibility of distinguishing between first- and higher-order phase transitions comes from observing that two different metastable states are present for the first-order transition and are absent for the higher-order transition. For example, one can analyze empirical distributions (histograms) of order parameters measured at pseudo-critical points. As explained for the Ising model, the two metastable states cause double peaks in the probability distributions. If a phase transition is "strongly" first-order, one can also observe hysteresis in the transition region. However, as CDT results show, one should again very carefully analyze finite-size effects, as it can happen that the hysteresis (or the two-peak separation) shrinks to zero in the $\bar{N}_4 \to \infty$ limit. The appearance of double peaks in the histograms is well quantified by the, so-called, Binder cumulant, related to the fourth moment of the probability distribution. Note that here, and in general in the CDT phase transition studies, we use a definition of the Binder cumulant which is shifted (by a -2/3 constant) versus the original Binder's definition [24]:

区分一级相变和高级相变的另一种方法是利用以下性质: 一级相变存在两个不同的亚稳态，高级相变则不存在。例如，可以分析准临界点处测得的序参量的经验分布 (直方图)。正如伊辛模型中解释的那样，两个亚稳态会导致概率分布出现双峰。如果相变是“强”一级相变，还可以在相变区域观测到滞后现象。但正如 CDT 的结果所示，仍然需要非常仔细地分析有限尺寸效应，因为在 $\bar{N}_4 \to \infty$ 极限下，滞后 (或双峰间距) 可能会收缩至零。直方图中双峰的出现可以用所谓的宾德累积量很好地量化，它与概率分布的四阶矩相关。注意，此处以及一般 CDT 相变研究中，我们使用的宾德累积量定义相比宾德原始定义 [24] 做了平移 (偏移常数-2/3):

$$B_{\mathcal{O}} \equiv \frac{1}{3}\left(1 - \frac{\langle \mathcal{O}^4 \rangle}{\langle \mathcal{O}^2 \rangle^2}\right). \tag{88}$$

For a first-order transition, where the histograms have two shifted peaks, $B_{\mathcal{O}}$ measured at the critical point will move away from zero when $\bar{N}_4 \to \infty$ as the two peaks become more and more apparent (the probability distribution approaches two shifted δ -functions). If instead the transition is higher-order, then the histograms have only one peak and $B_{\mathcal{O}}$ should tend to zero for $\bar{N}_4 \to \infty$. Thus, a deviation of $B_{\mathcal{O}}$ (measured at the critical point) from zero in the limit $\bar{N}_4 \to \infty$ can indicate a first-order transition, while a value close to zero suggests a higher-order transition. In Table 1 we summarize the characteristics of both types of phase transitions which were used in CDT to distinguish between the first- and the higher-order transitions.

对于一级相变，直方图存在两个分开的峰，临界点处测得的 $B_{\mathcal{O}}$ 会随 $\bar{N}_4 \to \infty$ 偏离零，这是因为两个峰变得越来越明显 (概率分布趋近于两个分开的 δ 函数)。如果相变是高级的，直方图只有单峰，那么当 $\bar{N}_4 \to \infty$ 时 $B_{\mathcal{O}}$ 应当趋于零。因此，在 $\bar{N}_4 \to \infty$ 极限下，(临界点测得的) $B_{\mathcal{O}}$ 偏离零意味着一级相变，而接近零则暗示高级相变。表 1 总结了 CDT 中用于区分一级相变和高级相变的两类相变的特征。

Last but not least, one should discuss what order parameters have been used in CDT. In the Ising model example, the order parameter (the magnetization m) was conjugate to the external field h appearing in the Hamiltonian and playing a role of a coupling constant in the model. Similarly, in CDT one has three coupling constants, k_0, Δ , and k_4 , and one can thus use the conjugate quantities, i.e., the global numbers $N_0, N_4^{(4,1)}$, and $N_4^{(3,2)}$ characterizing a CDT triangulation and appearing in the Regge action. Usually in the MC simulations, one fixes the total lattice volume $N_4^{(4,1)}$. Consequently one has the following order parameters (note that similarly to the Ising model, where one used an intensive magnetization per spin m , in CDT we also normalize by the lattice volume $N_4^{(4,1)}$)

最后，我们应当讨论 CDT 中使用过哪些序参量。在伊辛模型的例子中，序参量 (磁化强度 m) 与哈密顿量中出现的外场 h 共轭，该外场在模型中起到耦合常数的作用。类似地，CDT 中有三个耦合常数 k_0, Δ 和 k_4 ，因此可以使用共轭量，即刻画 CDT 三角剖分、出现在里奇作用量中的整体数 $N_0, N_4^{(4,1)}$ 和 $N_4^{(3,2)}$ 。通常在蒙特卡罗模拟中，人们会固定总晶格体积 $N_4^{(4,1)}$ 。因此我们得到如下序参量 (注意和伊辛模型类似，伊辛模型中使用单位自旋的强度磁化量 m ，在 CDT 中我们也对晶格体积 $N_4^{(4,1)}$ 做归一化)

$$\mathcal{O}_1 = \frac{N_0}{N_4^{(4,1)}}, \ \mathcal{O}_2 = \frac{N_4^{(3,2)}}{N_4^{(4,1)}}. \tag{89}$$

Table 1 Characteristics of the first- and the higher-order phase transitions

表 1 一级及更高阶相变的特征

Observable	First-order transition	Higher-order transition
Pseudo-critical point scaling according to (85)	$\tilde{\nu} \approx 1$	$\tilde{\nu} < 1$
Susceptibility scaling according to (87)	$\tilde{\gamma} \approx 1$	$\tilde{\gamma} < 1$
Hysteresis in the transition region	YES and remains when $\bar{N}_4 \to \infty$	NO or disappears when $\bar{N}_4 \to \infty$
Histograms measured at pseudo-critical points	Double peaks peak separation $\uparrow$ with $\bar{N}_4 \to \infty$	Single peak or peak separation $\downarrow$ with $\bar{N}_4 \to \infty$
Binder cumulant measured at pseudo-critical points	$B_{\mathcal{O}} < 0$ when $\bar{N}_4 \to \infty$	$B_{\mathcal{O}} \approx 0$ when $\bar{N}_4 \to \infty$

One can as well use more local information, not captured by the ”global” order parameters defined above. For example, even though the total lattice volume $N_4^{(4,1)}$ is fixed in the MC simulations, its distribution over spatial slices (the volume profile $N_3(k)$) is not, and the generic spatial volume distribution can vary among different phases. Similarly, there is a global relation between N_0 and $N_4^{(4,1)} + N_4^{(3,2)}$, captured by an average coordination number of a vertex (the coordination number is defined as a number of four-simplices sharing a given vertex), but the typical coordination numbers of individual vertices can be very much different between generic triangulations observed in different phases. Therefore, one can define two more order parameters:

我们也可以使用更多局部信息，这些信息无法被上述定义的「全局」序参量捕获。例如，即使总晶格体积 $N_4^{(4,1)}$ 在蒙特卡罗模拟中是固定的，它在空间切片上的分布 (体积轮廓 $N_3(k)$) 却不是，不同相的一般空间体积分布可以存在差异。类似地，N_0 和 $N_4^{(4,1)} + N_4^{(3,2)}$ 之间存在由顶点的平均配位数捕获的全局关系 (配位数定义为共享给定顶点的四单纯形数量)，但在不同相观测到的一般三角剖分中，单个顶点的典型配位数可以差异很大。因此，我们可以再定义两个序参量:

$$\mathcal{O}_3 = \frac{1}{N_4^{(4,1)}} \sum_k \left(N_3(k) - N_3(k+1)\right)^2, \mathcal{O}_4 = \frac{1}{N_4^{(4,1)}} \operatorname*{argmax}_v \left(c(v)\right), \tag{90}$$

where v denotes a set of all vertices in a triangulation and $c(v)$ is the coordination number. The behavior of all four order parameters in various CDT phases is presented in Fig. 8. At a first glance, it may seem a little bit surprising that in addition to the "typical" order parameters $\mathcal{O}_1$ and $\mathcal{O}_2$, which are conjugate to the bare couplings of CDT appearing in the Regge action (3), we have introduced new order parameters $\mathcal{O}_3$ and $\mathcal{O}_4$, not related to the bare action. We did it for pragmatic reasons, as the new order parameters enable us to study some phase transitions, like the $C_b - C_{dS}$ transition, which are not visible using the "typical" order parameters. Nevertheless one could say that the same happens in the "pure" (meaning without the external field, i.e., for $h = 0$) Ising model, which undergoes a higher-order phase transition at $\beta = \beta_c$. In order to define the expectation value and susceptibility of an order parameter (magnetization) in terms of derivatives of the free energy, one has to "enlarge" the Ising model by introducing a new coupling h , related to the external field. Similarly, in the case of CDT, one can "enlarge" the model by adding nontrivial couplings to local degrees of freedom, not appearing in the bare Regge action of CDT (3). For example, $\mathcal{O}_4$ has exactly such interpretation as it can be related to a nontrivial measure term (dependent on local order of vertices) introduced in some lattice models of quantum gravity, see Chap. 73, "Lattice Quantum Gravity: EDT and CDT". It turns out that indeed the order parameter $\mathcal{O}_4$ is very well suited to detect the $C_b - C_{dS}$ transition related to the appearance of high-order vertices, characteristic for phase C_b and not present in phase C_{dS} ; see Fig. 8.

其中 v 表示三角剖分中所有顶点的集合，$c(v)$ 是配位数。所有四个序参量在不同 CDT 相中的行为如图 8 所示。乍看之下可能有点意外: 除了「典型」序参量 $\mathcal{O}_1$ 和 $\mathcal{O}_2$ (它们与出现在里奇作用量 (3) 中的 CDT 裸耦合共轭)，我们还引入了和裸作用量无关的新序参量 $\mathcal{O}_3$ 和 $\mathcal{O}_4$ 。我们这么做是出于实用原因，因为新序参量能让我们研究某些相变，比如 $C_b - C_{dS}$ 相变，这些相变用「典型」序参量是无法观测到的。不过可以说，这在「纯」伊辛模型 (即没有外场，对应 $h = 0$ 的伊辛模型) 中也会发生，纯伊辛模型在 $\beta = \beta_c$ 处会发生高阶相变。要通过自由能的导数定义序参量 (磁化强度) 的期望值和磁化率，必须通过引入和外场相关的新耦合 h 来「扩展」伊辛模型。类似地，在 CDT 的情况中，我们可以通过向局部自由度添加非平凡耦合来「扩展」模型，这些耦合不会出现在 CDT 的裸里奇作用量 (3) 中。例如，$\mathcal{O}_4$ 恰好就是这种解释，因为它可以和某些量子引力晶格模型中引入的非平凡测度项 (依赖顶点的局部阶次) 相关，参见第 73 章「格点量子引力:EDT 和 CDT」。结果发现，序参量 $\mathcal{O}_4$ 确实非常适合检测 $C_b - C_{dS}$ 相变，该相变对应高阶顶点的出现，这是 C_b 相的特征，在 C_{dS} 相中不存在；参见图 8。

Using the order parameters $\mathcal{O}_1 - \mathcal{O}_4$, one can measure phase transition characteristics described above (see Table 1) and thus in principle distinguish between the first- and the higher-order transitions. In practice, the distinction is not always easy as phase transition signals are mixed for most CDT transitions. Therefore, we take a cautious approach, i.e., even in a case where most characteristics point to a higher-order transition but there are some signals of a first-order transition, we classify the transition in question as the first-order transition. Using these rules one has the following: in both the spherical and the toroidal CDT, the $A -$

C_{dS} transition was found to be a first-order transition [25, 26] , while the $B - C_b$ transition is a higher-order transition [25,27]. As regards other CDT phase transitions, the picture is more complicated. The $C_b - C_{dS}$ transition was found to be a higher-order transition in the spherical CDT [28], but a first-order transition in the toroidal CDT [9]. The $B - C_{dS}$ transition and the $A - B$ transition were so far studied only in the toroidal model, where both transitions were found to be first-order [29]. The above results are summarized in Table 2. The order of the transitions is also depicted in Fig. 2, where blue solid lines denote first-order transitions, while red solid lines are higher-order transitions.

利用序参量 $\mathcal{O}_1 - \mathcal{O}_4$ ，可以测量上述相变特征 (见表 1)，因此原则上可以区分一级相变和高阶相变。实际上，区分并不容易，因为大多数 CDT 相变的相变信号是混合的。因此我们采用谨慎的处理方式: 即便是大多数特征指向高阶相变，仅存在少数一级相变信号，我们仍将该待研究相变归类为一级相变。按照这一规则可得到以下结论: 在球面 CDT 和环面 CDT 中，均发现 $A - C_{dS}$ 相变是一级相变 [25, 26] ，而 $B - C_b$ 相变是高阶相变 [25,27]。至于 CDT 的其他相变，情况则更为复杂: 研究发现 $C_b - C_{dS}$ 相变在球面 CDT 中是高阶相变 [28]，但在环面 CDT 中是一级相变 [9]。到目前为止，仅在环面模型中研究过 $B - C_{dS}$ 相变和 $A - B$ 相变，发现二者均为一级相变 [29]。上述结果总结于表 2，相变的阶也展示在图 2 中: 蓝色实线表示一级相变，红色实线表示高阶相变。

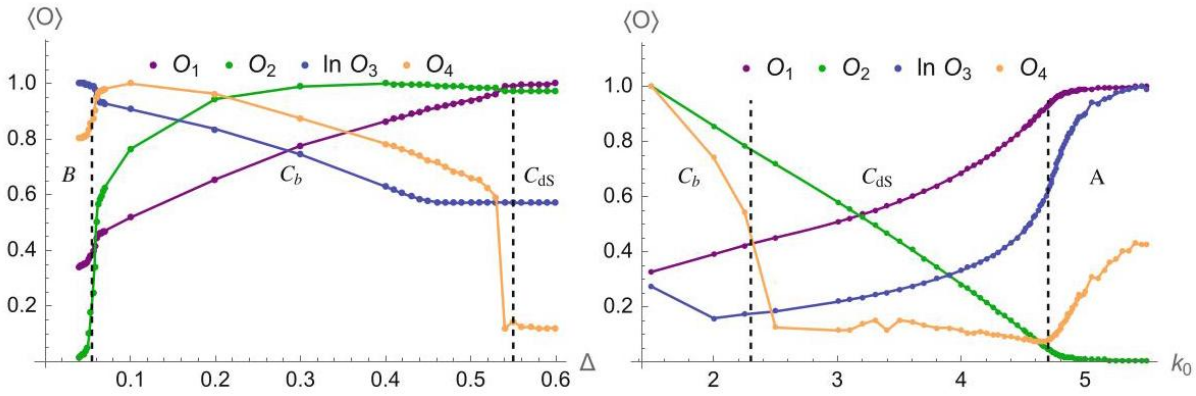

Fig. 8 CDT order parameters; see Equations (89) and (90), measured in the toroidal CDT for fixed $k_0 = 1.5$ (left panel) and for fixed $\Delta = 0.4$ (right panel). The order parameters were rescaled to fit into range [0, 1]. Phase transitions are indicated by dashed lines

图 8 CDT 的序参量；见式 (89) 和 (90)，在固定 $k_0 = 1.5$ (左图) 和固定 $\Delta = 0.4$ (右图) 的环面 CDT 中测量得到。序参量经过重新缩放以适配区间 [0, 1]。相变由虚线标出

Let us stress that the CDT phase transitions are nonstandard from the point of view of ordinary phase transitions, since they involve changes in spacetime geometry and the related effective topology, rather than changes in field configurations on a fixed spacetime, e.g., as in the Ising model. First, let us clarify what we mean by effective topology. In order to understand that, let us consider spacetime configurations observed in the de Sitter phase C_{dS} in the spherical CDT, i.e., when the fixed spatial topology is S^3 and (due to time-periodic boundary conditions) the global topology of the triangulations is that of $S^1 \times S^3$. By construction, any MC update of a triangulation cannot change the imposed global topology. However, a generic configuration in phase C_{dS} will effectively look like an S^4 -triangulation where the north pole and the south pole of the four-sphere are connected by a thin ”stalk” of cutoff size, cf. average spatial volume profiles in Fig. 4. The

”stalk” is necessary to preserve the imposed global topology of the triangulations, but if only it was allowed by the MC algorithm, it would completely disappear, yielding the change of the topology from $S^1 \times S^3$ to S^4 (which we call the effective topology). It is thus visible that not only the effective spacetime dimension but also the effective spacetime topology can be emergent concepts on the quantum level.

需要强调的是，从普通相变的角度来看，CDT 相变是非标准的，因为这类相变改变的是时空几何及相关有效拓扑，而非固定时空上的场组态，例如伊辛模型中的情况。首先我们来澄清有效拓扑的含义。为了理解这一概念，我们来看球面 CDT 德西特相 C_{dS} 中观测到的时空组态: 此时固定空间拓扑为 S^3，且由于时间周期性边界条件，三角剖分的整体拓扑为 $S^1 \times S^3$。根据构造，三角剖分的任意蒙特卡罗更新都无法改变预设的整体拓扑。然而，C_{dS} 相中的任意一般组态，有效看起来都像是 S^4 三角剖分——四球面的北极和南极由一个截断尺寸的细” 柄” 连接，参见图 4 中的平均空间体积轮廓。这个” 柄” 是维持预设的三角剖分整体拓扑所必需的，但如果蒙特卡罗算法允许它存在，它会完全消失，带来拓扑从 $S^1 \times S^3$ 到 S^4 的改变 (我们将其称为有效拓扑)。由此可见，不仅有效时空维度，有效时空拓扑也可以是量子层面上的涌现概念。

Now an interesting pattern emerges linking the order of the CDT phase transitions with the effective topology of spacetimes observed in the adjacent phases. As discussed above, the effective topology of phase C_{dS} in the spherical CDT is that of S^4. The same effective topology is also observed (both in the spherical and the toroidal CDT) in the bifurcation phase C_b. At the same time, the spherical CDT $C_b - C_{dS}$ transition is a higher-order transition. Also the effective topology of phase B is similar, and the $B - C_b$ transition is a higher-order transition (both in the spherical and the toroidal cases). All other phase transitions observed so far in CDT are first-order transitions, and they are related to a change of the effective topology. In the case of toroidal CDT, the $B - C_{dS}$ transition and the $C_b - C_{dS}$ transition involve a change of the effective topology from S^4 (observed in phases B and C_b) to T^4 (in the toroidal version of phase C_{dS}). The effective topology of phase A may be characterized as the topology of a disjoint union of spatial geometries, and thus it is different from the effective topologies encountered in other CDT phases, and again the $A - B$ and the $A - C_{dS}$ transitions are first-order transitions. The above results lead to the following conjecture:

目前我们发现了一个有趣的规律，它将 CDT 相变的阶数与相邻相观测到的时空有效拓扑联系了起来。如上文所述，球形 CDT 中相 C_{dS} 的有效拓扑为 S^4。同样的有效拓扑也在分岔相 C_b 中被观测到 (球形 CDT 和环形 CDT 中均是如此)。同时，球形 CDT 的 $C_b - C_{dS}$ 相变是高阶相变。并且相 B 的有效拓扑与之相似，$B - C_b$ 相变同样是高阶相变 (球形和环形情形下均成立)。迄今为止，CDT 中观测到的所有其他相变都是一级相变，它们都和有效拓扑的改变有关。对于环形 CDT 而言，$B - C_{dS}$ 相变与 $C_b - C_{dS}$ 相变都会引发有效拓扑改变: 从 (相 B 和相 C_b 中观测到的) S^4 变为相 C_{dS} 环形版本中的 T^4。相 A 的有效拓扑可以描述为空间几何的不相交并的拓扑，因此它与其他 CDT 相中遇到的有效拓扑都不同，对应的 $A - B$ 相变和 $A - C_{dS}$ 相变也同样是一级相变。上述结果引出了如下猜想:

Table 2 Summary of CDT phase transitions

表 2 CDT 相变总结

Phase transition	Spherical CDT	Toroidal CDT
$A - C_{dS}$	First-order	First-order
$B - C_{dS}$	?	First-order
$C_b - C_{dS}$	Higher-order	First-order
$B - C_b$	Higher-order	Higher-order
$A - B$	?	First-order

phase transitions which involve a change in effective topology will be first-order transitions.

涉及有效拓扑改变的相变都是一级相变。

At the same time, all CDT transitions which don't involve the effective topology change are most likely higher-order transitions.

同时，所有不涉及有效拓扑改变的 CDT 相变极有可能都是高阶相变。

RG Flow in CDT and the Perspective Continuum Limit

CDT 中的 RG 流与预期连续极限

Our main interest is to find a higher-order phase transition where one may be able to define a continuum limit of CDT. Since only the phase C_{dS} seems to offer acceptable infrared configurations, it is natural to look for the higher-order transition lines at the border of that phase. From the results reported above, we cannot use the toroidal CDT in such studies, since all such transition lines are first-order (there is still a chance that the triple points, i.e., the points where the three transition lines meet, see Fig. 2, may potentially be higher-order critical points, as it is quite common to observe a higher-order critical point in the end of a first-order transition line, but this is hard to check numerically). Therefore, we will focus on the spherical CDT, where one observes that the $C_b - C_{dS}$ transition line is higher-order. According to our conjecture, it is also likely that the spherical $B - C_{dS}$ transition (whose order has not been determined yet) is a higher-order transition, as it separates phases of the same effective topology. It also potentially makes the $C_b - B - C_{dS}$ triple point an interesting candidate for a UV fixed point. At least it would then be a critical point where three higher-order transition lines meet.

我们的核心目标是找到能够定义 CDT 连续极限的高阶相变。由于只有 C_{dS} 相能提供可接受的红外构型，在该相的边界寻找高阶相变线是自然而然的选择。根据上述已有结果，我们无法在这类研究中使用环形 CDT，因为它的所有这类相变线均为一级相变 (仍存在一种可能性: 三条相变线交汇的三临界点，即图 2 所示的点，有可能是高阶临界点，因为在一级相变线的端点观测到高阶临界点是十分常见的，但这一点很难通过数值方法验证)。因此我们将聚焦球形 CDT，在该模型中可以观测到 $C_b - C_{dS}$ 相变线是高阶的。根据我们的推测，球形 $B - C_{dS}$ 相变 (其阶数尚未确定) 很可能也是高阶相变，因为它分隔了具有相同有效拓扑的相。这也使得 $C_b - B - C_{dS}$ 三临界点有可能成为紫外不动点的有力候选。至少在该情况下，它会是一个三条高阶相变线交汇的临界点。

Having located the higher-order phase transition line(s), we now want to understand how to approach the critical point(s) from inside the physically interesting phase C_{dS} . The general idea is quite simple: we would like to adjust the dimensionless bare couplings of CDT in such a way that the RG trajectories in the

(k_0, Δ) coupling constant space, i.e., the lines of "constant physics" defined by some renormalized continuum observables, flow in the direction of decreasing lattice spacing a and hopefully lead to the higher-order critical point, implying that the correlation length $\xi_a \to \infty$ and the lattice spacing $a \to 0$. Then, such a critical point will correspond to a UV fixed point in which one obtains a continuum limit of the CDT lattice theory. The absence of a UV fixed point would be signaled by the fact that there is not any RG flow line ending at a higher-order transition point. In that case one cannot shrink the lattice spacing to zero and obtain a continuum limit. In CDT it is convenient to analyze the RG flow of the bare couplings under the additional assumption that the (average) physical volume of spacetime is fixed and finite along each RG flow trajectory:

定位到高阶相变线后，我们现在希望理解如何从物理上有意义的 C_{dS} 相内部逼近临界点。总体思路十分简单: 我们希望调整 CDT 的无量纲裸耦合，使得 (k_0, Δ) 耦合常数空间中的 RG 轨迹，也就是由部分重整化连续观测量定义的“恒定物理”线，朝着格点间距 a 减小的方向流动，并最终有望抵达高阶临界点，此时关联长度 $\xi_a \to \infty$ 和格点间距 $a \to 0$ 满足条件。这样的临界点就对应一个紫外不动点，我们可以在该不动点得到 CDT 格点理论的连续极限。若不存在 RG 流线终止于高阶相变点，则意味着不存在紫外不动点，此时我们无法将格点间距收缩至零得到连续极限。在 CDT 中，分析 RG 流时方便引入额外假设: 每条 RG 流轨迹上，时空的平均物理体积固定且有限:

$$V_4 \propto N_4 a^4 = \text{ const.} \tag{91}$$

Accordingly, one has to increase lattice volume N_4 in an appropriate way when the lattice spacing a is decreased, and the thermodynamical limit $N_4 \to \infty$ will coincide with the continuum limit $a \to 0$, if it exists.

相应地，当格点间距 a 减小时，必须以合适的方式增大格点体积 N_4 ，若连续极限存在，热力学极限 $N_4 \to \infty$ 将与连续极限 $a \to 0$ 重合。

The key question remains: how to define what constitutes a line of "constant physics"? In the following we will use a definition introduced in [30] (see also Chap. 76, "The Causality Road from Dynamical Triangulations to Quantum Gravity That Describes Our Universe" for discussion), where "constant physics" relies on two quite natural assumptions, namely, that (i) the "shape" of the (average) CDT geometry and (ii) the (relative) amplitude of quantum fluctuations remain constant on each RG flow trajectory. As will be shown below, such a definition has important consequences for the renormalized gravitational coupling constant if the semiclassical description in terms of the (Euclidean) de Sitter universe and the minisuperspace effective action introduced in section "Evidence for an Effective Minisuperspace Action" stays valid up to the UV scale.

核心问题依然是: 如何定义“恒定物理”线? 在下文中我们采用文献 [30] 中提出的定义 (相关讨论也可参见第 76 章“从动力学三角剖分到描述我们宇宙的量子引力: 因果性之路”)，该定义下“恒定物理”基于两个十分自然的假设:(i) 平均 CDT 几何的“形状”; (ii) 量子涨落的相对振幅，在每条 RG 流轨迹上保持不变。如下文所示，如果以欧氏德西特宇宙和“有效超空间作用量的证据”一节引入的超空间有效作用量描述的半经典图景在紫外标度下依然成立, 那么该定义对重整化引力常数有重要推论。

As discussed in section "Evidence for an Effective Minisuperspace Action," the (average) CDT geometry inside the semiclassical phase C_{dS} seems to be consistent (at least when the scale factor is considered) with the (Euclidean) de Sitter universe, i.e., a regular four-sphere S^4 . It implies a relation between the measured parameter $\widetilde{\omega}$, quantifying the width of the CDT geometry in lattice units, and its continuum counterpart ω ,

set by a condition that the total four-volume of the sphere equals V_4 ; see Equation (38):

正如“有效超空间作用量的证据”一节所讨论，半经典相 C_{dS} 内部的平均 CDT 几何 (至少对标度因子而言) 与欧氏德西特宇宙，即规则四维球 S^4 一致。这给出了测量参数 $\widetilde{\omega}$ (以格点单位量化 CDT 几何的宽度) 与其连续对应量 ω 之间的关系，该关系由四维球总体积等于 V_4 的条件确定；参见式 (38):

$$\widetilde{\omega} = \omega C_4^{1/4}.$$

There is also a relation between $\widetilde{\omega}, \omega$ and the coupling constants $\widetilde{\mu}, \mu$ appearing in the minisuperspace (39) and the CDT (40) effective actions, respectively; see Equation (42):

$\widetilde{\omega}, \omega$ 与分别出现在超空间 (39) 和 CDT(40) 有效作用量中的耦合常数 $\widetilde{\mu}, \mu$ 之间也存在一个关系，见式 (42):

$$\widetilde{\mu}\widetilde{\omega}^{8/3} = \mu\omega^{8/3} = \text{ const.}$$

Following [30], let us now consider anisotropic spacetime scaling scenarios à la Hořava-Lifshitz gravity [7, 31], also see Chap. 77, ”CDT and Hořava-Lifshitz QG in Two Dimensions”. One should note that such an approach manifestly breaks the four-dimensional diffeomorphism invariance of the continuum theory by introducing a preferred time foliation and thus makes the asymmetry between space and time a real physical phenomenon. In the cosmological minisuperspace truncation, one recovers the continuum semiclassical volume profile (35), as well as the continuum minisuperspace effective action (39), but now ω becomes a free parameter, which quantifies the spacetime anisotropy, and consequently the volume profile (35) corresponds to a deformed S^4 geometry, i.e., a four-ellipsoid, compressed, or elongated in time direction depending on ω (for $\omega = \left(\frac{\hat{3}}{8\pi^2}\right)^{1/4}$ one recovers the symmetric S^4). In such a case, the relation (42) between ω and μ also stays valid, and thus the spacetime asymmetry, quantified by ω , is set by the value of (dimensionless) coupling constant μ appearing in the minisuperspace action (39) $\left(\mu = 9\left(2\pi^2\right)^{2/3}\right.$ corresponds to a symmetric case consistent with

遵照文献 [30]，我们现在讨论霍拉瓦-利夫希茨引力框架下 [7,31] 的各向异性时空标度方案，也可参见第 77 章“二维 CDT 与霍拉瓦-利夫希茨量子引力”。需要注意的是，该方法通过引入优先时间叶状结构，明显破坏了连续理论的四维微分同胚不变性，从而让空间与时间的不对称性成为真实的物理现象。在宇宙学超空间截断中，我们仍可以得到连续半经典体积分布 (35) 以及连续超空间有效作用量 (39)，但此时 ω 成为量化时空各向异性的自由参数，相应的体积分布 (35) 对应变形后的 S^4 几何，即四椭球，根据 ω 的取值会在时间方向被压缩或拉伸 (当 $\omega = \left(\frac{\hat{3}}{8\pi^2}\right)^{1/4}$ 时我们回到对称的 S^4)。在这种情况下，ω 与 μ 之间的关系 (42) 仍然成立，因此由 ω 量化的时空不对称性由超空间作用量 (39) 中出现的 (无量纲) 耦合常数 μ 的取值决定，$\left(\mu = 9\left(2\pi^2\right)^{2/3}\right.$ 对应与广义相对论一致的对称情形)

General Relativity). As a result, through relation (38), different values of the lattice parameter $\widetilde{\omega}$ will translate into different values of the continuum parameter ω and thus to a physically different geometry of the quantum universe. Consequently

因此，通过关系 (38)，格点参数 $\widetilde{\omega}$ 的不同取值会转化为连续参数 ω 的不同取值，进而得到量子宇宙在物理上不同的几何。因此

$$\widetilde{\omega}\left(k_0, \Delta\right) = \text{ const.} \tag{92}$$

is required to keep the (average) continuum geometry fixed, and therefore it defines the lines of "constant physics" in the (k_0, Δ) coupling constant space.

需要保持 (平均) 连续几何固定，因此它在 (k_0, Δ) 耦合常数空间中定义了“恒定物理”线。

In order to define the RG flow, one should also require that the relative amplitude of quantum fluctuations stays constant on each line of "constant physics" when approaching the continuum limit, i.e., when the lattice volume N_4 is increased and the lattice spacing a is decreased in accordance with Equation (91). The condition

为了定义 RG 流，还需要满足: 趋近连续极限时，即按照式 (91) 增大格点体积 N_4 、减小格点间距 a 时，每条“恒定物理”线上量子涨落的相对振幅保持不变。该条件

$$\frac{\sqrt{\left\langle \delta V_3^2\left(t_k\right)\right\rangle}}{\left\langle V_3\left(t_k\right)\right\rangle} = \frac{\sqrt{\left\langle \delta N_3^2\left(k\right)\right\rangle_{\tilde{N}_4}}}{\left\langle N_3\left(k\right)\right\rangle_{\tilde{N}_4}} = \text{ const. }, \; t_k = ka \tag{93}$$

means that one investigates the same "real" continuum physics when changing the cutoff scale, and the result does not depend on N_4 nor a . It cannot be achieved for fixed k_0 and Δ , as in that case relative fluctuations vanish when $N_4 \to \infty$; see Equation (25). Accordingly, the RG flow toward a continuum limit requires following a path of "constant physics" (defined by the condition (92)) in the CDT coupling constant space $\left(k_0\left(N_4\right), \Delta\left(N_4\right)\right)$ when N_4 (and therefore $a \propto N_4^{-1/4}$) is changed. The amplitude of spatial volume fluctuations is set by the (renormalized) dimensionless gravitational coupling constant $\tilde{\Gamma}$ (cf. the CDT effective action (40)), and it scales as $\delta N_3 \propto \sqrt{\tilde{\Gamma}} N_4^{1/2}$ (see Equation (24)). At the same time, $N_3 \propto \widetilde{\omega}^{-1} N_4^{3/4}$ (see Equation (18)). Therefore, the condition (93) implies

意味着我们改变 cutoff 标度时，研究的是同一个“真实”连续物理，结果不依赖于 N_4 也不依赖于 a 。固定 k_0 和 Δ 无法满足这一点，因为这种情况下当 $N_4 \to \infty$ 时相对涨落会消失，见式 (25)。因此，流向连续极限的 RG 流需要在改变 N_4 (以及相应的 $a \propto N_4^{-1/4}$) 时，沿着 CDT 耦合常数空间 $\left(k_0\left(N_4\right), \Delta\left(N_4\right)\right)$ 中“恒定物理”(由条件 (92) 定义) 的路径移动。空间体积涨落的振幅由 (重整化后的) 无量纲引力耦合常数 $\tilde{\Gamma}$ 决定 (参见 CDT 有效作用量 (40))，其标度行为为 $\delta N_3 \propto \sqrt{\tilde{\Gamma}} N_4^{1/2}$ (见式 (24))。同时，$N_3 \propto \widetilde{\omega}^{-1} N_4^{3/4}$ (见式 (18))。因此，条件 (93) 意味着

$$\frac{\tilde{\Gamma} \widetilde{\omega}^2}{N_4^{1/2}} = \text{ const.} \tag{94}$$

It means that when the lattice volume N_4 is changed, one should follow a RG flow trajectory in the direction where the (renormalized) dimensionless gravitational coupling constant $\tilde{\Gamma}$ scales as

这意味着当改变格点体积 N_4 时，我们需要沿 RG 流轨迹运动，使得 (重整化后的) 无量纲引力耦合常数 $\tilde{\Gamma}$ 按如下方式标度

$$\tilde{\Gamma}\left(k_0\left(N_4\right), \Delta\left(N_4\right)\right) \propto N_4^{1/2}, \tag{95}$$

where we have explicitly included the dependence of $\tilde{\Gamma}$ on k_0 and Δ . As the amplitude of fluctuations scales as $\delta N_3 \propto \sqrt{\tilde{\Gamma}\left(k_0, \Delta\right)}$, the above condition compensates the $N_4^{-1/2}$ factor in Equation (94), resulting

from a different scaling of the fluctuations and the average volume profiles with N_4 . One should note that combining all RG flow conditions, i.e., Equations (91), (92), and (95), leads to (cf. Equation (44))

此处我们已明确给出 $\tilde{\Gamma}$ 对 k_0 和 Δ 的依赖关系。由于涨落的振幅按 $\delta N_3 \propto \sqrt{\tilde{\Gamma}(k_0,\Delta)}$ 标度，上述条件抵消了式 (94) 中的 $N_4^{-1/2}$ 因子，该因子源于涨落和平均体积剖面随 N_4 的不同标度行为。需要注意的是，组合所有 RG 流条件即式 (91)、(92) 和 (95) 后可得 (参见式 (44))

$$G \propto \tilde{\Gamma}\widetilde{\omega}^2 a^2 \propto \frac{\tilde{\Gamma}\widetilde{\omega}^2}{N_4^{1/2}} = \text{ const.} \tag{96}$$

Therefore, keeping the same continuum physics when approaching a continuum limit translates into keeping the (renormalized) dimensionful gravitational constant G fixed, at least if our effective semiclassical description holds up to this limit.

因此，在趋近连续极限时保持相同的连续物理，等价于保持 (重整化后的) 量纲引力常数 G 固定，至少在我们的有效半经典描述适用于该极限时成立。

Summarizing, we assume that each RG flow trajectory is defined by a path in the CDT bare dimensionless coupling constant space $(\kappa_0(N_4), \Delta(N_4))$ parametrized by N_4 (the lattice cutoff scale is $\propto N_4^{1/4}$) which fulfills the following conditions:

综上，我们假设每条 RG 流轨线均由 $(\kappa_0(N_4), \Delta(N_4))$ (CDT 裸无量纲耦合常数空间) 中以 N_4 参数化的路径定义 (格点截断标度为 $\propto N_4^{1/4}$)，且满足以下条件:

$$\widetilde{\omega}(k_0(N_4), \Delta(N_4)) = \text{ const.}, \ \tilde{\Gamma}(k_0(N_4), \Delta(N_4)) \propto N_4^{1/2}. \tag{97}$$

If the path continues to $N_4 \to \infty$ $(a \to 0)$, which is possible at a higher-order critical point (k_0^*, Δ^*) , then such a point will be a UV fixed point.

若路径延伸至 $N_4 \to \infty$ $(a \to 0)$ (这在高阶临界点 (k_0^*, Δ^*) 处是可能的)，则该点即为紫外不动点。

In order to check if the conditions (97) can be satisfied, one can perform a series of MC simulations in a grid of points (k_0, Δ) to measure the distributions $N_3(k)$ and then compute $\widetilde{\omega}(k_0, \Delta)$ and $\tilde{\Gamma}(k_0, \Delta)$. Our analysis assumes that $\widetilde{\omega}(k_0, \Delta)$ and $\tilde{\Gamma}(k_0, \Delta)$ do not depend on $\bar{N}_4$ which, as discussed in section "Evidence for an Effective Minisuperspace Action," is indeed the case inside the phase C_{dS} for large enough $\bar{N}_4$. It is therefore enough to carry out measurements for a fixed lattice volume $\bar{N}_4$. The results of such measurements [30] performed for $\bar{N}_4^{(4,1)} = 40\text{k}$ are visualized in Fig. 9, where we show contour plots of $\widetilde{\omega}(k_0, \Delta)$ (left panel) and $\sqrt{\tilde{\Gamma}(k_0, \Delta)}$ (right panel) in the (k_0, Δ) -plane. The lines visible on the left plot can be directly interpreted as lines of "constant physics," where $\widetilde{\omega}(k_0, \Delta) = \text{const.}$ Moving along any such line, one can read off from the right plot how $\sqrt{\tilde{\Gamma}(k_0, \Delta)}$ changes and thus in which direction one should follow when N_4 is increased (i.e., the lattice spacing a is decreased). It is seen that the lattice spacing decreases toward the right-bottom corner of the plots, i.e., toward the interesting region of the CDT phase diagram, where higher-order transition lines meet. It is also seen that most of the RG flow trajectories, which are deep inside the C_{dS} phase, go parallel to the $C_b - C_{dS}$ phase transition line but then turn away and go parallel to the $A - C_{dS}$ phase transition line. Therefore, such RG flow lines do not lead to any UV fixed point. However, there are potentially some lines

of ”constant physics” (very close to the $C_b - C_{dS}$ phase transition line) which may lead to a common critical point, cf. Fig. 10.

为检验条件 (97) 是否成立，可在点格 (k_0, Δ) 上开展一系列蒙特卡洛模拟，测量分布 $N_3(k)$，随后计算得到 $\widetilde{\omega}(k_0, \Delta)$ 和 $\tilde{\Gamma}(k_0, \Delta)$。我们的分析假设 $\widetilde{\omega}(k_0, \Delta)$ 和 $\tilde{\Gamma}(k_0, \Delta)$ 不依赖于 $\bar{N}_4$，正如“有效超空间作用量的证据”一节所讨论的，对于足够大的 $\bar{N}_4$，C_{dS} 相内确实满足这一关系，因此只需对固定格点体积 $\bar{N}_4$ 进行测量即可。这类针对 $\bar{N}_4^{(4,1)} = 40\text{k}$ 开展的测量得到的结果 [30] 可视化于图 9，我们在图中给出了 (k_0, Δ) 平面上 $\widetilde{\omega}(k_0, \Delta)$ (左图) 和 $\sqrt{\tilde{\Gamma}(k_0, \Delta)}$ (右图) 的等高线图。左图中可见的线可直接解释为“恒定物理”线，满足 $\widetilde{\omega}(k_0, \Delta) =$ 为常数。沿任意这类线移动，可从右图读出 $\sqrt{\tilde{\Gamma}(k_0, \Delta)}$ 的变化，进而得知当 N_4 增大 (即格点间距 a 减小) 时应当沿哪个方向移动。可以看到，格点间距向图的右下角不断减小，也就是朝向 CDT 相图中高阶相变线交汇的感兴趣区域。还可以观察到，大多数位于 C_{dS} 相深处的重整化群流轨迹都平行于 $C_b - C_{dS}$ 相变线延伸，随后转向并平行于 $A - C_{dS}$ 相变线延伸。因此这类重整化群流线无法通向任何紫外不动点。但存在一些“恒定物理”线 (非常靠近 $C_b - C_{dS}$ 相变线)，有可能通向共同临界点，参见图 10。

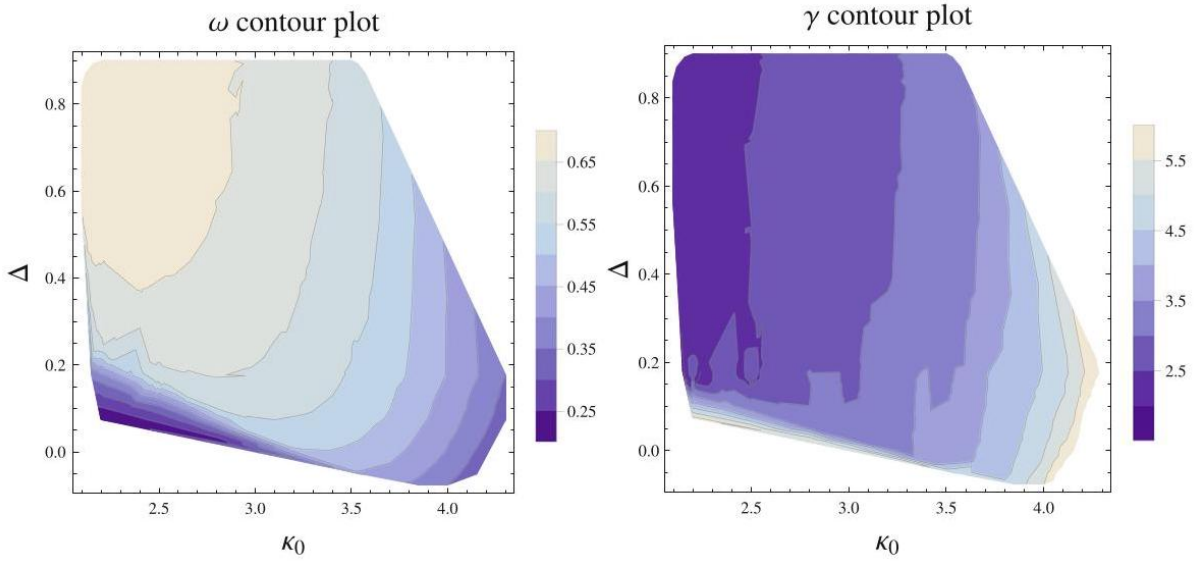

Fig. 9 The ”shape” parameter $\widetilde{\omega}$ (left panel) and the fluctuations amplitude $\gamma \propto \sqrt{\tilde{\Gamma}}$ (right panel) measured in the spherical CDT for $\bar{N}_4^{(4,1)} = 40\text{k}$. Courtesy of J. Ambjørn and A. Görlich

图 9 球形 CDT 中针对 $\bar{N}_4^{(4,1)} = 40\text{k}$ 测量得到的“形状”参数 $\widetilde{\omega}$ (左图) 和涨落振幅 $\gamma \propto \sqrt{\tilde{\Gamma}}$ (右图)。由 J. Ambjørn 和 A. Gör 惠赠

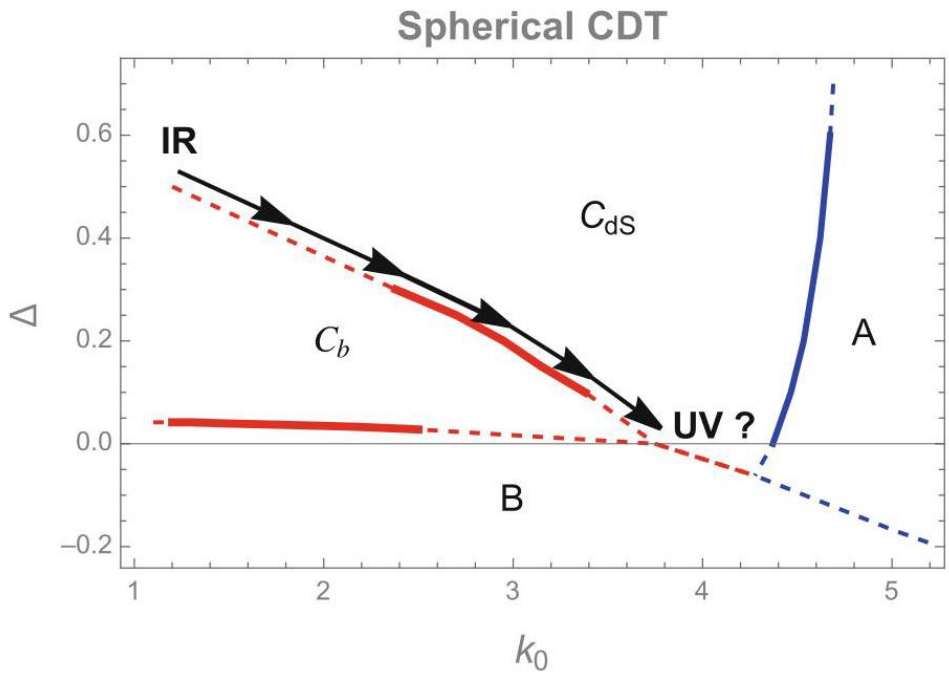

Fig. 10 Putative CDT renormalization group flow line(s) leading from the IR to the (perspective) UV fixed point

图 10 从红外通向 (潜在) 紫外不动点的推测 CDT 重整化群流线

Summary of the Search for a Continuum Limit

寻找连续极限的研究总结

Examples of simple lattice models, such as the Ising model, show that determining the order of a phase transition may be a difficult task and one has to carefully analyze finite-size effects. In the case of CDT, additional complication comes from the fact that the CDT phase transitions are not typical phase transitions studied in ”standard” lattice QFTs, defined on the fixed spacetime, but they rather involve changes in spacetime geometry or even spacetime (effective) topology. Nevertheless, using numerical MC simulations, one can study properties of the CDT phase transitions and in principle distinguish between the first- and the higher-order transitions. The results of the CDT phase transition studies performed so far lead to the conclusion that only in the case of the spherical CDT one can observe the higher-order phase transition lines (the $C_b - C_{dS}$ phase transition and potentially the $B - C_{dS}$ phase transition) bordering the physically interesting phase C_{dS} , inside which one observes the IR semiclassical universe. In that case one can also define the RG flow trajectories, related to keeping the physical ”shape” of the universe and (relative) amplitude of quantum fluctuations fixed and leading in the direction of decreasing lattice spacing. Combining RG flow conditions with an assumption that the physical four-volume of the universe is kept fixed leads to a condition that the dimensionful gravitational coupling constant G is kept fixed on each RG flow line up to the UV scale; see Equation (96). One should note that this result is not compatible with the standard functional renormalization group approach to asymptotic safety, where the dimensionless gravitational coupling stays nonzero but the dimensionful $G \to 0$ as the UV cutoff is removed. Thus, comparing results of both approaches is difficult

and requires further studies. Nevertheless, despite most of the RG flow trajectories in CDT do not end up in a common UV fixed point, there are some trajectories which potentially lead to a continuum limit, as schematically outlined in Fig. 10. The results are not conclusive as the precision of the MC measurements discussed above was not good enough to make sure that the RG flow really goes to the genuine UV fixed point(s).

伊辛模型这类简单格点模型的例子表明，确定相变的阶数并非易事，必须仔细分析有限尺寸效应。对于因果动态三角剖分 (CDT)，额外的复杂性来自于:CDT 的相变并非定义在固定时空上的“标准”格点量子场论中研究的典型相变，而是涉及时空几何甚至时空 (有效) 拓扑的改变。尽管如此，借助数值蒙特卡洛 (MC) 模拟，我们仍可以研究 CDT 相变的性质，原则上可以区分一级相变和更高阶相变。迄今为止 CDT 相变研究的结果得出结论: 只有在球面拓扑 CDT 的情况下，才能观测到与物理上感兴趣的相 C_{dS} 接壤的高阶相变线 ($C_b - C_{dS}$ 相变和潜在的 $B - C_{dS}$ 相变)，在 C_{dS} 相内部可以观测到红外半经典宇宙。在这种情况下，我们还可以定义重整化群 (RG) 流轨迹，它对应于保持宇宙的物理“形状”和量子涨落的 (相对) 振幅固定，并流向格点间距减小的方向。将 RG 流条件与宇宙物理四体积保持固定的假设结合，可以得到这样一个条件: 量纲引力耦合常数 G 在每条 RG 流线上直至紫外标度都保持固定；参见式 (96)。需要注意的是，这一结果与渐近安全的标准泛函重整化群方法并不相容，后者中无量纲引力耦合保持非零，但作为紫外截断的量纲 $G \to 0$ 被移除。因此，两种方法的结果难以比较，仍需进一步研究。尽管如此，CDT 中大多数 RG 流轨迹并不会终止于同一个紫外不动点，但仍存在一些轨迹有可能通向连续极限，如图 10 的概略示意图所示。目前的结果尚无定论，因为前述 MC 测量的精度不足以确认 RG 流确实流向真正的紫外不动点。

Conclusions

结论

Causal Dynamical Triangulations is based on lattice QFT techniques applied to the quantization of gravity and uses only a few additional assumptions about the topology of spacetime. Lattice QFTs turned out to be very successful in addressing many non-perturbative problems in other areas of physics, e.g., regarding Quantum Chromodynamics (QCD) beyond perturbation regime. QCD is an ordinary QFT in flat spacetime, and the regular hyper-cubic lattice used represents a simple discretization of the flat spacetime. However, if the field theory is gravity, spacetime itself becomes nontrivial and dynamical. Therefore, CDT generalizes the conventional lattice QFT to the case of fluctuating geometries, approximated by lattices constructed from a few types of simplices with fixed edge lengths. Using Regge prescription of how to compute spacetime curvature for a simplicial manifold, one can express Einstein-Hilbert action in terms of dimensionless lattice variables. The Regge action is defined in terms of geometric invariants, such as lengths and angles, and does not use spacetime coordinates, thus making CDT diffeomorphism-invariant. CDT is also manifestly background independent as all possible (lattice regularized) spacetime geometries enter the quantum-gravitational path integral. The key nontrivial assumption of CDT is that the quantum spacetime is globally hyperbolic and therefore can be foliated into spatial slices of constant cosmological time, which all have the same fixed topology. Although the distinguished notion of time in CDT looks superficially similar to the time foliation in Horava-Lifshitz gravity [31], its status is different because CDT does not possess any residual coordinate dependence. The role of time in CDT was partly clarified in a study in three dimensions, where it was verified explicitly that key results of CDT quantum gravity continue to hold in a version of the theory which does not possess a preferred time foliation [32]. This provides strong evidence that the notion of time that is naturally available in standard CDT is simply a convenient foliation choice (a la gauge fixing) and that its presence

does not affect the results of the theory in an unwanted way. The CDT time foliation enables one to precisely define what is meant by a Wick rotation from the Lorentzian to the Euclidean spacetime signature, and thus one can use the (Euclidean) model to investigate properties of the quantum-gravitational path integral using numerical Monte Carlo methods.

因果动态三角剖分基于应用于引力量子化的格点量子场论技术，仅对时空拓扑做出少量额外假设。事实证明，格点量子场论在解决物理学其他领域的诸多非微扰问题上非常成功，例如非微扰区的量子色动力学 (QCD)。QCD 是平直时空中的普通量子场论，所用的规则超立方格点是对平直时空的简单离散化。但当场论是引力时，时空本身会变得非平凡且具有动力学性。因此，CDT 将传统格点量子场论推广到了涨落几何的情形，这些几何由由几种固定边长的单形构造而成的格点近似。利用里奇方法计算单纯形流形的时空曲率后，我们可以将爱因斯坦-希尔伯特作用量用无量纲格点变量表示出来。里奇作用量由长度、角度等几何不变量定义，不依赖时空坐标，因此 CDT 满足微分同胚不变性。由于所有可能 (格点正则化后的) 时空几何都会进入量子引力路径积分，CDT 也明显满足背景独立性。CDT 的核心非平凡假设是: 量子时空整体双曲，因此可以分层切片为具有相同固定拓扑、宇宙学时间恒定的空间切片。尽管 CDT 中特殊的时间定义表面上看起来和霍拉瓦-栗弗席兹引力中的时间切片 [31] 相似，但二者地位不同，因为 CDT 不存在任何残余坐标依赖。三维空间的一项研究部分阐明了时间在 CDT 中的作用，该研究明确证实:CDT 量子引力的核心结果在不具备优先时间切片的理论版本中依然成立 [32]。这提供了强有力的证据，证明标准 CDT 中自然存在的时间概念仅仅是一种方便的切片选择 (类似规范固定)，它的存在不会以不符合预期的方式影响理论结果。CDT 的时间切片让我们可以准确定义从洛伦兹号差时空到欧几里得号差时空的 wick 转动，因此我们可以使用 (欧几里得) 模型，借助数值蒙特卡洛方法研究量子引力路径积分的性质。

One of the greatest achievements of CDT is that it correctly predicts the IR limit of quantum gravity, consistent with classical Einstein's field equations. The semiclassical limit is obtained in the, so-called, de Sitter phase C_{dS} , where one observes the emergent four-dimensional average geometry with superimposed quantum fluctuations. What is more, fluctuations of the global "shape" of the universe, quantified by the time evolution of the scale factor, are very well described by a simple minisuperspace effective action. One should note that despite the fact that the observed semiclassical solution for the scale factor is consistent with a homogeneous and isotropic universe, the abovementioned symmetries are not put in by hand in CDT (as it is done in minisuperspace models), but emerge dynamically, as also does the effective spacetime dimension four. It is quite remarkable that despite the fact that the geometries entering the gravitational path integral are very nonclassical, after performing a suitable average over configurations, the scale factor gets consistent with a homogeneous and isotropic spacetime. However, since the scale factor is just one mode of the metric, in order to verify that the observed semiclassical ground state geometry is really homogeneous and isotropic, one should use some other observables quantifying the "average geometry." This is still an open issue, but some progress has been recently made in this direction; see Chaps. 78, "Spectral Observables and Gauge Field Couplings in Causal Dynamical Triangulations" and 79, "Scalar Fields in Four-Dimensional CDT". Another nontrivial result is that the CDT effective action agrees with the standard Euclidean minisuperspace action only up to overall sign (cf. Equations (39) and (40), where both $\Gamma, \tilde{\Gamma} > 0$). The standard Euclidean minisuperspace action is unbounded from below due to negative sign of the kinetic term. The sign of the action does not matter for a classical trajectory, but in the path integral formalism, the unbounded action causes the path integral to be completely dominated by arbitrarily large fluctuations of the conformal mode, making the quantum theory ill-defined. A cure to the conformal mode problem can possibly come from a specific contour of integration for the conformal factor as Hartle and Hawking proposed in their minisuperspace truncation of the gravitational path integral [33]. In CDT the problem is cured in a natural way without resorting to the

Hartle-Hawking ”trick,” as one automatically obtains the inverted sign of the kinetic term, exactly consistent with the Hartle-Hawking proposal. This simply comes from a subtle interplay between the purely geometric degrees of freedom (entering the bare Regge action of CDT) and the entropic factor (counting the number of states with the same value of the bare action), which seems to stabilize the underlying quantum theory.

CDT 最重大的成果之一，是它正确预言了量子引力的红外极限，结果与经典爱因斯坦场方程一致。半经典极限是在所谓德西特相 C_{dS} 中得到的，在该相可以观测到涌现的四维平均几何，其上叠加了量子涨落。此外，由标度因子的时间演化量化的宇宙整体“形状”涨落，也可以用一个简单的超空间微扰有效作用量很好地描述。需要注意的是，尽管观测到的标度因子半经典解与均匀各向同性宇宙一致，CDT 并没有像超微空间模型那样手动引入上述对称性，这些对称性和有效时空维度为四维一样，都是动力学涌现的。值得注意的是，即使进入引力路径积分的几何高度非经典，在对构型做合适的平均后，得到的标度因子仍然符合均匀各向同性时空。但由于标度因子只是度规的一个模态，若要验证观测到的半经典基态几何确实是均匀各向同性的，还需要使用其他量化“平均几何”的可观测量。这目前仍是一个开放问题，但最近该方向已经取得了一些进展，参见第 78 章《因果动力学三角剖分中的谱可观测量与规范场耦合》和第 79 章《四维 CDT 中的标量场》。另一个重要结果是，CDT 有效作用量仅在整体符号上与标准欧几里得超微空间作用量一致 (对比式 (39) 和 (40), 两式中均为 $\Gamma, \tilde{\Gamma} > 0$)。标准欧几里得超微空间作用量由于动能项为负号，下方无界。对于经典轨迹，作用量的符号并不重要，但在路径积分形式中，无界作用量会导致路径积分完全被共形模任意大的涨落主导，使得量子理论定义不良。共形模问题的解决方法，可能源于哈特和霍金在引力路径积分超微空间截断中提出的共形因子特定积分围道。CDT 中无需借助哈特-霍金“技巧”就自然解决了该问题，因为 CDT 自动得到了动能项的反转符号，完全符合哈特-霍金的假设。这一性质纯粹来自纯几何自由度 (进入 CDT 裸雷格作用量) 和熵因子 (计数裸作用量取值相同的状态数) 之间的微妙相互作用，这种相互作用似乎稳定了底层量子理论。

Another good feature of the four-dimensional CDT is that it has a rich phase structure, where (in the case of spherical CDT) some of the phase transitions bordering the physically interesting semiclassical phase C_{dS} seem to be higher-order transitions. As a result one may hope to test the asymptotic safety scenario, where the UV fixed point of quantum gravity should appear as a higher-order critical point. Accordingly, one can try to define the RG flow of the CDT bare coupling constants toward the fixed point. If the RG flow leads to a higher-order critical point in such a way that the transition point could be associated with a gravitational UV fixed point, then one would obtain a non-perturbative description of a theory which can be viewed as the quantum theory of gravity defined at arbitrarily short distances or, alternatively, at arbitrarily large energy scales. The results reported in section ”RG Flow in CDT and the Perspective Continuum Limit” are not conclusive as the resolution of numerical data is not good enough to make sure if (at least some) of the RG flow lines lead to a higher-order critical point. One should also note that the above results were obtained [30] before the $C_b - C_{dS}$ phase transition was discovered [20], and therefore at that moment the results were missing our current understanding of the CDT phase structure. It would be then worth to repeat the RG flow measurements using current computer resources and improved algorithms of the MC simulations which would enable to study much larger systems, thus reducing finite-size effects and increasing accuracy of the numerical results. Having said this, let us comment about a possible scenario that the continuum limit cannot be found. First of all it can mean that our definition of what is considered to be a line of ”constant physics” (here defined as a constant ”shape” of the semiclassical CDT universe) is wrong and one should use some other notions of ”constant physics,” which can be well motivated by nonclassical features of quantum geometry found on Planckian scales. This is indeed possible as the CDT approach seems to be noncompatible with the standard renormalization group techniques used in asymptotic safety. It leads again to the problem

of defining good observables quantifying such features. But even in the most pessimistic scenario, where the new observables wouldn't help, CDT could still be considered as an effective QFT of gravity, valid up to some finite energy scale of order of the Planck scale.

四维 CDT 的另一个优良特性是它拥有丰富的相结构:(在球形 CDT 的情况下) 与有物理意义的半经典相 C_{dS} 接壤的一些相变似乎是高阶相变。因此我们有希望检验渐近安全情景——量子引力的紫外不动点应当会以高阶临界点的形式出现。相应地，我们可以尝试在 CDT 中定义裸耦合常数流向该不动点的重整化群流。如果重整化群流最终通向一个高阶临界点，且该转变点可以对应引力紫外不动点，那么我们就能得到该理论的非微扰描述，它可以被看作是在任意短距离 (等价于任意高能标) 下都良定义的量子引力理论。在“CDT 中的重整化群流与连续统极限展望”章节报告的结果尚无定论，因为数值数据的分辨率不足以确认 (至少部分) 重整化群流线是否通向高阶临界点。还需要指出，上述结果是在 $C_b - C_{dS}$ 相变被发现 [20] 之前得到的 [30]，因此当时的研究不具备我们目前对 CDT 相结构的认知。利用当前的计算资源和改进的蒙特卡洛模拟算法重复重整化群流测量是很有价值的，这些改进能够让我们研究大得多的系统，从而减小有限尺寸效应，提高数值结果的精度。说完这些，我们来讨论一下找不到连续统极限的可能情景。首先，这可能意味着我们对什么是“恒物理”线 (此处定义为半经典 CDT 宇宙保持恒定“形状”) 的定义是错误的，我们应当采用“恒物理”的其他定义——这些定义可以由普朗克尺度下量子几何的非经典特征合理导出。这确实是有可能的，因为 CDT 方法似乎和渐近安全中使用的标准重整化群技术不兼容，这又引出了定义能量化这类特征的合格可观测量的问题。但即使在最悲观的情景下——即使引入新可观测量也无济于事，CDT 仍然可以被看作是引力的有效量子场论，它在直到普朗克量级的有限能量标度内都成立。

Cross-References

交叉引用

CDT and Hořava-Lifshitz QG in Two Dimensions

二维中的 CDT 与霍拉瓦-利夫希茨量子引力

Scalar Fields in Four-Dimensional CDT

四维 CDT 中的标量场

Spectral Observables and Gauge Field Couplings in Causal Dynamical Triangulations

因果动态三角剖分中的谱可观测量与规范场耦合

The Causality Road from Dynamical Triangulations to Quantum Gravity That Describes Our Universe

从动态三角剖分到描述我们宇宙的量子引力的因果性路径

References

参考文献

1. S. Weinberg, Ultraviolet Divergences in Quantum Theories of Gravitation, in General Relativity: An Einstein Centenary Survey. Cambridge University Press, UK (1980), pp. 790-831

2. J. Ambjørn, A. Görlich, J. Jurkiewicz, R. Loll, Phys. Rept. 519, 127 (2012)

3. R. Loll, Class. Quant. Grav. 37, 013002 (2020)

4. J. Ambjørn, Z. Drogosz, J. Gizbert-Studnicki, A. Görlich, J. Jurkiewicz, D. Németh, Universe 7, 79 (2021)

5. T. Regge, Nuovo Cim. 19, 558 (1961)

6. J. Ambjørn, J. Jurkiewicz, R. Loll, Nucl. Phys. B 610, 347 (2001)

7. J. Ambjørn, A. Görlich, S. Jordan, J. Jurkiewicz, R. Loll, Phys. Lett. B 690, 413 (2010)

8. J. Ambjørn, D. Coumbe, J. Gizbert-Studnicki, J. Jurkiewicz, JHEP 08, 033 (2015)

9. J. Ambjørn, J. Gizbert-Studnicki, A. Görlich, J. Jurkiewicz, D. Németh, JHEP 06, 111 (2018)

10. M. Reitz, D. Németh, D. Rajbhandari, A. Görlich, J. Gizbert-Studnicki, Generalised Spectral Dimensions in Non-Perturbative Quantum Gravity (2022). https://arxiv.org/abs/2207.05117

11. M. Craioveanu, M. Puta, T. Rassias, Old and New Aspects in Spectral Geometry. Springer Dordrecht (2001). https://doi.org/10.1007/978-94-017-2475-3

12. J. Ambjørn, J. Jurkiewicz, R. Loll, Phys. Rev. Lett. 95, 171301 (2005)

13. O. Lauscher, M. Reuter, Phys. Rev. D 65, 025013 (2001)

14. D. Benedetti, Phys. Rev. Lett. 102, 111303 (2009)

15. P. Horava, Phys. Rev. Lett. 102, 161301 (2009)

16. L. Modesto, Class. Quant. Grav. 26, 242002 (2009)

17. J. Ambjørn, A. Görlich, J. Jurkiewicz, R. Loll, Phys. Rev. D 78, 063544 (2008)

18. J. Ambjørn, A. Görlich, J. Jurkiewicz, R. Loll, J. Gizbert-Studnicki, T. Trześniewski, Nucl. Phys. B 849, 144 (2011)

19. J. Ambjørn, J. Gizbert-Studnicki, A. Görlich, J. Jurkiewicz, JHEP 09, 017 (2012)

20. J. Ambjørn, J. Gizbert-Studnicki, A. Görlich, J. Jurkiewicz, JHEP 06, 034 (2014)

21. J. Ambjørn, Z. Drogosz, J. Gizbert-Studnicki, A. Görlich, J. Jurkiewicz, D. Németh, Phys. Rev. D 94, 044010 (2016)

22. J. Ambjørn, J. Gizbert-Studnicki, A.Görlich, K. Grosvenor, J. Jurkiewicz, Nucl. Phys. B 922, 226 (2017)

23. K. Binder, D.P. Landau, Phys. Rev. B 30, 1477 (1984)

24. K. Binder, Phys. Rev. Lett. 47, 693 (1981)

25. J. Ambjørn, S. Jordan, J. Jurkiewicz, R. Loll, Phys. Rev. D 85, 124044 (2012)

26. J. Ambjørn, D. Coumbe, J. Gizbert-Studnicki, A. Görlich, J. Jurkiewicz, Class. Quant. Grav. 36, 224001 (2019)

27. J. Ambjørn, G. Czelusta, J. Gizbert-Studnicki, A. Görlich, J. Jurkiewicz, D. Németh, JHEP 05, 030 (2020)

28. D. Coumbe, J. Gizbert-Studnicki, J. Jurkiewicz, JHEP 02, 144 (2016)

29. J. Ambjørn, J. Gizbert-Studnicki, A. Görlich, D. Németh, JHEP 04, 103 (2022)

30. J. Ambjørn, A. Görlich, J. Jurkiewicz, A. Kreienbuehl, R. Loll, Class. Quant. Grav. 31, 165003 (2014)

31. P. Horava, Phys. Rev. D 79, 084008 (2009)

32. S. Jordan, R. Loll, Phys. Lett. B 724, 155 (2013)

33. J. Hartle, S. Hawking, Phys. Rev. D 28, 2960 (1983)